Magmatic ore deposits in mafic-ultramafic intrusions of the Giles Event, Western Australia

W.D. Maier[1], H.M. Howard[2], R.H. Smithies[2], S.H. Yang[3], S-J. Barnes[4], H. O'Brien[5], H. Huhma[5], and S. Gardoll[6]

[1]School of Earth and Ocean Sciences, Cardiff University, Cardiff, Wales,UK

[2]Geological Survey of Western Australia, Perth, Australia

[3]Oulu Mining School, University of Oulu, Oulu 90014, Finland

[4]Sciences de la Terre, Université du Quebec á Chicoutimi, Chicoutimi G7H 2B1, Canada

[5]Geological Survey of Finland (GTK), FI-02151 Espoo, Finland

[6]Department of Applied Geology, Curtin University, GPO Box U1987, Perth WA 6845.

Abstract

More than 20 layered intrusions were emplaced at c. 1075 Ma across >100 000 km^2 in the Mesoproterozoic Musgrave Province of central Australia as part of the c. 1090–1040 Ma Giles Event of the the Warakurna Large Igneous Province (LIP). Some of the intrusions, including Wingellina Hills, Pirntirri Mulari, The Wart, Ewarara, Kalka, Claude Hills, and Gosse Pile contain thick ultramafic segments comprising wehrlite, harzburgite, and websterite. Other intrusions, notably Hinckley Range, Michael Hills, and Murray Range, are essentially of olivine-gabbronoritic composition. Intrusions with substantial troctolitic portions comprise Morgan Range and Cavenagh Range, as well as the Bell Rock, Blackstone, and Jameson–Finlayson ranges which are tectonically dismembered blocks of an originally contiguous intrusion, here named Mantamaru, with a strike length of >170 km and a width of > 20 km, constituting one of the world's largest layered intrusions.

Over a time span of > 200 my, the Musgrave Province was affected by near continuous high-temperature reworking under a primarily extensional regime. This began with the 1220–1150 Ma intracratonic Musgrave Orogeny, characterized by ponding of basalt at the base of the lithosphere, melting of lower crust, voluminous granite magmatism, and widespread and near-continuous, mid-crustal ultra-high-temperature (UHT) metamorphism. Direct ascent of basic magmas into the upper crust was inhibited by the ductile nature of the lower crust and the development of substantial crystal-rich magma storage chambers. In the period between c. 1150 and 1090 Ma magmatism ceased, possibly because the lower crust had become too refractory, but mid-crustal reworking was continuously recorded in the crystalisation of zircon in anatectic melts. Renewed magmatism in the form of the Giles Event of the Warakurna LIP began at around 1090 Ma and was characterized by voluminous basic and felsic volcanic and intrusive rocks grouped into the Warakurna Supersuite. Of particular interest in the context of the present study are the Giles layered intrusions which were emplaced into localized extensional zones. Rifting, emplacement of the layered intrusions, and significant uplift all occurred between 1078 and 1075 Ma, but mantle-derived magmatism lasted for >50 m.y., with no time progressive geographical trend, suggesting that magmatism was unrelated to a deep mantle plume, but instead controlled by plate architecture.

The Giles layered intrusions and their immediate host rocks are considered to be prospective for (i) platinum group element (PGE) reefs in the ultramafic–mafic transition zones of the intrusions, and in magnetite layers of their upper portions, (ii) Cu–Ni sulfide deposits hosted within magma feeder conduits of late basaltic pulses, (iii) vanadium in the lowermost magnetite layers of the most fractionated intrusions, (iv) apatite in unexposed magnetite layers towards the evolved top of some layered intrusions, (v) ilmenite as granular disseminated grains within the upper portions of the intrusions, (vi) iron in tectonically thickened magnetite layers or magnetite pipes of

the upper portions of intrusions, (vii) gold and copper in the roof rocks and contact aureoles of the large intrusions, and (viii) lateritic nickel in weathered portions of olivine-rich ultramafic intrusions.

Keywords: Musgrave Province, Giles event, layered intrusions, PGE deposits, magnetite layers

1. Introduction

The Musgrave Province of central Australia hosts one of the most important clusters of mafic–ultramafic layered intrusions globally (Fig. 1), referred to as the Giles Complex (Daniels, 1974) or the Giles intrusions (Smithies et al., 2009). Together with broadly contemporaneous bimodal volcanism of the Bentley Supergroup and basic magmatism of the Warakurna Large Igneous Province (LIP)(Wingate et al., 2004), the Giles intrusions constitute the Warakurna Supersuite, formed during the c. 1090 to 1040 Ma Giles Event. The prospectivity of the Giles intrusions for magmatic ore deposits remains poorly understood. This is partly due to sparse exposure and because much of the study area belongs to the Ngaanyatjarra – Anangu Pitjantjatjara – Yankunytjatjara Central Reserve into which access is strictly regulated. However, the enormous volume of mafic igneous rocks and the remarkable size of some of the intrusions (up to several 1000 km^2) reflect a high flux of mantle derived magma and heat into the crust. This is considered to be favorable for the formation of magmatic and hydrothermal ore deposits. Two world-class deposits have been discovered so far, namely the Nebo–Babel magmatic Ni–Cu deposit (Seat et al., 2007, 2009) and the Wingellina Ni laterite deposit (Metals X Ltd, 2013). In the present paper we review the ore potential of the Giles intrusions and related mafic intrusive rocks of the Warakurna Supersuite.

2. Past work

Systematic geologic research on the Musgrave Province began with a mapping program (at 1:250 000 scale) in the 1960s (Geological Survey of Western Australia - reported in Daniels, 1974), during which the Blackstone, Murray, and Morgan ranges, and parts of the Cavenagh and Jameson ranges, were mapped (see Fig 1 for localities). Nesbitt and Talbot (1966) subsequently proposed that some of the layered intrusions are tectonised remnants of an originally much larger body. Other important early contributions on the layered intrusions include the papers by Goode and Krieg (1967), Goode (1970, 1976a,b, 1977a,b,c, 1978), and Goode and Moore (1975). A large multidisciplinary study of the Musgrave Province beginning in the late 1980s (Australian Geological Survey Organisation, now Geoscience Australia: Glikson, 1995; Glikson et al., 1996) also focused mainly on the Giles intrusions (Ballhaus and Glikson, 1989, 1995; Ballhaus and Berry, 1991; Clarke et al., 1995a,b; Glikson, 1995; Sheraton and Sun, 1995; Stewart, 1995). Recent work includes studies by Seat et al. (2007, 2009) and Godel et al. (2011), on the Nebo–Babel Ni–Cu ore deposit, and by Evins et al. (2010a,b) and Aitken et al (2013), on the structural evolution during the Giles Event.

3. Regional geology

In the present paper, the term 'Musgrave Province' is used to refer to high-grade metamorphic rocks affected by the 1220-1150 Ma Musgrave Orogeny, covering an area up to 800 km long and 350 km wide in central Australia (Fig. 1). The Western Australian segment of the Musgrave Province is referred to as the 'west Musgrave Province'. On geophysical images the Province is delineated by a series of east-trending anomalies. It is tectonically bound by the Neoproterozoic to Paleozoic sedimentary rocks of the Amadeus Basin in the north and the Officer Basin in the south (Edgoose et al., 2004).

95 The Musgrave Province lies at the junction between the North, South and West Australian
96 Cratons. While some models suggest these cratonic elements of the Australian Craton
97 amalgamated as early as c. 1700 Ma (e.g. Li, 2000; Wingate and Evans, 2003), most models agree
98 that final amalgamation pre-dates the Musgrave Orogeny at c. 1220 Ma (Giles et al., 2004; Betts
99 and Giles, 2006; Caeood and Korsch, 2008; Smithies et al., 2010, 2011; Kirkland et al., 2013).
100 With the exception of c. 1575 Ma rocks in the Wannarn area, the basement to the west
101 Musgrave Province is not exposed. However, isotopic data on the detrital components in
102 paragneisses, and on zircon xenocrysts, indicate that the basement is dominated by two major
103 juvenile crust formation events, at 1600–1550 Ma and 1950–1900 Ma (Kirkland et al., 2013).
104 The oldest magmatic rocks in the study area comprise felsic calc-alkaline rocks of the
105 Papulankutja Supersuite at c. 1400 Ma (Howard et al., 2011b; Kirkland et al., 2013). However, the
106 oldest event recognizable throughout the west Musgrave Province is the Mount West Orogeny,
107 characterized by emplacement of calc-alkaline granites of the Wankanki Supersuite mainly within
108 the central and southeastern part of the west Musgrave Province (Evins et al., 2009; Smithies et
109 al., 2009). Crystallization ages cluster between c. 1326 and 1312 Ma (Gray, 1971; Sun et al., 1996;
110 White et al., 1999; Bodorkos et al., 2008a–e; Kirkland et al., 2008a–f; Smithies et al., 2009). The
111 rocks are typically metaluminous, calcic to calc-alkaline granodiorites and monzogranites,
112 compositionally resembling Phanerozoic granites of the Andean continental arc (Smithies et al.,
113 2010). The Mount West Orogeny may have been triggered by the amalgamation of the North,
114 West, and South Australian Cratons and associated subduction and accretion (Giles et al., 2004;
115 Betts and Giles, 2006; Smithies et al., 2010, 2011; Kirkland et al., 2013).
116 The 1220–1150 Ma Musgrave Orogeny formed in an intracratonic (Wade et al., 2008;
117 Smithies et al., 2009, 2010) or back-arc setting (Smithies et al., 2013). Deformation and
118 metamorphism was of high grade resulting in abundant mylonites. The main magmatic

components are charnockitic and rapakivi granites of the Pitjantjatjara Supersuite. The earliest Pitjantjatjara granites are strongly Yb-depleted interpreted to have formed through deep-crustal melting in the presence of garnet. A transition from these to Yb-undepleted granites derived from shallower depth is diachronous, attributed to removal of the lower crust and mantle lithosphere, previously thickened during the Mount West Orogeny (Smithies et al., 2010, 2011). Intrusion of the high-T Pitjantjatjara granites (Smithies et al., 2010, 2011) coincided with a 70–100 m.y. period of regional ultra-high-temperature (UHT) metamorphism (King, 2008; Kelsey et al., 2009, 2010; Smithies et al., 2010, 2011), characterized by lower to mid-crustal temperatures of >1000°C, along a geothermal gradient of ≥35–40°C/km (King, 2008; Kelsey et al., 2009, 2010). Such conditions are consistent with removal of the lithospheric mantle. Thermal modeling and zircon geochronology indicates that mid-crustal temperatures remained elevated (>800°C) in the period between the Musgrave Orogeny and the Giles Event (Smithies et al., 2015), mainly due to the accumulation of the highly radiogenic Pitjantjatjara granites.

The c. 1090 to 1040 Ma Giles Event was characterized by voluminous mafic to felsic magmatism (Fig. 2), including the layered mafic-ultramafic 'Giles intrusions' (G1), massive gabbro (G2) locally mixed and mingled with granite, various dyke suites including the Alcurra Dolerite suite, granite plutons, as well as mafic and felsic lavas, volcaniclastic and sedimentary rocks forming the Bentley Supergroup. All these components are grouped into the Warakurna Supersuite interpreted to have accumulated in the long-lived intracontinental Ngaanyatjarra Rift (Evins et al., 2010b; Aitken et al., 2013). Based in part on the extensive outcrop of the Warakurna Supersuite across ~ 1.5 million km^2 the Giles magmatism has been interpreted as the result of a mantle plume (Wingate et al., 2004; Morris and Pirajno, 2005). However, the most conservative estimates for the duration of mantle magmatism are >30 m.y. with a likelihood it continued for significantly longer (Smithies et al., 2015, and in press), with no time-progressive geographical

143 trend or track, inconsistent with a simple plume model (Smithies et al., 2013, 2015, in press; Evins
144 et al., 2010a,b).
145 Younger events include the 580–530 Ma intracratonic Petermann Orogeny, during which
146 many of the Giles intrusions were fragmented. Additional younger events are reflected by several
147 regional dolerite dyke suites (at c. 1000, c. 825, and c. 750 Ma) and low-volume felsic magmatism
148 (at c. 995 Ma and c. 625 Ma)(Howard et al., 2015).
149
150 **4. Tectonic subdivision**
151 Past workers divided the Musgrave Province into a number of sub-zones that show distinct
152 structural and metamorphic characteristics. The sub-zones are separated by major west- and
153 west-northwesterly trending faults, including the south-dipping Woodroffe Thrust (Fig. 1). In the
154 eastern portion of the west Musgrave Province, there is a marked north-to-south change in the
155 pressure of granulite-facies metamorphism. In the northern segment, high-pressure (10–14 kbar)
156 metamorphism during the Petermann Orogeny has masked the effects of older metamorphism
157 (Scrimgeour and Close, 1999). To the south, the metamorphic overprint of the Petermann
158 Orogeny is not as marked and evidence for relatively low-pressure, but high-temperature
159 Mesoproterozoic metamorphism is preserved (Clarke et al., 1995b). The boundary between these
160 two regimes lies close to the west-trending, near vertical Mann Fault (Fig. 1).
161 The western part of the study area is subdivided into three distinct zones, namely the Walpa
162 Pulka, Tjuni Purlka, and Mamutjarra Zones (from northeast to southwest; Howard et al., 2014; Fig.
163 2). The Tjuni Purlka Zone represents a northwest-trending belt of multi-generational (c. 1220,
164 1075, and 550 Ma) shearing and mafic magmatism of the Warakurna Supersuite (Fig. 2) that
165 remained active throughout much of the Giles Event. The Walpa Pulka Zone (Fig. 2) is a deep-
166 crustal domain hosting abundant c. 1220–1150 Ma granites of the Pitjantjatjara Supersuite that

were emplaced during the Musgrave Orogeny. Mafic intrusions are rare and restricted to small bodies north of the Hinckley Range. The Mamutjarra Zone in the south (Fig. 2) contains several Giles intrusions and the c. 1345–1293 Ma calc-alkaline granites of the Wankanki Supersuite, emplaced during the Mount West Orogeny.

5. Analytical methods

Samples were prepared for analysis at GSWA using a jaw crusher followed by milling in a tungsten carbide mill. The mill was tested for possible contaminants, with only cobalt being significant (≤157 ppm in grinding tests). Major elements were determined by wavelength-dispersive X-ray fluorescence spectrometry (XRF) on fused disks using methods similar to those of Norrish and Hutton (1969). Precision is better than 1% of the reported values. Concentrations of Ba, Cr, Cu, Ni, Sc, V, Zn, and Zr were determined by wavelength-dispersive XRF on pressed pellets using methods similar to those of Norrish and Chappell (1977), whereas Cs, Ga, Nb, Pb, Rb, Sr, Ta, Th, U, Y, and REE were analysed by inductively coupled plasma–mass spectrometry (ICP-MS) using methods similar to those of Eggins et al. (1997), on solutions obtained by dissolution of fused glass disks. Precision for trace elements is better than 10% of the reported values. All whole-rock major and trace element data for the silicate rocks are listed in Table 1 of the supplementary data. All analyses and analytical details can be obtained from the WACHEM database (at <http://geochem.dmp.wa.gov.au/geochem/>). Selected major and trace elements for the massive magnetite seams were determined by instrumental neutron activation analysis (INAA) at The University of Québec at Chicoutimi, Canada (Table 2, supplementary data).

Platinum, Pd, and Au were analysed by lead collection fire assay of 40 g of sample, followed by ICP quantitation. The detection limit was 1 ppb for each element. For selected samples, complete PGE spectra were obtained by ICP-MS at The University of Quebec at Chicoutimi.

Analytical details are given in Barnes et al. (2010). Platinum group element data are shown with the bulk of the lithophile element data in Table 1, supplementary data.

Sulfur isotopes were analysed by Rafter GNS Sciences at the New Zealand National Isotope Centre at Lower Hutt, New Zealand. Samples were measured in duplicate in tin capsules with equal amounts of V2O5 on a EuroVector elemental analyzer connected to a GVI IsoPrime mass spectrometer. All results are averages and standard deviations of duplicates are reported with respect to Vienna Canyon Diablo Troilite (VCDT) standard, normalized to internal standards R18742, R2268, and R2298 with accepted $\delta^{34}S$ values of –32‰, +3.3‰, and +8.6‰, respectively. The external precision for this instrument is better than 0.3 for $\delta^{34}S$. All data are listed in Table 3, supplementary data.

In situ Sr isotope data were determined by laser ablation ICP-MS at the Geological Survey of Finland (GTK). Analytical procedures are provided in Yang et al. (2013b), and the data are provided in Table 4, supplementary data.

For most samples, Sm–Nd isotopic analyses were determined by isotope dilution at the VIEPS Radiogenic Isotope Laboratory, Department of Earth Sciences, La Trobe University, Victoria. Analytical techniques follow those of Waight et al. (2000). All quoted εNd values are initial values calculated at the time of igneous crystallization. For some samples, Nd isotopes were determined at GTK Espoo. Analytical details are given in Maier et al. (2013a). All Sm–Nd isotope data are listed in Table 5, supplementary data.

The composition of olivine was determined at The University of Oulu in Oulu, Finland, using a JEOL JXA-8200 electron microprobe at an accelerating voltage of 15 kV and a beam current of 30 nA, which allowed an approximately 150 ppm detection limit for nickel. The accuracy of analyses was monitored using reference material of similar compositions. Compositional data are listed in Table 1.

6. Geology and petrology of the Giles intrusions

6.1. Introduction

The Giles intrusions in western Australia show considerable variation in terms of size (from a few km^2 to >3000 km^2), depth of emplacement (from < 1kbar to possibly as much as 12 kbar), whole rock and mineral composition, as well as style of associated mineral deposits. In the following section, we group the intrusions by their predominant lithologies. Intrusions with important ultramafic segments of wehrlite, harzburgite, websterite and (olivine) orthopyroxenite include Wingellina Hills, Pirntirri Mulari, The Wart (Fig. 1). Intrusions that are predominantly leucogabbronoritic are more common, comprising Hinckley Range, Michael Hills, Latitude Hill, Murray Range, Morgan Range, Cavenagh Range and Saturn. The Blackstone, Jameson-Finlayson, and Bell Rock ranges also belong to this group, but they are now believed to be tectonically segmented portions of an originally single body, hereafter called the Mantamaru intrusion. In addition, a number of smaller intrusions or fragments of intrusions occur to the north of the Tjuni Purlka Zone including Mt Muir and Lehmann Hills.

Several of the mafic intrusions contain thick troctolitic successions, namely the Cavenagh and Morgan ranges and Mantamaru. Anorthosites may form relatively thin layers (centimetres to several tens of centimetres) in the mafic intrusions, but attaining thicknesses of several tens of metres at Kalka in South Australia.

6.2. Mafic-ultramafic layered intrusions

6.2.1. Pirntirri Mulari

The intrusion is located ~30 km north of Blackstone Community (Fig. 2). It was grouped with the gabbronoritic Murray Range by Ballhaus and Glickson (1995), but in view of the distinct lithologies and composition of the intrusions (ultramafic-mafic for Pirntirri Mulari, mafic for Murray) this interpretation is rejected here. The exposed portion of the intrusion has the shape of a wedge, with the upper mafic portion being markedly wider than the lower ultramafic portion (Fig. 3). The layers strike about 150° and mostly dip steeply to the southwest (60–90°). The body is about 5 km wide and has a stratigraphic thickness of about 3 km.

Most of the rocks are medium-grained (olivine) websterites, peridotites, (olivine) orthopyroxenites, and (olivine) gabbronorites. At the southwestern and northeastern margins of the intrusion occur interlayered websteritic and gabbronoritic orthocumulates, whereas adcumulate peridotites and orthopyroxenites are concentrated in the centre. Based on compositional and field evidence, we propose that the succession youngs to the northeast, implying that the intrusion is slightly overturned. Many of the rocks show textural equilibration, expressed by 120° grain boundaries, abundant bronzite and spinel exsolutions in clinopyroxene, small granoblastic plagioclase grains containing spinel inclusions, orthoclase exsolution blebs and two-pyroxene spinel symplectite at contacts between plagioclase and olivine. These features are common to many other Giles intrusions and were previously interpreted to reflect relatively high crystallization pressures and temperatures (Ballhaus and Glikson, 1989).

The basal contact of the intrusion is not exposed, but in view of the increased proportion of orthocumulates towards the southwestern exposed edge, we argue that the basal contact is proximal to this. The top contact is likely of a tectonic nature, as suggested by the presence of a mylonite zone and by the relatively unevolved chemical composition of the uppermost gabbros (Mg# 0.7, Cr/V > 1) (Table 1 data repository).

Most exposed contacts between layers are sharp (Fig. 4a). In the centre of the intrusion (GSWA189374), coarse-grained websterite underlies gabbronorite with an undulose contact, and has locally injected the gabbronorite (Fig. 4b). The gabbronorite is more deformed than the pyroxenite, and is altered near the contact, consistent with intrusion of pyroxenite below older gabbronorite. Elsewhere (e.g., GSWA189368), fine-grained lherzolite overlies coarse-grained peridotite with an undulose, sharp contact. The lherzolite contains inclusions of the peridotite and is interpreted to have crystallized from a new magma influx that was quenched and partially eroded its floor. Other ultramafic layers are underlain by pegmatoidal gabbronoritic orthocumulate layers (Fig. 4c), consisting of 40% plagioclase, 30% orthopyroxene, 20% clinopyroxene, and accessory phlogopite and chromite. Relatively high concentrations of incompatible trace elements (e.g. P, LREE, Nb, Rb) in the pegmatoid suggest that it may have formed in response to upward percolation of evolved melt or fluid.

The lower portion of the intrusion, particularly below and above pyroxenite layers, contains several horizons showing textural evidence for considerable syn-magmatic cumulate mobility, such as abundant ultramafic and anorthositic schlieren within gabbronorite (Fig. 4d).

The concentrations of the platinum group elements (PGE) in the intrusion are mostly <10 ppb (Fig. 5), and Cu/Pd is at the level of the primitive mantle (4000–7000), suggesting that the magma was fertile and sulfur undersaturated during crystallization. However, at a stratigraphic height of ~ 2600 m above the base of the intrusion, Cu/Pd increases sharply, suggesting that a sulfide melt had fractionated from the magma at this stage. This sample has low PGE concentrations, although it contains nearly 500 ppm Cu. It is located in the mafic–ultramafic transition interval, analogous to the stratigraphic position of PGE reefs in the Bushveld Complex and many other PGE-mineralized intrusions. A sulfide-bearing pyroxenite from an equivalent stratigraphic level collected along the southeastern edge of the intrusion (Fig. 3) has similar

chromium, copper, and nickel concentrations to the equivalent internal horizon, but higher Pt+Pd (172 ppb) and gold (17 ppb) concentrations. Assay results using a NITON portable XRF showed elevated Ni and Cu over a stratigraphic interval of 5–10 m, and peak concentrations of 0.43% Cu and 0.7% Ni in weathered rock (Redstone Resources Ltd, 2008a). No detailed sampling of this interval has yet been conducted to establish the width and grade of a putative reef horizon.

6.2.2. Wingellina Hills

The intrusion is approximately 12 km long and up to 3 km wide (Fig. 6). Drilling by Acclaim Minerals and Metals X Ltd, and mapping by GSWA, established dips of about 65–75° to the southwest, and younging in the same direction indicating that the intrusion is not overturned. The strike of the layering is 110-120°. The exposed stratigraphic thickness amounts to 2.5 km, assuming that the stratigraphy is not duplicated by tectonism. The gabbros and pyroxenites tend to be unaltered at the surface, whereas the peridotites are commonly deeply weathered to a depth of about 60 m to >200 m, particularly in shear zones.

The central portion of the intrusion contains numerous cyclic units consisting of basal pegmatoidal (ortho) pyroxenite, overlain by clinopyroxenite and then peridotite (olivine–spinel cumulate), wehrlite, and gabbronorite (Ballhaus and Glickson, 1989). The gabbronorite may contain fragments and schlieren of ultramafic material, and it may display convoluted and folded layering on a scale of 1–2-centimetres, analogous to Pirntirri Mulari (Fig. 4).

The composition of the basal to central portion of the intrusion has been studied in several stratigraphic boreholes. The basal contact has been intersected by a reverse circulation (RC) borehole (WPRC23, see Maier et al., 2014 for details). It is interpreted as intrusive because there is a well-defined, > 100 m wide basal compositional reversal that is characteristic of layered intrusions (Latypov et al., 2011). Overlying the contact is a 1-2m thick zone consisting of hybrid,

309 possibly contaminated gabbroic rocks (~10% MgO). A rock chip collected ~2 m above the contact
310 consists of medium-grained, moderately deformed olivine gabbronorite, implying relatively
311 insignificant tectonism of the contact zone (R Coles, 2013, written comm., 27 May).
312 In the next 300 m of the drill core, basal olivine gabbronorite is first overlain by pyroxenite
313 and then by progressively more magnesian harzburgite. This, in turn, is followed by peridotite and
314 wehrlite and then by about 20 m of websterite and >40 m of olivine gabbronorite. The contacts
315 between rock types can be either sharp or gradational. Within the websterite occurs a PGE reef
316 (described below) that has been identified along a strike length of 2–3 km (Fig. 6). The remainder
317 of the intrusion consists of layers of peridotite, wehrlite, pyroxenite, and olivine gabbronorite,
318 described in more detail in Ballhaus and Glickson (1989).
319 The compositional variation in the interval hosting the PGE reef is shown for borehole
320 WPRCO-064 (Fig. 7). The contact between websterite and wehrlite is sharp, reflected by a marked
321 decrease in MgO and an increase in Cr concentration. Platinum-group element concentrations
322 increase through the websterite layer to a maximum of 2ppm Pt+Pd+Au, at a level about 5–7 m
323 beneath the top of the layer. The peak grades occur over a 1-m interval, and grades in excess of 1
324 ppm PGE occur over 3–5 m. Above the reef, the concentrations of the PGE decrease relatively
325 rapidly over a height of a few meters. Gold and Cu concentrations remain relatively low (<5 ppb
326 Au, <10 ppm Cu) throughout the PGE-enriched zone, but peak just above the PGE reef, with up to
327 330 ppb Au in a 1-m interval, and up to 400 ppm Cu in rocks located a further 2 m above the Au
328 peak. Gold and Cu concentrations then decrease with further stratigraphic height, although at a
329 slower rate than the PGE levels. Similar metal distribution patterns have been observed in several
330 other layered intrusions (e.g., the c. 2.58 Ga Great Dyke, Wilson et al., 1989; the c. 2.925 Ga Munni
331 Munni intrusion, Barnes, 1993; and the c. 3.03 Ga Stella intrusion, Maier et al., 2003b), where they
332 were referred to as ‘offset patterns’ (Barnes, 1993). In comparison to the Bushveld PGE reefs (~1–

2% S), the PGE reefs at Wingellina Hills are relatively sulfur-poor (mostly <500 ppm S), possibly due to metamorphic devolatization. This renders the reefs nearly invisible in hand specimen.

The thickness and grade of the PGE reef shows considerable variation along-strike. In two of the three analysed boreholes (WPRC0-064 and WPRCD0-083) concentrations of >500 ppb PGE occur over a thickness of 8 m. The bulk concentrations of PGE+Au normalized to a width of 1 m are similar in the two holes (10.6 ppm in WPRC0-064, 9.6 ppm in WPRCD0-083). Borehole WPRC0-043 contains >100 ppb PGE+Au over 12 m, and total PGE+Au contents of 5.5 ppm normalized to 1 m, lower by about 40% than in the two other holes. This is unlikely to be the result of alteration, but implies significant variation in PGE grade of the reef along strike. Notably, the bulk PGE contents normalized to a width of 1m of the reef interval (at least in holes WPRCD0-064 and WPRCD0-083) are broadly similar to the PGE contents of the combined Merensky Reef and UG2 chromitite of the Bushveld Complex. However, the Bushveld reefs are much narrower and thus more economic to mine.

The Wingellina Hills laterite consists of yellow-brown to dark brown ochre material composed of goethite, manganese oxides, gibbsite, and kaolinite produced by weathering of peridotite. This constitutes the Wingellina nickel laterite deposit, discovered by INCO in 1956 (187 Mt at about 1% Ni and 0.08% Co; >167 Mt is classified as probable mining reserve; Metals X Ltd, 2013). Limonitic ochre is also present at Claude Hills (4.5 Mt at 1.5% Ni; Goode, 2002), in the Pirntirri Mulari intrusion, and in the southeastern part of the Bell Rock intrusion where excavations revealed laterite, ochre, and chalcedonic veins above a zone of saprolite (Howard et al., 2011b). The laterites formed by selective leaching of SiO_2 and MgO, resulting in residual concentration of alumina, iron oxides, and nickel, developed particularly prominently along shear zones. The ore is exposed at surface and has an average thickness of 80 m (maximum 200 m). The deposit has a high aspect- and very low strip ratio. It is locally cut by semiprecious, pale green

chrysoprase mined artisinally since the 1960s, particularly in the Kalka area (Goode, 2002). The lateritic profiles may have some potential for scandium deposits, particularly where the parent rock consisted of clinopyroxenite, but to our knowledge, no relevant investigations have so far been conducted.

6.2.3. The Wart

The Wart is a relatively small mafic-ultramafic body, located about 20 km south of the community of Wingellina. The main block of the intrusion measures about 5 km x 2 km striking about 130° and dipping steeply at 80–90° to the southwest. Several smaller mafic slivers occur to the northwest of the main body. The stratigraphic thickness of the body is ~1–2 km. Ballhaus and Glikson (1995), who studied the Wart in some detail suggested that it represents the lower portion of the Bell Rock intrusion.

The Wart shares certain lithological and compositional characteristics with Pirntirri Mulari. Both contain layers of medium-grained mesocumulate wehrlite–peridotite within a package of adcumulates and mesocumulates of clinopyroxenite and melagabbronorite. Many of the ultramafic layers have sharp contacts and have been interpreted as sills (Ballhaus and Glikson, 1995). We collected only a small number of gabbroic and ultramafic samples because the body is culturally sensitive. However, abundant mineral compositional data are given in Ballhaus and Glikson (1995).

6.3. Predominantly mafic intrusions

6.3.1. Latitude Hill – Michael Hills

Latitude Hill is located 5–10 km to the east of The Wart and the Bell Rock intrusions (Fig. 2). Ballhaus and Glikson (1995) proposed that it may be a folded segment of the 8000m thick Michael

Hills gabbro, whereas Pascoe (2012) suggested that Latitude Hill is in faulted contact with Bell Rock. Latitude Hill has an intrusive contact with granulite analogous to Wingellina Hills and The Wart (Ballhaus and Glikson, 1995; present work). It contains numerous layers and lenses of olivine gabbronorite and olivine pyroxenite, as well as rare peridotite, but the dip direction of the layers remains uncertain.

6.3.2. Morgan Range

The Morgan Range is located ~ 10 km north of Blackstone Community (Fig. 2). It measures approximately 10 km x 5 km (~50 km^2) in size, striking broadly 120° and with a stratigraphic thickness of >1 km. The intrusion consists mostly of relatively unaltered olivine gabbronorites and troctolites that display modal layering on a scale of centimetres to metres. It forms a boat-shaped structure with steep dips (up to 80°) to the interior, except for the centre where the dip is sub-horizontal. The syncline plunges at a relatively shallow angle towards the southeast and compositional data suggest that the intrusion is not overturned.

At the northeastern tip of the intrusion is a relatively small (~300 m x 300 m) interlayered mafic-ultramafic block consisting of dunite, troctolite and melagabbronorite. The rocks strike ~100° and dip steeply (80°) to the north. They show certain compositional similarities to Wingellina Hills and Pirntirri Mulari, but because the contact with the main Morgan Range is concealed by regolith it is presently unclear whether this segment forms an integral part of the Morgan Range intrusion, or whether it is a fragment of another intrusion that was tectonically adjoined to the Morgan Range.

6.3.4. Hinckley Range

404 This is a large (~30 km x 10 km), highly deformed, relatively poorly layered body that has a
405 stratigraphic thickness of about 5800 m, strikes about 100°, and dips steeply to the north at 70–
406 80°. The rocks consist of (olivine) gabbros, troctolites, and microgabbros, with a few layers or
407 lenses of anorthosite, and minor pyroxenite. Abundant pseudotachylite are related to the
408 Petermann Orogeny. Many of our samples have relatively high concentrations of K_2O and
409 incompatible trace elements, suggesting that the mafic magma assimilated, or mixed with, a
410 granitic component. Our most primitive samples were collected at the southern edge of the
411 intrusion, suggesting that the intrusion youngs towards the northeast (cf Ballhaus and Glickson,
412 1995).

413 Where the Hinckley Range intrusion is in contact with the West Hinckley Range intrusion
414 (MGA 472843E 7118953N), mingling textures between gabbro and granite are prominent. These
415 have been described in Howard et al. (2011b) and Maier et al. (2014), from whom the following
416 description is taken. The gabbro belongs to the unlayered G2 variety which tends to crosscut,
417 engulf, and post-date the layered G1 intrusions. The G2 gabbros locally form agmatites or injection
418 migmatites (Fig. 8), and angular blocks engulfed by granite. Brittle fractures in gabbro may be
419 infilled by granite veins. This indicates that the granite has intruded partially solidified gabbro.
420 Contacts between the felsic and mafic portions may also be cuspate, indicating that the mafic
421 component behaved in a ductile manner in the presence of the felsic material. Similar
422 relationships occur some 20 km to the northwest, at Amy Giles Hill (Fig. 2). A leucogranite showing
423 well-developed co-mingling textures with gabbro (Howard et al., 2006a) has been dated at 1074 ±
424 3 Ma (GSWA 174589; Bodorkos and Wingate, 2008b).

425 In the West Hinckley Range, mingled gabbro forms a kilometre-scale fold with a steep
426 northwest-trending axial plane that has been intruded by syndeformational leucogranite. A strong
427 ‘gneissic’ fabric has locally formed in mixed or agmatitic rocks as the axial planar fabric continued

to develop, and this has been again engulfed within subsequent injections of leucogranite. A sample of undeformed leucogranite from within one of these axial planar zones, approximately 2 km south of the mingled gabbro–granite described above, yielded a crystallization date of 1075 ± 7 Ma (GSWA 174761; Kirkland et al., 2008e). Syn-mylonitic leucogranite has also pooled into boudin necks in a northwest-trending mylonite directly south of Charnockite Flats (~2.5 km northwest of the West Hinckley Range intrusion), and has been dated at 1075 ± 2 Ma (GSWA 185509; Kirkland et al., 2008f). The combined data define a very narrow period of intrusion of massive G2 gabbro and multi-phase intrusion of leucogranites (1078–1074 Ma), northwest-directed folding, and northwest-trending shearing. The relationships between gabbro and granite in the Hinckley Range intrusion confirm earlier suggestions by Clarke et al. (1995b) that substantial deformation occurred during the Giles Event.

6.3.5. Murray Range

The gabbroic Murray Range comprises two distinct segments, (i) a layered portion of >25 km^2 consisting of gabbronorite or olivine gabbronorite, with the most primitive rocks occuring in the centre of the intrusion, and (ii) extensive areas covered by massive gabbro, particularly to the east and northeast of Pirntirri Mulari. The strike of the layering is mostly 50–70°, and the dip is sub-vertical. The intrusion contains abundant stratiform layers and lenses of microgabbro and cross-bedded medium-grained gabbronorites. Due to its location at the contact between the Tjuni Purlka and Walpa Pulka Zones the intrusion was tectonically dismembered, obscuring the true stratigraphic thickness and structure of the intrusion. Like the Hinckley Range, the Murray Range is one of the G1 intrusions that was substantially intruded by G2 gabbro, consistent with the model that during the emplacement of the G2 gabbros, the contact between the Tjuni Purlka and Walpa

Pulka Zones was a syn-magmatic shear zone (Evins et al., 2010a,b). It is thus not surprising that deformation and alteration are commonly more pronounced than in the other Giles intrusions.

6.3.6. Cavenagh Range

The Cavenagh Range remains one of the least known amongst the Giles intrusions because access to it is restricted on cultural grounds. The intrusion is located 10 km south of the Blackstone Range (Fig. 2) and is defined by several circular remnant magnetic highs occurring over an area of approximately 22 km x 18 km. The southern portion forms a syncline with a stratigraphic thickness of about 1 km. It consists predominantly of olivine gabbronorites, olivine gabbros, troctolites, and norites. Websterites, anorthosites and microgabbros form bands and discontinuous pods, schlieren, and autoliths. Xenoliths of basement gneiss have been encountered near the southeastern edge. An east-trending fault separates the southern segment from the northern portion of the intrusion which dips at about 15–30° to the northeast and has a stratigraphic thickness of about 2–4 km (barring structural duplication). It consists dominantly of poorly layered olivine gabbronorite, troctolite, and magnetite-bearing olivine gabbronorite.

Layering in the Cavenagh intrusion is defined predominantly by modal variation between olivine, pyroxene, and plagioclase. Boundaries between layers are mostly gradational, but pyroxenites, anorthosites, and many microgabbros tend to have sharp contacts. The latter rocks also tend to form lenses, schlieren, and fragments within gabbronorite and troctolite.

The southern to central portion of the Cavenagh intrusion is the least chemically evolved. The northern portion shows a subtle trend toward more differentiated compositions with height. Simultaneously, the concentrations of PGE increase, reaching 80–100 ppb PGE in two samples. The microgabbros are interlayered with medium-grained gabbronorite and may contain autoliths of anorthosite and thin bands, irregular clasts, and circular concretions of granular websterite and

clinopyroxenite adcumulate. These field relationships suggest that the microgabbros and the associated medium-grained rocks intruded contemporaneously. The microgabbros tend to have equigranular textures with 120° grain boundaries. In places, olivine and pyroxene grains may form strings oriented in a radial configuration that are here interpreted to have resulted from crystal growth in a flowing, supercooled magma. Large olivine oikocrysts can form wispy crystals that are surrounded by rims of anorthosite. The latter may have formed when rapid crystallization due to supercooling or degassing led to depletion in the olivine component within a boundary layer surrounding the growing crystals. The microgabbros may also contain clinopyroxene oikocrysts with abundant inclusions of irregular and rounded exsolved oxide grains.

The microgabbros have variable compositions, broadly overlapping with the medium grained host rocks. Many of the samples contain a cumulus component, as indicated by whole-rock chromium concentrations of up to 1900 ppm, positive strontium anomalies on multi-element variation diagrams, and depleted incompatible trace element levels (e.g., <5 ppm Zr). Microgabbros in the Giles intrusions and elsewhere were previously explained by intraplutonic quenching (Ballhaus and Glikson, 1989, Tegner et al., 1993).

6.3.7. Lehmann Hills, Mt Muir, and other small intrusions north of the Blackstone and Wingellina Communities

The intrusions outcrop over relatively small areas and consist of gabbronorites, olivine gabbronorites and troctolites (Fig. 9a). The rocks may have a distinct flow structure, containing elongated lenses and schlieren of anorthosite in pyroxenite, and autoliths of pyroxenite within anorthosite. At Lehmann Hills, sulfides (up to 1% combined pyrrhotite and chalcopyrite) are relatively abundant.

A number of small mafic bodies occur up to 20 km to the north of the Hinckley Range, in the Mt Gosse – Mt Daisy Bates area (termed 'Northeast' in Table 1, data repository). These bodies consist of metagabbros and metagabbronorites. They tend to show partial granoblastic textures, with garnet forming fine-grained rims around pyroxene and magnetite, or more rarely porphyroblasts. Pyroxene is commonly replaced by hornblende, and biotite is also common.

6.3.8. Mantamaru

Mantamaru is the Ngaanyatjarra name for the community of Jameson. The intrusion forms one of the world's largest layered igneous bodies, with an original size of at least 3400 km^2. This body was dismembered during the Petermann orogeny resulting in the Jameson-Finlayson, Blackstone and Bell Rock ranges.

Jameson–Finlayson Range

The Jameson–Finlayson Range extends for 66 km along a strike of ~120° and is ~ 30 km wide (Fig. 2). Layering is in normal orientation and dips at about 20° to 30° to the southwest, implying a stratigraphic thickness of up to about 10 km. Several layer-parallel mylonitic zones occurring near the base of the intrusion could account for limited structural repetition, but we argue that this does not significantly affect the overall thickness estimates.

The bottom and top contacts of the intrusion are not exposed. At the base is magnetite–ilmenite-bearing lherzolite; the rocks contain 20–50 vol.% opaques that have estimated V_2O_5 contents of about 1.4 wt% (Daniels, 1974). This is overlain by rhythmically layered troctolite and olivine gabbronorite (Fig. 9b). At the top of the intrusion, in the southwest, there is a layered succession of troctolite, olivine gabbro, and olivine gabbronorite, containing at least 11 major

titaniferous magnetite seams (Fig. 9c). However, due to poor outcrop, the thickness and contact relationships of most of the seams remain poorly known.

The magnetite seams mostly form bands of rubble. They appear to be separated by silicate intervals several hundreds of metres thick (Fig. 10). All layers that have been sampled consist of massive iron oxide, with <5% silicates. Grain sizes are relatively coarse (≤3 mm), possibly reflecting sintering (Reynolds, 1985). The main minerals are magnetite, granular ilmenite, fine ilmenite lamellae, abundant hematite replacement patches and lamellae (≤20 vol.%), as well as goethite. Layers enriched in apatite were not encountered.

The most reliable observations have been made on the basal magnetite layer. It has been traced along a strike of about 19 km forming an aeromagnetic anomaly with sporadic broken outcrop (Fig. 10). The seam may reach a thickness of 50 m, with up to three sub-seams locally developed. Whether the sub-seams formed due to primary magmatic processes or structural duplication is uncertain. The contacts of the seam with the magnetite-bearing leucotroctolite and anorthosite hanging and footwall are sharp. The host rocks show evidence for deformation. The mineralogy of the seam consists of magnetite and granular ilmenite, as well as fine ilmenite lamellae within magnetite. Hematite and goethite replacement is locally abundant.

Concentrations of Pt, Pd, and Au have been analysed in 39 samples of the layer along strike and in 3 traverses across the layer (Traka Resources, unpublished report). In addition, we analysed three samples of the layer for the complete PGE spectrum (Table 1, data repository). The PGE concentrations reach approximately 2 ppm Pt+Pd+Au (Fig. 11). The seam is thus markedly PGE enriched relative to the Bushveld Main Magnetite Layer (Fig. 12), but has significantly lower PGE contents than the main PGE mineralized magnetite layer of the Stella intrusion of South Africa (Maier et al., 2003b). The metal concentration patterns of the Jameson seam show depletion in Os–Ir–Ru relative to Rh–Pt–Pd, characteristic of evolved magmatic rocks (Fig. 12). The layer has

relatively constant vanadium concentrations throughout (up to 7400 ppm V, 1.35 wt% V_2O_5; Fig. 11), whereas the PGE tend to be markedly elevated at the base. Sulfur concentrations are mostly 100–150 ppm, locally reaching 700 ppm. Sulfur concentrations do not correlate with Cu and PGE (Fig. 11), suggesting some of the sulfur could have been lost in response to equilibration of sulfide with magnetite (Naldrett and Lehmann, 1988), or in response to low-grade metamorphic devolatisation. The average Pd/Ir ratio is relatively low (34), consistent with a magmatic origin of the PGE mineralization. Platinum/Pd ratios are above unity, analogous to other PGE mineralized magnetites and magnetite gabbros (see Maier, 2005 and references therein).

Magnetite layers 2, 3, 6 and 7 are not exposed, but their presence is suggested by prominent magnetic anomalies (Fig. 10). Layers 4 and 5 are pervasively altered to goethite and hematite, although they also contain abundant granular ilmenite. Layer 8 may be a plug-like body. Layer 11 is partly exposed and forms a massive, well-layered, possibly rotated layer dipping about 30° to the southwest. The compositional variation in the upper seams is poorly understood, although it is evident that the vanadium and noble metal contents are much lower than in layer 1, whereas iron, chromium, and phosphorus concentrations increase with height (Table 2, supplementary data).

Blackstone Range

The body is ~50 km long and up to 5km wide. It strikes about 90° and layering dips at between 70 and 80° to the south and is not overturned. The exposed stratigraphic thickness is about 4 km. The body is interpreted to be the exposed northern limb of an upright west-trending structural syncline (the Blackstone Syncline). Relics of its north-dipping southern limb are sporadically exposed 20 km to the south, directly north of the Cavenagh intrusion. The size of the combined body is about 1400 km^2. It is conformably overlain by felsic volcanic rocks of the Tollu Group (Bentley Supergroup).

The rocks are relatively unaltered and undeformed. Layering can be pronounced where defined by thin (centimetre-scale) magnetite layers. Most of the rocks are (olivine) gabbronorites and troctolites, each constituting approximately 50% of the total mass of the intrusion. Troctolitic rocks occupy the central and southern portions of the intrusion. The troctolites contain less than 20% olivine, with the exception of two relatively olivine-rich layers (40% olivine, 100–150 m thickness) that can be traced along much of the intrusion, one in the centre (sample GSWA 155669) and another near the southern edge. These two layers are also present in the Bell Rock intrusion where they contain up to 80% olivine. The occurrence of these layers in both intrusions is consistent with an interpretation whereby the two intrusions are fragments of a large, tectonically dismembered proto intrusion (Nesbit and Talbot, 1966; Glikson, 1995). At the southern margin of the intrusion occurs a ~ 1 m-thick magnetite layer that contains 1.5% V_2O_5. Relatively elevated Cu concentrations of up to 250 ppm suggest the presence of minor sulfides, common to all magnetite-rich rocks in the upper portions of the Blackstone intrusion. Whether this layer can be correlated to magnetite layer 1 in the Jameson–Finlayson intrusion is uncertain, as it is highly PGE depleted whereas the Jameson basal layer is relatively PGE rich.

Bell Rock Range

This body extends for ~ 50 km along a strike of ~ 120°. The exposed width is ~ 5–6 km, and the rocks dip at 70° to the southwest. Field exposures of graded and cross-bedded layers, as well as whole rock and mineral compositional data indicate younging of the intrusion to the southwest. A detailed compositional study of the Bell Rock intrusion was conducted by Ballhaus and Glikson (1995), from which some of the following information is taken. Our own sample base is relatively small, comprising 14 samples taken across the body.

The exposed stratigraphic thickness is about 3800 m, but since the contacts of the body are not exposed, this is a minimum estimate. The top of the intrusion is likely in contact with volcanic rocks of the Bentley Supergroup; This implies that either the intrusion has been deeply eroded after its emplacement or the top contact is faulted. The basal rocks consist of medium- to coarse-grained troctolites and gabbros, whereas the central portion consists of magnetite-bearing troctolite and the upper portion contains centimetre- to tens of centimetre-thick magnetite seams, dunitic layers, numerous microgabbro sills, and a few anorthosite layers. Modal cyclicity occurs on a centimetre to metre scale. A recent drillhole collared at the western edge of the Latitude Hill intrusion with a dip of 70° toward the southwest (MDDH0001, drilled by Anglo American Exploration (Australia) Pty Ltd as part of the Department of Mines and Petroleum's Exploration Incentive Scheme), has intersected deformed magnetite-enriched troctolites that are interpreted to belong to the Bell Rock intrusion (Pascoe, 2012). This suggests that magnetite seams could be present below cover.

6.3.9. Alcurra Dolerite suite

The components of the Alcurra Dolerite suite comprise dolerite dykes and sills that constitute the bulk of the 1078-1073 Ma Warakurna Large Igneous Province (Wingate et al., 2004), small basic and intermediate bodies and dykes emplaced near the margins of older G1 layered mafic intrusions, G2 massive gabbro, and comingled gabbro–granite.

Contact relationships constrain the emplacement dates of the Alcurra suite to <1078 Ma, and dating of some of the intrusions indicates that magmatism continued to at least c. 1067 Ma (Howard et al., 2009). However, geochemical data suggest that Alcurra-type rocks were likely formed over a much longer period, including lavas of the Bentley Supergroup until at least 1047

615 Ma (Howard et al., 2009, 2011a; Smithies et al., 2013). The Alcurra Dolerite suite thus reflects
616 relatively long-lived mantle melting (Smithies et al., 2013).
617 The c. 1076 Ma mafic to intermediate rocks forming part of the Alcurra Dolerite suite
618 typically consist of fine- to medium-grained olivine gabbro, olivine norite, ferronorite, and
619 ferrodiorite. The latter rocks have evolved and Fe-rich tholeiitic compositions, resulting in a
620 pronounced aeromagnetic signature and high specific gravity.
621 Rocks of the Alcurra Dolerite Suite occur throughout the West Musgrave Province, including
622 the Blackstone Syncline, within the marginal zones of the G1 Jameson Range and Murray Range
623 where they intruded along the layer contacts and between the intrusions and their country rocks.
624 The northeast-trending, coarse-grained ferrogabbro dykes that crosscut the G1 Jameson intrusion,
625 and which also occur throughout the northern parts of the COOPER map sheet, used fractures and
626 faults related to the earlier Musgrave Orogeny.
627
628 **6.3.10. Saturn**
629 The Saturn intrusion defines an elliptical aeromagnetic anomaly with a diameter of approximately
630 10 km, located between the Cavenagh and Blackstone ranges (Figs. 2 and 13). Cross cutting field
631 relationships indicate that Saturn is younger than the Blackstone Range. However, a date of 1072
632 ± 8 Ma determined by using the U–Pb method on baddeleyite in olivine gabbro (Redstone
633 Resources Ltd, 2007, written comm.) is within error of the c. 1078 to 1075 Ma range for both the
634 G1 and G2 mafic phases of the Giles Event. The concentric magnetic pattern implies zones of
635 magnetite enrichment, but massive magnetite layers have not been found on the surface.
636 Possibly, this is due to the very poor outcrop. The only exposed rocks consist of scattered massive,
637 medium-grained, leucocratic olivine gabbros, typically containing elevated concentrations of

638 biotite and up to 5% magnetite. The rocks are massive or show flow-banded textures, defined by
639 schlieren of fine-grained gabbronorite (for example, at the 'Camp' site, Fig. 13).
640 The rocks have relatively evolved compositions, overlapping with Blackstone and Bell Rock.
641 Samples collected along the Phoebe traverse (Fig. 13, 14) contain up to 6.7% TiO_2 and 800 ppm V,
642 comparable to magnetite gabbros from the Jameson and Blackstone ranges. The rocks in the
643 centre of the Saturn intrusion are somewhat more primitive than those at the margin, having
644 higher Mg# and lower Ti concentrations (Fig. 14), consistent with a dome-like structure. Sulfide
645 contents are around 1%, higher than in most other Giles intrusions. Copper and PGE
646 concentrations are mostly relatively low, but they increase approximately halfway up the
647 magmatic stratigraphy (Fig. 14). Based on its age, the crosscutting relationships with rocks in the
648 Blackstone syncline, and compositional characteristics such as the enrichment in mica and sulfide,
649 the Saturn intrusion may be of transitional composition between the Alcurra Dolerite Suite and
650 the G1/G2 intrusive phase.
651
652 **6.3.11. Intrusions in the Halleys – Helena – DB Hill area**
653 The mafic rocks to the northeast and south of the Saturn intrusion were explored by Redstone
654 Resources at the Halleys, Halleys NW, Helena, and DB Hill prospects (Report at General Meeting,
655 2008b; Fig. 13). The intrusion(s) lack the strong remanent magnetic signature of the Cavenagh
656 intrusion and are thus interpreted to be distinct bodies. The crosscutting magnetic patterns
657 suggest that they intruded into the G1 intrusions as well as the volcanic, volcaniclastic, and clastic
658 rocks of the Kunmarnara and lower Tollu Groups.
659 Most of the rocks are medium-grained, leucocratic ferrogabbros or ferronorites. They have
660 up to 20% intercumulus or oikocrystic magnetite, up to 5% biotite, and several percent sulfide
661 minerals. The rocks tend to be massive, or show a weak, west-trending magmatic foliation.

Although whole-rock and mineral compositions are slightly more differentiated than in the upper portions of the Blackstone or Cavenagh intrusions, Cr/V ratios are locally elevated due to chromium enrichment (≤1.6 wt%) within magnetite. The rocks have markedly higher concentrations of mica, sulfide, and incompatible trace elements, and Au/PGE ratios than the Cavenagh and Blackstone intrusions. Instead, the Halleys rocks have distinct chemical and petrographic affinities with the Alcurra Dolerite suite.

Drilling delineated a pipe-like PGE enriched body, with up to 0.33 wt% Cu and 0.24 ppm PGEs over 74 m, and 0.5 wt% Cu and 0.53 ppm PGE over 16 m (Redstone Resources, 2008, comm. at Annual General Meeting, 27 November). The noble metal patterns are less fractionated than in the magnetite seams of the Bushveld Complex or the Stella, Jameson, and Saturn intrusions, having lower PPGE/IPGE ratios. This is consistent with a magmatic origin of the Halleys mineralization.

6.3.12. Nebo–Babel

The 1068+-4 Ma Nebo–Babel intrusion is located about 25 km south of Jameson Community (Fig. 2). The Nebo–Babel Ni–Cu–PGE deposit was studied in detail by Seat et al. (2007, 2009) and Seat (2008), and the following section has been compiled mostly from their work.

The intrusion has a tubular ('chonolithic') shape traceable for about 5km and trending north-northeast to east. It is 1 km wide and has a stratigraphic thickness of approximately 0.5 km. The chonolith plunges gently to the west-southwest and dips to the south at about 15°. It is offset by the Jameson Fault, dividing it into 2 portions, the Nebo section in the east and the Babel section in the west. Geochemical data indicate that the body is overturned. It was emplaced along a shearzone in felsic orthogneiss of the Pitjantjatjara Supersuite. The magma flow direction was

685 proposed to have been towards the northeast because some of the units thin in this direction and
686 becomes progressively more fractionated.
687 At the stratigraphic base of the intrusion is a breccia zone (MBZ), overlain by a chilled margin
688 (7–9% MgO), variably textured leucogabbronorite (VLGN), melagabbronorite (mela-GN) and
689 barren gabbronorite (BGN), which in the Nebo sector is associated with oxide–apatite
690 gabbronorite (OAGN). The latter constitutes about 20–30% of the intrusion and is characterized by
691 oxide-rich layers that are 5–30 cm thick, with gradational bases and sharp upper contacts. The
692 Babel segment additionally contains the key mineralized gabbronorite unit (MGN) and a 15m thick
693 massive and coarse-grained troctolite unit located between VLGN and BGN in the upper part of
694 the intrusion.
695 In April 2002, Western Mining Corporation announced a drill intersection of 26 m containing
696 2.45% Ni, 1.78% Cu, and 0.09% Co at the Nebo–Babel prospect. The resource estimates are 392 Mt
697 at 0.30% Ni and 0.33% Cu, based on 90 drillholes (Seat et al., 2007). The sulfides consist of
698 monoclinic pyrrhotite, pentlandite, chalcopyrite, and pyrite and occur as massive ores with
699 associated sulfide breccias and stringers, and as disseminated ores, typically forming interstitial
700 blebs in the gabbronorite unit (MGN). Sulfur isotopic data show a remarkably narrow range of $\delta^{34}S$
701 values from 0 to +0.8‰. The massive sulfides formed through fractional crystallization of a sulfide
702 liquid, resulting in a cumulate of monosulfide solid solution relatively enriched in Os, Ir, Ru, and Rh
703 and depleted in Pt, Pd, and Au.
704
705 **6.3.13. Dyke suites**
706 The dyke suites in the west Musgrave Province have been studied by a number of authors,
707 including Nesbitt et al. (1970), Zhao and McCulloch (1994), Clarke et al. (1995b), Glikson et al.
708 (1996), and Scrimgeour and Close (1999). Howard et al. (2006b) identified seven distinct suites of

dykes. The oldest dyke suite (c. 1170 Ma, ~8% MgO) forms part of the Pitjantjatjara Supersuite. Dykes associated with the Giles Event include those belonging to the Alcurra Dolerite suite (6–9% MgO; Zhao et al., 1994; Edgoose et al., 2004) and further include unnamed plagioclase-rich dolerites (~8% MgO) that clearly post-date the G1 intrusions, but may be synchronous with the G2 intrusions. Post-Giles dolerites comprise a suite of unnamed olivine- and plagioclase-porphyritic dykes at c. 1000 Ma (~8% MgO), 825 Ma quartz dolerite dykes of the Gairdner-Willouran LIP (~8% MgO), and c. 800 Ma dykes of the Amata Dolerite (Zhao et al., 1994; Glikson et al., 1996; Wingate et al., 1998). A further suite of dykes (~ 9.5% MgO) may be of broadly coeval, or younger, than the Gairdner Dyke Swarm.

Godel et al. (2011) distinguished five distinct dyke suites (NB1–5) in the Nebo–Babel area. Types NB1–3 are low-Ti basalts with 5–20% MgO, postulated to be derived from the sub-continental lithospheric mantle (SCLM). Types NB4 and NB5 are high-Ti basalts with 5–14% MgO interpreted to be sourced from a mantle plume. The NB1 type is of approximately similar composition to the plagioclase-phyric dykes of Howard et al. (2006b), containing about 10–13% MgO. NB4 was proposed to represent the Alcurra Dolerite suite.

7. Geochemistry of the intrusions

7.1. Lithophile elements and Nd–Sr–S isotopes

The concentration of the major elements in the G1 layered intrusions is largely controlled by variation in the proportions of olivine, orthopyroxene, clinopyroxene, plagioclase, and magnetite. The modal proportion of plagioclase in the ultramafic rocks is mostly <10%, resulting in relatively high MgO and FeO contents and low Al_2O_3 contents (Fig. 15a). Most of the remaining samples collected are gabbronorites or troctolites with <15% MgO and >10% Al_2O_3. Application of the lever rule indicates that the modal proportion of plagioclase in the latter rocks is typically >50%, with

733 the Cavenagh intrusion being least feldspathic (Fig. 15a,b). Titanomagnetite is an important phase
734 in the Mantamaru, Halleys, and Saturn intrusions, as indicated by high TiO_2 at low MgO and Al_2O_3
735 concentrations (Fig. 15b). Elevated K_2O concentrations in the Hinckley and Murray Range
736 intrusions are likely the result of relatively enhanced crustal contamination (Fig. 15c), whereas the
737 elevated K_2O levels at the Halleys prospect possibly result from advanced fractionation since the
738 country rocks are K-poor mafic intrusive rocks. Relatively high P_2O_5 levels at the Halleys prospect
739 and the Saturn, Jameson, and Blackstone intrusions suggest the presence of apatite (Fig. 15d).
740 Relatively P enriched rocks have also been intersected by drilling along the eastern edge of the Bell
741 Rock intrusion (Pacoe, 2012).
742 The ultramafic intrusions are characterized by relatively high Cr and Ni contents, controlled
743 mainly by olivine, clinopyroxene, and orthopyroxene (Fig. 16). The basal rocks at Wingellina Hills
744 plot along a trend from olivine to orthopyroxene, reflecting their harzburgitic and olivine-
745 orthopyroxenitic composition. The remainder of the ultramafic rocks at Wingellina Hills and
746 Pirntirri Mulari are wehrlites and websterites. Cumulus chromite is largely confined to Wingellina
747 Hills where Cr contents exceed the levels that can be hosted in pyroxene. Most of the gabbroic
748 intrusions contain <1000 ppm Cr, with the exception of samples from the Wingellina Hills and
749 Halleys intrusions. The elevated Cr concentrations at Halleys are the result of abundant Cr-bearing
750 magnetite.
751 In most intrusions, Ni shows a good positive correlation with MgO (Fig. 16b). Samples with
752 significant amounts of olivine are mostly confined to the Wingellina Hills intrusion which have
753 MgO > 30 wt% and Ni > 1000 ppm. The trend of the Wingellina Hills samples in Ni-MgO space can
754 be extrapolated to a Ni concentration in olivine of about 2500–3000 ppm, broadly overlapping
755 with measured olivine compositions from Pirntirri Mulari (~3000 ppm Ni). Two ultramafic samples
756 from Pirntirri Mulari and one from the Morgan Range have distinctly higher Ni contents than the

757 other ultramafic rocks. This is possibly a result of alteration, in view of their relatively high loss-on-
758 ignition (LOI) values. The presence of sulfide and magnetite could explain the elevated Ni levels in
759 the Halleys and Blackstone intrusions (up to ~1500 ppm Ni), compared to the other gabbroic–
760 troctolitic intrusions, which tend to contain <500 ppm Ni. Even higher Ni contents occur at the
761 Nebo Babel Ni-Cu sulfide deposit which have a tenor of 5-6% Ni in the sulfides.
762 The state of differentiation of the intrusions can be compared in a plot of Cr/V ratio vs Mg#
763 (Fig. 17). Wingellina Hills, Pirntirri Mulari, The Wart, and Morgan Range are least evolved, showing
764 some overlap with the Lower Zone of the Bushveld Complex, except that the Bushveld has higher
765 Cr/V ratios due to higher chromite contents. Intrusions with intermediate compositions include
766 Cavenagh, Murray Range, Hinckley Range, the massive G2 gabbros, and the slightly more
767 differentiated Mt. Muir together with the intrusive fragments to the north of Mt Muir and
768 Hinckley Range ('North' and 'Northeast' in Table 1, supplementary data). The most evolved
769 intrusions are Mantamaru (although Bell Rock contains some relatively unevolved samples),
770 Saturn, Halleys, and dykes belonging to the Alcurra Dolerite suite. However, in the Alcurra Dolerite
771 suite there are also relatively unevolved samples that have up to 9 wt% MgO.
772 The mafic intrusions show fractionated lithophile multi-element (spider) patterns, with
773 relative enrichments in the most incompatible elements, but negative Nb anomalies (Maier et al.,
774 2014). Positive Ti anomalies are found at Mantamaru, Halleys, and Lehman Hills and in many
775 samples from Saturn, reflecting the presence of magnetite. The Saturn and Halleys intrusions have
776 distinctly elevated incompatible trace element contents relative to most other intrusions,
777 including Cavenagh and Blackstone, consistent with a distinct magmatic lineage. Notably, the trace
778 element patterns of gabbros from Wingellina Hills are identical to those of Wingellina Hills
779 pyroxenites, indicating crystallization from magmas of broadly similar composition.

780 Data from sample suites that contain a higher liquid component are plotted in Fig. 18. The
781 Alcurra Dolerite suite (Fig. 18a), G2 gabbros (Fig. 18b), NB1 dykes, and the fine grained marginal
782 rocks from Nebo–Babel show considerable similarity including pronounced negative Nb and Ta
783 anomalies and, in the case of the G2 gabbros and Nebo–Babel chilled margins, negative Ti
784 anomalies. In all suites, the incompatible trace element contents are typically higher than in the
785 G1 intrusions, but the shapes of the multi-element patterns for all mafic intrusives are remarkably
786 similar. Microgabbros from Cavenagh have less fractionated, but more 'spiky' patterns than the
787 other liquid-rich mafic rocks (Fig. 18d). This reflects the elevated cumulate component in most
788 microgabbros.
789 Mantamaru has systematically higher εNd (0 to +2) and lower Ce/Nb ratios (mostly 2–7) than
790 the other intrusions (Fig. 19). Some of the least radiogenic Nd isotope compositions occur in the
791 G2 gabbros and the G1 Cavanagh and Morgan Range intrusions (εNd = –1 to –4, Ce/Nb = 3–13),
792 and in the Kalka intrusion in South Australia (Wade, 2012). Rocks of the Alcurra Dolerite suite have
793 intermediate compositions (εNd = –1 to +2, Ce/Nb ~ 3–5). Most Nebo–Babel samples have
794 compositions overlapping with the Alcurra Dolerite suite (εNd = –1.7 to 0.3, Ce/Nb = 5–7, except
795 for the marginal rocks, which show lithological evidence for crustal assimilation and have εNd as
796 low as –3). The data of Seat et al. (2011) indicates that basement rocks at Nebo–Babel have εNd
797 values of –4.5 to –5 and Ce/Nb ratios of 9, whereas the regionally extensive Pitjantjatjara granite
798 suite has εNd of –2 to –4 and highly variable Ce/Nb (5 to >20).
799 *In situ* Sr isotope analyses on plagioclase (Maier et al., 2014) are consistent with these
800 results in that the least-radiogenic Sr isotopic values are found in the Mantamaru and Halleys
801 intrusions, whereas Morgan Range, Lehman Hills, and Cavenagh have higher initial Sr isotope
802 ratios. Microgabbros from Cavenagh have less radiogenic Sr isotope ratios (Sr_i = (87Sr/86Sr)i =
803 0.7042 – 0.7057) than associated medium-grained gabbros (Sr_i = 0.7052 – 0.7068), and the

804 medium-grained samples show greater isotopic heterogenity. This is interpreted to reflect lining of
805 the magma conduits by early, relatively contaminated magma pulses, allowing the relatively late-
806 stage microgabbro magma to be emplaced while undergoing relatively less crustal interaction. Of
807 note is that almost the entire range in Sr isotopic ratios seen within the west Musgrave mafic-
808 ultramafic intrusions is present within the Kalka intrusion in South Australia, and in both cases, the
809 ultramafic rocks have the highest initial Sr isotope ratios, whereas anorthosites, leucogabbros, and
810 troctolites have relatively more mantle-like compositions.

811 Whole-rock sulfur isotope data have been generated for rocks of the Jameson intrusion, the
812 G2 gabbros, and the Alcurra Dolerite suite (Table 3, supplementary data). In addition, we collected
813 sulfur isotope data for sulfide-bearing rhyolites from the Bentley Supergroup in the Palgrave area
814 (Fig. 2), as well as *in situ* (laser ablation ICP-MS) sulfur isotope data from Halleys. These data can
815 be compared to those from Nebo-Babel (Seat et al., 2009). All mafic intrusive rocks plot near the
816 composition of the mantle. By contrast, rhyolites of the Mount Palgrave Group have a much wider
817 sulfur isotopic range of $\delta^{34}S$, from +3.2 to +7. The data could either suggest that the sulfides in the
818 mafic rocks are of mantle derivation, or that any crustal sulfides were juvenile or underwent no
819 sulfur isotopic fractionation, or that assimilated crustal sulfides equilibrated with the magma at
820 high R-factors (mass ratio of silicate melt to sulfide melt; Campbell and Naldrett, 1979; Lesher and
821 Burnham, 2001). Notably, recent data from the Manchego prospect (Karykowski, 2014) show
822 strong negative $\delta^{34}S$, representing the only igneous suite amongst the Giles intrusions with
823 markedly non-magmatic S isotope signatures.

824

825 **7.2. Sulfur and chalcophile elements**

826 Most of the Giles intrusions have relatively low sulfur concentrations, at <200 ppm (Fig. 20a).
827 Slightly higher sulfur concentrations are present at Wingellina Hills, The Wart, Murray Range,

828 Hinckley Range, the 'North' and 'Northeast' intrusive fragments, some of the G2 massive gabbros,
829 and the Alcurra Dolerite suite (up to 2000 ppm). Even higher sulfide contents (in places > 1 vol. %)
830 occur at Saturn, and in olivine gabbro and olivine gabbronorite of the upper Jameson intrusion,
831 with Cu concentrations up to 860 ppm (at 0.12 wt% SO_3). The relatively high sulfide and Cu
832 contents could be due to protracted fractionation and resulting saturation in sulfide liquid in the
833 magma, analogous to the troctolitic Kiglapait intrusion in Labrador, where sulfur saturation is
834 reached after 93% fractionation (Morse, 1981). Alternatively, the upper stratigraphic portions of
835 the Jameson Range could have undergone incipient hydrothermal alteration and addition of Cu
836 and S, possibly related to the voluminous volcanic activity that formed the Mount Palgrave Group,
837 directly to the southwest. However, sulfur isotopic data for two troctolitic samples (GSWA 189475
838 and 189478) indicate $\delta^{34}S$ of between +2.1 and +2.8, broadly consistent with a magmatic origin.
839 No sulfur data are available for Halleys, but petrographic examination indicates locally
840 several percent sulfides, consistent with Cu concentrations of >4000 ppm in some samples.
841 Sulfide-rich mafic intrusive rocks, locally containing net textured and massive sulfides were
842 recently intersected at the Manchego Prospect (Phosphate Australia, 2014; Karykowski, 2014). The
843 highest sulfide contents among the Giles intrusions occur at Nebo–Babel, including thick intervals
844 of massive and disseminated sulfides (Seat et al., 2007).
845 The mafic-ultramafic intrusions are typically relatively Cu poor (<200 ppm Cu, Fig. 20b). The
846 relatively unevolved (ultramafic) rocks have particularly low Cu contents, whereas Cu contents
847 progressively increase in the evolved (mafic) rocks, consistent with incompatible behavior of Cu in
848 fractionating sulfur-undersaturated magma. The highest Cu contents are found in the Nebo Babel
849 (sulfide tenor of 2-8% Cu), Halleys and Manchego intrusions (Seat et al., 2007, Karykowski, 2014).
850 Slightly lower Cu contents in some samples from Saturn, and the uppermost portions of the
851 Jameson intrusion, where some of the massive magnetite layers contain up to 700 ppm Cu.

852 Elevated Cu concentrations are also found in the Wingellina Hills PGE reefs (up to 500 ppm Cu),
853 and in a pyroxenite from the upper portion of Pirntirri Mulari that has 350 ppm Cu.
854 The majority of the Giles intrusions have low PGE contents (<30 ppb Pt+Pd, Fig. 20c). Higher
855 values occur in the PGE reefs of the Wingellina Hills intrusion, containing up to several ppm PGE,
856 the pyroxenite in the upper portion of Pirntirri Mulari (200 ppb PGE, not shown in Fig. 20c due to
857 lack of major element data), and in samples from Halleys (up to 200 ppb PGE). Other PGE-rich
858 rocks not plotted include those from Nebo–Babel (up to 0.5 ppm PGE in whole rocks, up to ~7 ppm
859 PGE in sulfide) and Manchego (up to approximately 1 ppm PGE in sulfide, Karykowski, 2014). The
860 lowermost magnetite layer in the Jameson intrusion has up to about 2 ppm PGE, at very low
861 sulfide contents. Scattered PGE enrichment, not accompanied by sulfide enrichment, occurs in the
862 Morgan Range (≤80 ppb), The Wart (one sample with 120 ppb), and Cavenagh (three samples with
863 75–100 ppb).
864 In almost all intrusions, including the sulfide-bearing Nebo Babel, Halleys and Manchego
865 intrusions, Cu/Pd ratios are above the range of the primitive mantle (~7000); thus, they are PGE-
866 depleted relative to mantle (Fig. 20d). This could suggest that the magma had equilibrated with
867 sulfide prior to final emplacement, in the mantle or the crust, or that it assimilated Cu-rich crust,
868 or that the mantle source was relatively enriched in Cu. Cu/Pd ratios progressively increase with
869 decreasing Mg# and samples with Cu/Pd < primitive mantle are mostly confined to Wingellina
870 Hills, Pirntirri Mulari, and the Morgan Range, as well as some Cavenagh samples, that is, rocks with
871 Mg# mostly >60. We interpret this to reflect sulfide liquid saturation in response to primarily
872 magmatic fractionation rather than contamination. We do not consider it likely that the PGE
873 depletion is due to a relatively small degree of mantle melting, as NB1 is strongly S undersaturated
874 and has lower TiO2 contents (0.8%) than typical MORB (>1%, Gale et al., 2013).

875 Most of the sample suites that represent liquids rather than cumulates (NB1 dykes, the
876 Alcurra Dolerite suite, and Nebo–Babel chilled margins) are PGE depleted, with Cu/Pd ratios above
877 primitive mantle values. The main exceptions are the unevolved G2 gabbros, which contain up to
878 10–15 ppb Pt and Pd each and have Cu/Pd ratios overlapping with primitive mantle. Notably, Nebo
879 Babel chilled margins too have PGE concentrations typical of basaltic magmas (~10–20 ppb Pt and
880 Pd each), but Cu/Pd > 10 000.
881
882 **7.3. Mineral chemistry**
883 We determined the compositions of olivine, orthopyroxene, clinopyroxene, and plagioclase in
884 more than 50 rock samples from the Giles intrusions, excluding the the Alcurra Dolerite suite and
885 the G2 massive gabbros. A summary of some key compositions are given in Table 1, and a detailed
886 discussion of the data can be found in Maier et al. (2014). In the present paper, we focus on
887 discussing olivine compositions. The mineral has between 40 and 87 mole % Fo (Fig. 21). Olivine
888 from the Blackstone intrusion and parts of Cavenagh show the lowest Fo values, whereas the
889 highest Fo contents occur at Wingellina Hills, Pirntirri Mulari, The Wart, and Morgan Range.
890 Samples from Jameson, Saturn, Hinckley Range, Murray Range, Nebo–Babel, Lehman Hills, and
891 Latitude Hill contain olivine with intermediate Fo contents.
892 Olivine from the mafic and mafic-ultramafic Giles intrusions has up to 3500 ppm Ni (Fig.
893 21a). Ni contents show a positive correlation with Fo content and are higher than in olivines of
894 comparable Fo content from many basic magmas globally, although relatively high Ni
895 concentrations appear to be characteristic of many layered intrusions (Fig. 21b). The highest Ni
896 contents in magmatic olivine identified so far occurs in the Kevitsa intrusion of Finland (with up to
897 1.5 wt% Ni; Yang et al., 2013).

For the origin of the Ni enrichment in olivine of the layered intrusions several models may be considered. (i) Equilibration of olivine with trapped melt could lower the Fo content without significantly affecting Ni concentrations. This model would be consistent with the observed decoupling of Fo from Ni contents in olivine, and from An contents of plagioclase. However, Godel et al. (2011) found Ni enrichment in olivines from the NB1 dykes. Thus, the observed Ni enrichment must, at least in part, reflect an early magmatic process. (ii) Equilibration of olivine with percolating sulfide liquid. However, there is little evidence for sulfide in most intrusive rocks related to the Giles Event. (iii) Assimilation of Ni-rich sulfide before final magma emplacement. This model is presently also considered unlikely as the West Musgrave crust is relatively poor in magmatic Ni sulfides. (iv) Magma derivation from a pyroxenitic–eclogitic mantle source (Sobolev et al., 2011). This model is equally rejected as it implies that most layered intrusions globally are derived from pyroxenitic mantle sources, for which there is presently no evidence. (v) Contamination leading to magma reduction and relatively low Fo contents. However, the oxygen fugacity of the Giles layered intrusions is thought to be similar to most other mafic-ultramafic crustal rocks, at around the quartz-fayalite-magnetite buffer (Staubman, 2010). (vi) Polybaric fractionation, with initial high-P crystallization of pyroxene at depth leading to depletion of the magma in MgO relative to Ni, followed by ascent and final emplacement of the magma at low pressure conditions where olivine may become stable. Such a magma, and any olivine crystallising from it, could have relatively high Ni to MgO ratios (Maier et al., 2013). In addition, the D_{Ni} into olivine increases with falling pressure (Li and Ripley, 2010). The model would be consistent with the distinctly lower Cr/Al ratios of pyroxenes in the Giles intrusions relative to the Bushveld Complex (Maier et al., 2014), potentially reflecting high-P pyroxene crystallization. Ballhaus and Glickson (1995) noted that olivine in the Giles intrusions shows a continuous range of Fo contents, in contrast to other layered intrusions such as the Bushveld Complex which lack olivines of

922 composition Fo 60–80, normally interpreted to be the result of the peritectic reaction of olivine to
923 pyroxene, temporarily destabilizing olivine. The authors proposed that the lack of an “olivine gap”
924 in the Giles intrusions is due to polybaric fractionation.
925
926 **8. Discussion**
927 **8.1. Nature of parent magmas to the Giles intrusions**
928 Knowledge of the composition of the parent magma to cumulate rocks is of considerable interest
929 to petrologists and economic geologists because this potentially allows to constrain the nature of
930 the mantle source, the degree of crustal contamination of the magma, the crystallization history of
931 an intrusion, and the prospectivity for magmatic mineral deposits. One of the most common
932 approaches to estimate the parent magma composition is based on the study of chilled contact
933 rocks of intrusions. However, such rocks are commonly contaminated and thus not necessarily
934 representative of the primary magma. Another approach could be to examine microgabbroic rocks
935 that are abundant within several Giles intrusions, but many of these rocks contain a cumulate
936 component.
937 A technique that has been successfully applied in the Bushveld Complex and more recently
938 in the Giles intrusions comprises the study of fine-grained sills or dykes associated with the
939 intrusion (Sharpe, 1981; Barnes et al., 2010). For the ultramafic segments of the G1 intrusions, a
940 suitable parent magma candidate would be the fine-grained low-Ti tholeiitic ‘plagioclase-rich
941 dykes’ initially documented in the Bell Rock Range area by Howard et al. (2007). These dykes are
942 compositionally equivalent to the NB1 dyke type of Godel et al. (2011). A further suitable parent
943 magma type could be the unevolved members of the massive G2 gabbros. They contain ~ 10–13
944 wt% MgO, 12 wt% FeO_T, 350 ppm Ni, up to 700 ppm Cr, and 10–15 ppb Pt and Pd each.
945 Crystallization of the Wingellina Hills intrusion from either NB1- or primitive G2-type magma is

consistent with the relatively low Ti content of these magmas (Fig. 53 in Maier et al., 2014). Modeling using the PELE software (Boudreau, 1999) indicates that at low to intermediate pressure NB1 has a crystallization order of chromite > olivine+chromite > olivine+chromite+clinopyroxene > chromite+clinopyroxene+plagioclase+orthopyroxene. This is broadly consistent with petrographic observations on the Pirntirri Mulari and Wingellina Hills intrusions, namely the occasional occurrence of chromite grains within olivine. The modeled Fo content at 1–5 kb is 87 mol.%, consistent with analyses. Furthermore, calculations by Godel et al. (2011) indicate that NB1 reaches sulfur saturation after 30% crystallization, at about the time plagioclase appears on the liquidus, consistent with the stratigraphic position of the PGE reefs at the top of the ultramafic zone in the Wingellina Hills intrusion. None of the other c. 1070 Ma dyke suites analysed by Howard et al. (2006b) or Godel et al. (2011) provides a suitable fit for the ultramafic intrusions. Considering the parental magmas to the gabbroic intrusions, possible candidates are the Nebo–Babel chilled margin (7–9 wt% MgO, Mg# of 51–61) or the compositionally similar NB3 dyke type. For the Halleys and Saturn intrusions, the Alcurra Dolerite suite (or the compositionally equivalent NB4 dyke type of Godel et al., 2011) would be a potential parent magma, based on similarities in incompatible trace element and noble metal ratios (e.g., high Cu/Pd) and common enrichment in mica and sulfide (Howard et al., 2009). The most primitive members of the Alcurra Dolerite suite have 8–9 wt% MgO and Cr/V ratios of 2–4 (Table 1, supplementary data).

8.2. Mantle sources of the magmas

Godel et al. (2011) proposed that NB 1 magmas were derived from the sub-continental lithospheric mantle (SCLM). Their model was based on the relatively low Ti contents and MREE to HREE ratios in the magmas, implying the presence of amphibole in the source. However, several arguments can be made against this model: (i) Magmas believed to be derived from the SCLM, e.g.

970 Bushveld B1 magmas, have much lower S contents (400 ppm, Barnes et al., 2010) than NB1, which
971 has S contents typical of many other global basalts (~1000 ppm; Godel et al., 2011). (ii) SCLM
972 derived magmas may have high Pt/Pd above unity (Barnes et al., 2010) whereas NB1 has Pt/Pd
973 below unity, in the range of most other basalts. (iii) Between c. 1220 and c. 1120 Ma, the west
974 Musgrave Province experienced ultra-high temperature (UHT) metamorphism in the middle crust
975 (Kelsey et al., 2009). Smithies et al. (2010, 2011) argued that this requires removal of the regional
976 SCLM, consistent with a dramatic lowering in the pressure of crustal melting at the beginning of
977 the Musgrave Orogeny. If there was SCLM at the beginning of the Giles Event, it must have formed
978 after the Musgrave Orogeny, which means it would have been still young, hot, and weak, and have
979 too radiogenic Nd isotopic compositions to be parental to the NB1 dykes ($\varepsilon Nd = -2$). Based on
980 these data, we do not subscribe to the model of Godel et al. (2011). The evidence for an
981 asthenospheric mantle source to NB1 is more persuasive, e.g., the resemblance of Yb–Ti–Zr–Nb
982 concentrations of NB1 to those in MORB. The enrichment in LILE and LREE within NB1 could be
983 modeled by low degree (<<5%) crustal contamination of asthenospheric high-Mg basalt.
984 The origin of the magma forming the Alcurra Dolerite suite also remains unresolved. Godel et al.
985 (2011) proposed that the NB4 dykes, which they considered analogues of the Alcurra Dolerite
986 suite, were plume melts. The main argument rests on the relatively high Ti contents and
987 MREE/HREE ratios of NB4, ostensibly requiring the presence of residual garnet in a deep mantle
988 source. However, the high La/Yb ratios of the Alcurra-type rocks (5 - 9.7) are not accompanied by
989 depletions in Yb (average 3.34 ppm) with respect to MORB and are thus better explained through
990 minor contamination (<<1%) with HFSE-rich crust. Crustal contamination could potentially also
991 explain the relatively high Cu/Pd and Au/PGE ratios of the Alcurra-type magmas, whereas the
992 origin of the elevated Pt/Pd remains presently poorly understood.
993

994 **8.3. Crustal contamination of the magmas**

995 The Giles intrusions have εNd from +2 to –5 (Fig. 19 and Table 4, supplementary data). These data
996 could be explained by variable crustal contamination, or melting of compositionally diverse mantle
997 sources, or both. At least some degree of *in situ* crustal contamination is suggested by the field
998 evidence, e.g. the mingling of the G2 gabbros with granite and abundant xenoliths in several G1
999 intrusions such as Hinckley Range (Fig. 6) and Kalka (Gray and Goode, 1989).

1000 In the ultramafic intrusions, crustal contamination is suggested by the existence of 2 distinct
1001 crystallization paths. The basal portions of the Wingellina Hills and Kalka (South Australia)
1002 intrusions, and most of the central portions of Pirntirri Mulari, have a crystallization sequence of
1003 olivine > orthopyroxene+olivine+chromite > orthopyroxene+clinopyroxene, in contrast to the
1004 central portion of the Wingellina Hills intrusion (Ballhaus and Glickson, 1995) which has a similar
1005 crystallization order as that modeled (using PELE) for NB1, i.e. chromite - olivine+chromite -
1006 olivine+chromite+clinopyroxene - chromite+clinopyroxene+plagioclase+orthopyroxene. Two
1007 distinct liquid lines of descent have also been found at the Muskox intrusion, Canada, where the
1008 basal rocks show a crystallization sequence of olivine > clinopyroxene+olivine, whereas the upper
1009 units show olivine > olivine+orthopyroxene, interpreted to result from contamination with partial
1010 melts of the roof (Irvine, 1970).

1011 Among the gabbroic G1 intrusions, Cavenagh has the lowest εNd (εNd as low as –5),
1012 overlapping with those of basalts of the Mummawarrawarra and Glyde Formations of the Bentley
1013 Supergroup (and Warakurna Supersuite). As there are no Musgrave crustal rocks currently known
1014 to have εNd values below –6, the required degree of contamination of the Cavenagh magma may
1015 seem unrealistically high. However, granites of the regionally occurring Pitjantjatjara Supersuite
1016 are extremely rich in HFSE, which may greatly reduce the required amounts of contamination
1017 (Kirkland et al., 2013). Relatively strong contamination of the Cavenagh intrusion is consistent with

1018 the high Ce/Sm and Ce/Nb ratios (Fig. 22). In contrast, Nd and Sr isotopic data for the troctolitic
1019 intrusions (namely Mantamaru) approximate the chondritic uniform reservoir (CHUR) (εNd mostly
1020 from 0 to +2, ISr ~ 0.704), have markedly higher εNd or lower Sri than any Musgrave crust present
1021 at the time and relatively low Ce/Sm and Ce/Nb ratios (Fig. 22). These data indicate very minor
1022 (<5%) crustal contamination in most troctolitic intrusions.
1023 The Alcurra Dolerite suite has slightly lower εNd (+1 to –1) than the Mantamaru intrusion.
1024 Smithies et al. (2013) showed that less than 10% bulk contamination of the most primitive samples
1025 of the Alcurra Dolerite suite with average Pitjantjatjara Supersuite granite can explain the entire
1026 isotopic variation and much of the highly incompatible trace element variation within the Alcurra
1027 Dolerite suite. If one assumes as contaminant a low-degree (20%) partial melt of average
1028 Pitjantjatjara Supersuite granite, the required assimilation is <4%. Such low degrees of
1029 contamination would produce only slight shifts to lower εNd isotope values, and it would thus
1030 appear unlikely that the mantle source was strongly depleted. Thus, the unevolved magmas of the
1031 Alcurra Dolerite suite were likely derived by relatively shallow melting (<80 km) of weakly
1032 depleted mantle, followed by early and very minor (<4%) contamination with highly enriched
1033 crustal material, and then closure of the continuously fractionating system to further
1034 contamination. The latter process can be applied to all Giles intrusions, consistent with the broad
1035 similarity in εNd within individual bodies, at variable Ce/Nb and La/Sm.
1036
1037 **8.4. Magma emplacement**
1038 The emplacement conditions of the Giles intrusions were discussed by Maier et al. (2014), from
1039 which the following summary has been compiled. Field relationships and compositional data
1040 indicate that the depth of emplacement varied considerably between intrusions. In the case of
1041 Mantamaru, country-rock inclusions and intrusive contacts indicate that the body was emplaced

at the stratigraphic level of the Mummawarrawarra Basalt (Kunmarnara Group). Based on the low metamorphic grade (greenschist facies) of the basalts, it is argued that the Mantamaru intrusion crystallised in an upper crustal, extensional environment. Constraints on its crystallization age are the minimum depositional age of the Kunmarnara Group (defined by intrusion of granite at c. 1078 Ma; Sun et al., 1996; Howard et al., 2011b), and a direct U–Pb zircon date of 1076 ± 4 Ma (Kirkland et al., 2011; GSWA 194762).

Particularly in the Hinckley Range, in the eastern part of the study area, massive G2 gabbro cuts the layered G1 intrusions and tends to show evidence of comingling with leucogranite. The latter may form pluton-scale bodies in the basement, for example the Tollu pluton. In the vicinity of major shear zones this bimodal gabbroic-granitic magmatism was accompanied by shearing and west-northwest folding, at between 1078 ± 3 and 1074 ± 3 Ma (Howard et al., 2011b). These dates overlap with the crystallization ages of the layered (G1) intrusions, but field relationships indicate that the G2 intrusions always post-date G1.

In the Blackstone Sub-basin, to the south of Blackstone Community, rhyolites of the Smoke Hill Volcanics directly overlie the G1 Blackstone Range without an obvious fault. Crystallization ages for the rhyolites [1071 ± 8 Ma (GSWA 191728; Coleman, 2009); 1073 ± 7 Ma (GSWA 191706; Coleman, 2009), and 1073 ± 8 Ma (GSWA 189561; C Kirkland, 2014, written comm.) are within analytical error of the emplacement date of the G1 and G2 intrusions, and the composition of the rhyolites resembles that of leucogranites associated with the G2 intrusions. In addition, several field exposures indicate that the Blackstone intrusion was emplaced into the lower basaltic portions of the Kunmarnara Group (Bentley Supergroup).This requires extensive and rapid crustal uplift, erosion, and exhumation of the layered G1 intrusions, immediately followed by felsic volcanism.

Previous authors have proposed that some of the ultramafic Giles intrusions have been emplaced at relatively high pressure (Goode and Moore, 1975; Ballhaus and Berry, 1991), based on high Al concentrations of pyroxene, spinel exsolution in pyroxene and plagioclase, rutile exsolution in pyroxene, antiperthitic exsolution in plagioclase, and orthopyroxene–clinopyroxene–spinel–albite coronas between olivine and plagioclase. For example, Goode and Moore (1975) suggested that the Ewarara intrusion was emplaced at a pressure of 10–12 kbar. If the thickness of the crust at the end of the Musgrave Orogeny, just 40my before the Giles event, was 35 km (Smithies et al., 2011), the Ewarara intrusion would have intruded near the base of the crust. Ballhaus and Glikson (1989) proposed an emplacement depth of 6.5kbar (~20km) for the Wingellina Hills and Pirntirri Mulari intrusions. However, because the coeval gabbroic intrusions are up to 10 km thick, the emplacement depth of the ultramafic bodies may have been as shallow as 10 km.

Emplacement into relatively deep crustal levels could explain why the ultramafic intrusions are less abundant than the gabbroic and troctolitic bodies, and why the former are proportionally more abundant in South Australia than in Western Australia - the South Australian crust is exposed at a deeper level (Goode, 2002). Equally consistent with this model is the observation that the ultramafic intrusions tend to be exposed in the cores of regional folds (i.e., the anticline north of Blackstone Community which hosts the Pirntirri Mulari and Morgan Range intrusions), or along faults.

Field relationships also allow to place some constraints on emplacement dynamics. For example, the close spatial association of many microgabbros with fragments and schlieren of pyroxenite suggests that the emplacement of the microgabbros was accompanied by disaggregation of semi-consolidated pyroxene-rich cumulate slurries. This points to a semi-consolidated magma chamber that was frequently replenished by unevolved magma.

8.5. Fragmentation of intrusions

The idea that some or all of the Giles layered intrusions could be tectonically dismembered remnants of a much larger body can be traced back to Sprigg and Wilson (1959) and Nesbitt and Talbot (1966). Other authors who favoured this model include Glikson (1995), Smithies et al. (2009), Howard et al. (2011b) and Aitken et al. (2013). Geophysical, lithological, and compositional data reported in the present study indicate that the Jameson–Finlayson, Blackstone, and Bell Rock intrusions are fragments of an originally contiguous body, named the Mantamaru intrusion by Maier et al. (2014). This has a minimum preserved size of 3400 km^2, in the same range as the Great Dyke, Stillwater, Sept Iles, and Dufek intrusions which measure between 3000–5000 km^2. It has been further proposed that the Cavenagh intrusion may form the southern limb of the synclinal Blackstone intrusion (Nesbitt and Talbot, 1966; Aitken et al., 2013), potentially adding at least another 540 km^2 to the size of the Mantamaru intrusion. However, the Blackstone intrusion is much more differentiated than the Cavenagh intrusion, and it contains a massive magnetite layer that appears to be absent from the Cavenagh intrusion. Furthermore, the Cavenagh intrusion shows elevated PGE concentrations in its upper portion whereas the Blackstone intrusion is uniformly PGE depleted. Finally, the Blackstone intrusion has distinctly higher εNd values than the Cavenagh intrusion. These data place some doubts on a possible connection between the Cavanagh and Blackstone intrusions, although other layered intrusions such as Bushveld and Kalka can have a wide range of trace element and isotopic compositions.

Based largely on compositional data, Seat (2009) proposed that the Nebo and Babel intrusive blocks are overturned fragments of an originally contiguous intrusion. This model is consistent with field evidence from, e.g., the western end of the Hinckley intrusion and the NW edge of the Blackstone Range, that deformation accompanied magmatism, locally developing open to tight folds.

1113 It is tempting to speculate that all the ultramafic intrusions located in the Tjuni Purlka Zone
1114 (Wingellina Hills, Pirntirri Mulari, The Wart, Morgan Range, Kalka, Gosse Pile, and Ewarara)
1115 originally formed a single body. This would imply lateral movement of up to 50 km within the Tjuni
1116 Purlka Zone. The intrusions share some similarities (e.g., olivine and pyroxene compositions,
1117 stratigraphic position of the Wingellina PGE reef and the Cu–PGE-rich horizon at Pirntirri Mulari)
1118 but they also show differences (e.g., thicker olivine and chromite rich segments and higher PGE
1119 concentrations at Wingellina Hills than in the other bodies, variation in plagioclase composition
1120 between Wingellina Hills and The Wart vs. Pirntirri Mulari). Further work is required to resolve this
1121 question.
1122
1123 **8.6. Comparison to other large layered intrusions**
1124 In order to better understand the petrogenesis and prospectivity of the Giles intrusions, it is useful
1125 to draw comparisons with other well-characterized and mineralized layered intrusions, e.g. the
1126 Bushveld Complex (Fig. 23). The Pirntirri Mulari, Wingellina Hills, and The Wart intrusions are the
1127 approximate stratigraphic and compositional equivalents of the Lower and Critical Zones of the
1128 Bushveld Complex. They have broadly similar olivine compositions and they show basal
1129 compositional reversals, thick ultramafic portions, and a number of ultramafic–mafic cyclic units.
1130 Reef-style PGE enrichments have been identified in the Wingellina Hills intrusion, and there are
1131 some indications that a similar horizon may exist in the Pirntirri Mulari intrusion. The equivalent
1132 prospective horizon of The Wart, Kalka, Ewarara, Gosse Pile, Ngulana, and Alvey Hills remains
1133 poorly studied, partly due to restricted access.
1134 A major difference between the Giles ultramafic intrusions and the Bushveld Complex is that
1135 the former appear to lack chromitite seams. If this is due to the early crystallization of Cr-rich

clinopyroxene, as suggested by Ballhaus and Glickson (1995), this would imply a low prospectivity for chromite deposits in the Giles intrusions.

The gabbroic Morgan Range intrusion contains a lens of ultramafic rocks at its northern edge and thus could represent the stratigraphic equivalent to the Upper Critical Zone - Main Zone transition of the Bushveld Complex, unless the ultramafic lens was tectonically adjoined to the Morgan Range. The lens does have some potential to host a PGE reef analogous to Wingellina Hills. In contrast, the Cavenagh, Michael Hills, Latitude Hill, Hinckley Range, Murray Range, Lehman Hills, and Mt Muir intrusions have lower PGE prospectivity as they appear to be stratigraphic equivalents of the Bushveld Main Zone, sharing intermediate compositions and relatively subdued layering.

The Mantamaru intrusion is stratigraphically approximately equivalent to the upper Main Zone and Upper Zone of the Bushveld Complex. Both intrusions contain several magnetite layers (~25 in the Bushveld, at least 11 at Jameson) that can reach a thickness of more than 10 m (i.e., layer 1 at Jameson, magnetite layer 21 in Bushveld). In addition, in both intrusions the vanadium concentration progressively decreases from the basal to the upper magnetite layers (Fig. 19), and also within individual layers. However, the vanadium contents of the Bushveld Main Magnetite Layer are twice as high as those at Jameson (13000 vs 7500 ppm). Other differences between the two intrusions include significantly higher PGE contents in the Jameson basal magnetite seam and the apparent absence of an apatite-rich layer at Jameson.

8.7. Tectonic setting

The Musgrave Province is located between the lithospheric keels of the West Australian, South Australian, and North Australian Cratons. Channeling of mantle plumes along the cratonic keels could have resulted in strong adiabatic mantle partial melting and mafic magmatism (Begg et al.,

2009). However, Smithies et al. (2012) argued that the >200Ma time span of continuing mantle magmatism and UHT metamorphism is inconsistent with a mantle plume. The Musgrave Province instead represented a stationary zone of mantle upwelling, resulting in a persisting hot zone. Magmatism may have been driven by processes such as plate motions, lithospheric delamination, volatile transfer from the SCLM or the crust to the convecting mantle, or mantle flow along the irregular base of the lithosphere (Silver et al., 2006). Similar scenarios were envisaged by Silver et al., (2006) and Foulger (2010) for the Ventersdorp, Great Dyke, Bushveld, and Soutpansberg continental magmatic events in southern Africa.

The stage was set during and after the 1345–1293 Ma Mount West Orogeny which resulted in crustal thickening, partial melting, and densification of lower crust. The REE geochemistry of Musgrave granites suggests that at the beginning of the 1220–1150 Ma Musgrave Orogeny the depth of crustal melting changed from relatively deep to shallow, caused by delamination of residual lower crust and the underlying lithospheric mantle. The ensuing UHT metamorphism from 1220 to 1120 Ma testifies to a sustained regime of highly thinned crust and mantle lithosphere. Any magmatism was predominantly felsic because the lower crust had become a zone of melting, assimilation, storage, and homogenization (MASH), inhibiting ascent of relatively dense mafic magmas. This crustal thermal structure strongly influenced conditions at the beginning of the Giles Event (Smithies et al., 2015, in press). The latter was triggered by far-field forces acting on the margins of the West Australian Craton (Evins et al., 2010b; Smithies et al., 2015, in press). Initial subsidence and deposition of the Kunmarnara Group was followed by draining of melts ponded at the base of the crust (G1, G2, Alcurra Dolerite suite). The relatively early G1 and G2 magmas were variably contaminated during ascent into the crust (Fig. 24). Subsequent magmas of the Alcurra Dolerite suite underwent relatively little contamination suggesting that the crust had become more refractory. At the same time, the Alcurra magmas are more differentiated because the crust

thickened during the Giles event, allowing more intra-crustal ponding and fractional crystallization. The relatively low PGE concentrations, high Cu/Pd, Pt/Pd, and Au/PGE ratios of the Alcurra magmas could be explained by melting of hybrid crust-rich mantle, in response to foundering of crust and new SCLM (Fig. 24a).

8.8. Origin of mineralization

8.8.1. PGE reefs within the Wingellina Hills layered intrusion

The bulk of the world's PGE resources occur in the form of stratiform layers or so-called reefs hosted by layered mafic-ultramafic intrusions. Economic deposits are presently confined to just three intrusions, namely the Bushveld Complex of South Africa, the Stillwater Complex in Montana, USA, and the Great Dyke of Zimbabwe, but sub-economic deposits that may be mined in the future occur in many other intrusions. The reefs consist of relatively narrow (<1-2m), but laterally extensive layers of ultramafic or mafic rocks that typically contain <1-3 % sulfides. The host intrusions are relatively sulfur poor, and most reefs show mantle-like sulfur isotopic signatures (Liebenberg, 1970; Li et al., 2008) suggesting that saturation of the magma in sulfide melt was reached due to fractionation rather than contamination. At least in the case of the Bushveld Complex, mixing between compositionally different magmas was probably not instrumental in reef formation because the magmas were highly sulfur undersaturated (Barnes et al., 2010). The concentration of the sulfides to form the reefs was possibly aided by hydrodynamic cumulate sorting in response to syn-magmatic subsidence of the intrusions (Maier et al., 2013b).

The main PGE reef of the Wingellina Hills intrusion shows certain similarities to the Great Dyke and Munni Munni PGE reefs, including the stratiform nature, the stratigraphic position towards the top of the ultramafic zone of the intrusion (Fig. 25), and the offset stratigraphic positions of the various chalcophile elements. The bulk PGE content in the Wingellina Hills reef is

in the same range as that in the Main Sulfide Zone of the Great Dyke. In both intrusions, there is no marked variation in trace element ratios across the reef (unpublished data of Maier). The origin of the Wingellina Hills main PGE reef can be explained by a model of sulfide saturation from fractionating NB1-type magma. The intrusion features several additional layers of PGE enrichment above the main PGE reef, but these have not been studied by us. They could reflect magma replenishments to the chamber, as the resident magma was likely relatively PGE depleted after the formation of the main reef.

The low PGE grade of the Wingellina Hills PGE reef relative to the Bushveld and Great Dyke reefs could reflect less-efficient metal concentration due to faster cooling rates in the relatively small Wingellina Hills intrusion, whereas the low sulfide contents may reflect metamorphic sulfur loss, consistent with sub-cotectic sulfide proportions in most Wingellina Hills rocks.

8.8.2. Cu–Ni–PGE–Au mineralization at Halleys

Reef-style PGE–Cu–Au mineralization is typical of the upper portions of many layered intrusions (Maier, 2005). The enrichment of magnetite together with sulfide at the Halleys prospect could thus suggest that the Halleys intrusive body represents the evolved portion of an adjacent large layered intrusion, possibly the Blackstone Range of the Mantamaru intrusion, the Cavanagh Range, or the Saturn intrusion. A petrogenetic link to Blackstone and Cavenagh is presently considered unlikely as Halleys has much higher gold and sulfur concentrations as well as mica contents than Blackstone and Cavenagh. Furthermore, field relationships indicate that Halleys crosscuts the southern segment of the Blackstone Range. A petrogenetic relationship between Halleys and the Saturn intrusion is more plausible as both share the compositional features of the Alcurra Dolerite suite. However, a direct connection between Halleys and Saturn is inconsistent with the distinct magnetic signature of the intrusions.

An alternative model could be that the Halleys mineralization represents contact-style mineralization at the base or sidewall of a layered intrusion analogous to, e.g., the Platreef of the Bushveld Complex or the Suhanko deposit of the Portimo Complex, Finland. These deposits are considered to have formed through sulfide liquid saturation in response to fractional crystallization accompanied by floor contamination. The proximity of the floor and the resulting high cooling rate of the magma produced wide, disseminated mineralization rather than narrow reefs. Sulfides at Halleys have $\delta^{34}S$ of –0.9, providing little added constraints on the nature of the sulfur source. More work is clearly required to further constrain the petrogenesis of the intrusion and its mineralization.

8.8.3. Vanadium and PGE mineralization in magnetite seams of the Jameson Range, Mantamaru intrusion

Advanced fractional crystallization of basaltic magmas leads to cotectic crystallization of magnetite with silicates, resulting in magnetite-bearing gabbroic and dioritic rocks. The formation of massive oxide layers requires that magnetite is effectively separated from the silicate minerals as the cotectic proportions of magnetite and silicates are between 5 and 30% (Toplis and Carroll, 1996). The mechanism of oxide fractionation has been debated for decades. One of the main problems has been to explain the knife-sharp contacts of many magnetite layers, requiring extremely effective separation of oxide crystals from silicate magma. The many structural similarities between layered cumulates and certain types of sedimentary rocks has led Irvine et al. (1998) to propose a mechanism of density currents sweeping down along the walls of magma chambers. Maier et al. (2013b) rejected this model for the Bushveld Complex because density currents would not preserve the abundant, highly elongated, sub-horizontally oriented anorthosite autoliths within many oxide seams. The authors instead suggested that oxide-silicate slurries were

mobilized and sorted during subsidence of the Bushveld chamber. This process would be less turbulent and may preserve some of the compositional layering of the cumulates. The slurries could be injected into the semi-consolidated crystal pile, and locally form transgressive pipes.

Other models for the formation of the oxide seams proposed in the past include shifts in phase stability fields of oxides caused by changes in pressure (Cameron, 1980; Lipin, 1993), temporary supersaturation in magnetite triggered by an increase in the oxygen fugacity of the magma in response to contamination (Ulmer, 1969), or a combination of magma mixing, pressure change, and oxidation in response to magma replenishment. However, one of the most popular models for the formation of massive magnetite layers remains iron oxide liquid immiscibility, originally advanced by Philpotts (1967). Experiments have produced immiscible iron oxide liquids in silicate liquids (Freestone, 1978; Roedder, 1978; Naslund, 1983), but whether the silicate melts used in the experiments are good analogues to natural magmas remains debated. Toplis and Carrol (1995, 1996) and Tollari et al. (2006, 2008) showed that using silicate melt compositions close to natural basalts and diorites, magnetite or ilmenite crystallize before the magmas become saturated with iron oxide liquid.

The potential for apatite deposits in the Giles intrusions remains unknown. Most of the samples analysed here are apatite free, although Traka Resources (2013) found somewhat elevated phosphorus concentrations (up to 250 ppm P) in seam 5 of the Jameson intrusion. Anglo American intersected elevated phosphorus concentrations (up to 8000 ppm P) in magnetite-rich rocks to the south of the Bell Rock intrusion, suggesting there could be apatite potential in unexposed magnetite seams. Minor amounts of apatite were also described from Kalka (Goode, 2002). Based on analogy with the Bushveld Complex where nelsonite forms the uppermost of the magnetite seams, the target horizon for apatite rich layers is at the very top of the intrusions.

8.8.4. Nebo–Babel Ni–Cu deposit

Analogous to most other significant Ni-Cu deposits globally, Nebo–Babel is hosted by a tubular (chonolithic) body interpreted as a magma feeder conduit (Seat et al., 2007, 2009). The chilled margin contains sulfides, which led Seat et al. (2007) to propose that some of the magmas entrained sulfide liquid. The authors argued that the concentration of the entrained sulfides was in part controlled by changes in magma flow velocity, in turn related to changes in the shape of the conduit. However, in contrast to many other deposits elsewhere that are interpreted to have formed by addition of external sulfur to the magma, sulfide liquid saturation in the Nebo–Babel conduit was interpreted to have been triggered by magma mixing (of Alcurra-type magma with NB1-type magma) and contamination with orthogneiss, i.e. without addition of external sulfur (Seat et al., 2007; Godel et al., 2011). The orthomagmatic model is feasible in terms of sulfur mass balance: extracting 100 ppm S from 1 km^3 of magma can produce a massive sulfide lens 1 km long, 10 m high, and 20 m wide. However, orthomagmatic derivation of the Nebo Babel sulfides would require an extremely effective concentration mechanism as the cotectic proportion of sulfide precipitating from sulfur-saturated troctolitic–gabbronoritic magma is very small (perhaps as little as 0.1 wt%).

Seat et al. (2007) based their model on the observation that the sulfides at Nebo Babel have mantle-like sulfur isotopic compositions, and that the rocks of the Pitjantjatjara Supersuite, which forms the immediate country rock to the deposit, tend to be sulfur-poor. However, mapping by GSWA has revealed that the Pitjantjatjara granites are only a very minor lithological component within this part of the Mamutjarra Zone. More abundant are rocks of the Wirku Metamorphics, Winburn Granite, and Bentley Supergroup. Amongst these, the Winburn Granite and volcanic and volcaniclastic rocks of the Bentley Supergroup typically contain visible pyrite and can locally be sulfide-rich, with up to 3000 ppm S in some samples of ignimbrite and rhyolite (see also Fig. 79 in

1304 Howard et al., 2011, showing sulfide enrichment in drill hole WA02, Strzelecki Metals). The
1305 chamber system required for the Bentley volcanics must have been enormous - and even at the current
1306 level of exposure, Nebo Babel is located only ~ 1km north of unexposed (i.e., interpreted) areas of Bentley
1307 volcanics, and ~ 7 km east of the Winburn granite with is part of the felsic chamber system. It is possible
1308 that at a slightly deeper level, the NB magmas may have intruded into the Bentley volcanic system.
1309 Deposition of the lower portion of the Bentley Supersuite (the Mount Palgrave Group and
1310 much of the Kaarnka Group), pre-dates intrusion of the Nebo–Babel gabbro (Smithies et al., 2013).
1311 The presently available sulfur isotopic data for the units of the Bentley Supergroup indicate a
1312 range of compositions, with those from the lower part having $\delta^{34}S$ between +1.8 and +7,
1313 potentially representing a suitable external sulfur source for the Nebo–Babel deposit. We thus
1314 argue that addition of external sulfur to the Nebo–Babel magma remains a possibility. The
1315 contamination model would be consistent with the relatively high Cu/Pd and Cu/Ni ratios (possibly
1316 reflecting addition of crustal Cu) and high Au/Pd ratios (possibly due to addition of crustal Au) (see
1317 data of Seat et al., 2007).
1318 The question arises as to why only one major Ni–Cu deposit has so far been found in the
1319 Musgrave Province. Mineral deposits tend to form clusters, suggesting that more Ni-Cu deposits
1320 should occur in the Musgrave Province. Exploration during the last decade has identified several
1321 low-grade deposits (Halleys, Manchego, Succoth) suggesting the true potential of the west
1322 Musgrave Province for Ni–Cu sulfide deposits remains unrealized.
1323

1324 **9. Conclusions**

1325 The Musgrave Province was the focus of long-lived mantle upwelling producing large volumes of
1326 magnesian basaltic to tholeiitic magma and their felsic derivatives. Magmatism led to crustal
1327 melting, lithospheric delamination, and a high crustal heat flux over >200 m.y. The Province

contains one of the greatest concentrations of mafic-ultramafic layered intrusions globally, amongst them Mantamaru which is one of the world's largest layered intrusions. These data illustrate that large layered intrusions are not confined to cratons. What is required is a stable tectonic environment where magmas can ascend in locally extensional, possibly transpressional zones allowing the formation of thick sill-like bodies.

Due to the large size of the Giles intrusions, cooling rates were relatively slow. This led to crustal loading, subsidence of magma chambers, and sagging of cumulates prior to complete solidification. The mobilized cumulates unmixed and formed lenses and layers of peridotite and magnetitite that are locally enriched in PGE. Syn- to post-magmatic tectonism led to fragmentation of many of the intrusions. The degree of crustal contamination was mostly relatively minor (<5%), although locally, basaltic magmas mingled with coeval granitic magmas. The mineralization potential of the Giles intrusions and their host rocks is considerable. Large magmatic events, particularly those dominated by mafic-ultramafic magmas may cause increased heat flux into the crust, triggering crustal melting, devolatization, and large-scale fluid flow. Deposit types favored by such regimes include magmatic PGE–Cr–V-Fe–P deposits in large layered intrusions, Ni–Cu sulfide deposits in magma feeder conduits or at the base of layered intrusions, and hydrothermal deposits of variable style, notably in the roof and sidewalls of the largest intrusions.

10. Acknowledgements

Much of the work documented here arose through a regional-scale geological mapping project jointly coordinated through the Ngaanyatjarra Council and the Geological Survey of Western Australia (GSWA), and guided by the local Indigenous people in the region between the

communities of Wingellina and Warburton. The authors thank GSWA for permission to publish the data. Richard Ernst and Steve Barnes are thanked for their constructive reviews.

References

Ahmat A. L. 1986. Petrology, structure, regional geology and age of the gabbroic Windimurra complex, Western Australia. PhD thesis, University of Western Australia, Perth (unpubl.).

Aitken, AR, Dentith, MC, Evans, SF, Gallardo, LA, Joly, A, Thiel, S, Smithies, RH and Tyler, IM 2013, Imaging crustal structure in the west Musgrave Province from magnetotelluric and potential field data: Geological Survey of Western Australia, Report 114, 81p.

Ballhaus, C and Berry, RF 1991, Crystallization pressure and cooling history of the Giles Layered Igneous Complex, central Australia: Journal of Petrology, v. 32, p. 1–28.

Ballhaus, C and Glikson, AY 1989, Magma mixing and intraplutonic quenching in the Wingellina Hills intrusion, Giles Complex, central Australia: Journal of Petrology, v. 30, p. 1443–1469.

Ballhaus, C and Glikson, AY 1995, The petrology of layered mafic-ultramafic intrusions in the Giles Complex, western Musgrave block, central Australia: AGSO Journal, v. 16, p. 69–89.

Barnes, SJ 1993, Partitioning of the PGE and gold between silicate and sulphide magmas in the Munni Munni Complex, Western Australia: Geochimica et Cosmochimica Acta, v. 57, p. 1277–1290.

Barnes, S-J and Maier, WD 1999, The fractionation of Ni, Cu and the noble metals in silicate and sulphide liquids, in Dynamic processes in magmatic ore deposits and their application to mineral

exploration edited by RR Keays, CM Lesher, PC Lightfoot, and CEG Farrow: Geological Association of Canada; Short Course Notes 13, p. 69–106.

Barnes, S-J, Maier, WD and Curl, E 2010, Composition of the marginal rocks and sills of the Rustenburg Layered Suite, Bushveld Complex, South Africa: implications for the formation of the PGE deposits: Economic Geology, v. 105, p.1491–1511.

Becker, H, Horan, MF, Walker, RJ, Gao, S, Lorand J-P and Rudnick, RL 2006, Highly siderophile element composition of the Earth's primitive mantle: constraints from new data on peridotite massifs and xenoliths: Geochimica et Cosmochimica Acta, v. 70, p. 4528–4550.

Begg, GC, Griffin, WL, Natapov, LM, O'Reilly, SY, Grand, SP, O'Neill, CJ, Hronsky, JMA, Poudjom Djomani, Y, Swain, CJ, Deen, T and Bowden, P 2009, The lithospheric architecture of Africa: seismic tomography, mantle petrology, and tectonic evolution: Geosphere, v. 5, p. 23–50.

Bodorkos, S, and Wingate, MTD 2008a, 174594: metamorphosed leucogabbro, Mirturtu Camp; Geochronology Record 716: Geological Survey of Western Australia, 4p.

Bodorkos, S and Wingate, MTD 2008b, 174589: quartz syenite dyke, Amy Giles Hill; Geochronology Record 715: Geological Survey of Western Australia, 4p.

Bodorkos, S, Wingate, MTD and Kirkland, CL 2008a, 174538: metamonzogranite, Mount Daisy Bates; Geochronology Record 712: Geological Survey of Western Australia, 4p.

Bodorkos, S, Wingate, MTD and Kirkland, CL 2008b, 174558: metamorphosed quartz diorite, Mount Fanny; Geochronology Record 713: Geological Survey of Western Australia, 4p.

Bodorkos, S, Wingate, MTD and Kirkland, CL 2008c, 174736: granofelsic metasyenogranite, Mount Fanny; Geochronology Record 717: Geological Survey of Western Australia, 4p.

1392 Bodorkos, S, Wingate, MTD and Kirkland, CL 2008d, 174737: foliated metamonzogranite, Mount
1393 Fanny; Geochronology Record 718: Geological Survey of Western Australia, 5p.

1394 Bodorkos, S, Wingate, MTD and Kirkland, CL 2008e, 174747: metagabbro, Mount Fanny;
1395 Geochronology Record 719: Geological Survey of Western Australia, 4p.

1396 Boudreau, AE 1999, PELE–a version of the MELTS software programme for the PC platform:
1397 Computers and Geosciences, v. 25, p. 201–203.

1398 Cameron, EN 1980, Evolution of the Lower Critical Zone, central sector, eastern Bushveld Complex:
1399 Economic Geology, v. 75, p. 845–871.

1400 Campbell, IH and Naldrett, AJ 1979, The influence of silicate : sulfide ratios on the geochemistry of
1401 magmatic sulfides: Economic Geology, v. 74, p. 1503–1505.

1402 Cawood, PA and Korsch RJ 2008, Assembling Australia: Proterozoic building of a continent.
1403 Precambrian Research, v 166, p. 1-38.

1404 Clarke, GL, Buick, IS, Glikson, AY and Stewart, AJ 1995b, Structural and pressure-temperature
1405 evolution of host rocks of the Giles Complex, western Musgrave Block, central Australia: evidence
1406 for multiple high-pressure events: AGSO Journal of Australian Geology and Geophysics, v. 16, p
1407 127–146.

1408 Clarke, GL, Sun, S-S and White, RW 1995a, Grenville age belts and associated older terranes in
1409 Australia and Antarctica: AGSO Journal of Australian Geology and Geophysics, v. 16, p. 25–39.

1410 Coleman, P 2009, Intracontinental orogenesis in the heart of Australia: structure, provenance and
1411 tectonic significance of the Bentley Supergroup, western Musgrave Block, Western Australia:
1412 Geological Survey of Western Australia, Record 2009/23, 48p.

1413 Daniels, JL 1974, The Geology of the Blackstone region, Western Australia: Geological Survey of
1414 Western Australia, Bulletin 123, 257p.

1415 Edgoose, CJ, Scrimgeour, IR and Close, DF 2004, Geology of the Musgrave Block, Northern
1416 Territory: Northern Territory Geological Survey, Report 15, 48p.

1417 Eggins, SM, Woodhead, JD, Kinsley, LPJ, Mortimer, GE, Sylvester, P, McCulloch, MT, Hergt, JM and
1418 Handler, MR 1997, A simple method for the precise determination of >40 trace elements in
1419 geological samples by ICPMS using enriched isotope internal standardisation: Chemical Geology, v.
1420 134, p. 311–326.

1421 Evins, PM, Smithies, RH, Howard, HM, Kirkland, CL, Wingate, MTD and Bodorkos, S 2010a,
1422 Redefining the Giles Event within the setting of the 1120–1020 Ma Ngaanyatjarra Rift, west
1423 Musgrave Province, Central Australia: Geological Survey of Western Australia, Record 2010/6, 36p.

1424 Evins, PM, Smithies, RH, Howard, HM, Kirkland, CL, Wingate, MTD and Bodorkos, S 2010b, Devil in
1425 the detail: the 1150–1000 Ma magmatic and structural evolution of the Ngaanyatjarra Rift, west
1426 Musgrave Province, Central Australia: Precambrian Research, v. 183, p. 572–588.

1427 Evins, PM, Smithies, RH, Howard, HM and Maier, WD 2009, Holt, WA Sheet 4546: Geological
1428 Survey of Western Australia, 1:100 000 Geological Series.

1429 Foulger, GR 2010, Plates vs plumes: Wiley-Blackwell, Chichester, 328p.

1430 Freestone, IC 1978, Liquid immiscibility in alkali-rich magmas: Chemical Geology, v. 23, p. 116–123.

1431 Gale A, Dalton CA, Langmuir CH, Su Y, Schilling J-G (2013) The mean composition of ocean ridge
1432 basalts. Geochemistry, geophysics, geosystems, Volume 14, Number 3,
1433 doi:10.1029/2012GC004334

Glikson, AY (editor) 1995, The Giles mafic-ultramafic complex and environs, western Musgrave Block, central Australia: Thematic issue: AGSO Journal of Geology and Geophysics, v. 16, no. 1–2, 193p.

Glikson, AY, Stewart, AT, Ballhaus, GL, Clarke, GL, Feeken, EHT, Level, JH, Sheraton, JW and Sun, S-S 1996, Geology of the western Musgrave Block, central Australia, with reference to the mafic-ultramafic Giles Complex: Australian Geological Survey Organisation, Bulletin 239, 206p.

Godel, B, Seat, Z, Maier, WD and Barnes, S-J 2011, The Nebo–Babel Ni-Cu-PGE sulfide deposit (West Musgrave Block, Australia): part 2 — constraints on parental magma and processes, with implications for mineral exploration: Economic Geology, v. 106, p. 557–584.

Goode, ADT 1970, The petrology and structure of the Kalka and Ewarara layered basic intrusions, Giles Complex, central Australia: The University of Adelaide, Adelaide, PhD thesis (unpublished).

Goode, ADT 1976a, Small scale primary cumulus igneous layering in the Kalka layered intrusion, Giles Complex, central Australia: Journal of Petrology, v. 17, p. 379–397.

Goode, ADT 1976b, Sedimentary structures and magma current velocities in the Kalka layered intrusion, central Australia: Journal of Petrology, v. 17, p. 546–558.

Goode, ADT 1977a, Vertical igneous layering in the Ewarara layered intrusion, central Australia: Geological Magazine, v. 114, p. 215–218.

Goode, ADT 1977b, Flotation and remelting of plagioclase in the Kalka Intrusion, central Australia: petrological implications for anorthosite genesis: Earth and Planetary Science Letters, v. 34, p. 375–380.

1455 Goode, ADT 1977c, Intercumulus igneous layering in the Kalka layered intrusion, central Australia:
1456 Geological Magazine, v. 114, p. 215–218.

1457 Goode, ADT 1978, High temperature, high strain rate deformation in the lower crustal Kalka
1458 Intrusion, central Australia: Contributions to Mineralogy and Petrology, v. 66, p. 137–148.

1459 Goode, ADT 2002, The Western Musgrave Block – Australia: Data Metallogenica, District Overview.
1460 42p.

1461 Goode, ADT and Krieg, GW 1967, The geology of Ewarara Intrusion, Giles Complex, central
1462 Australia: Journal of the Geological Society of Australia, v. 14, p. 185–194.

1463 Goode, ADT and Moore, AC 1975, High pressure crystallisation of the Ewarara, Kalka and Gosse
1464 Pile intrusions, Giles Complex, central Australia: Contributions to Mineralogy and Petrology, v. 51,
1465 p. 77–97.

1466 Gray, CM 1971, Strontium isotope studies on granulites: The Australian National University,
1467 Canberra, PhD thesis (unpublished), 242p.

1468 Gray, CM, Cliff, RA and Goode, ADT, 1981, Neodymium–strontium isotopic evidence for extreme
1469 contamination in a layered basic intrusion: Earth and Planetary Science Letters, v. 56, p. 189–198.

1470 Gray, CM and Goode, ADT 1989, The Kalka layered intrusion, central Australia: a strontium isotopic
1471 history of contamination and magma dynamics: Contributions to Mineralogy and Petrology, v. 103,
1472 p. 35–43.

1473 Howard, HM, Smithies, RH, Kirkland, CL, Evins, PM and Wingate, MTD 2009, Age and geochemistry
1474 of the Alcurra Suite in the west Musgrave Province and implications for orthomagmatic Ni-Cu-PGE

1475 mineralization during the Giles Event: Geological Survey of Western Australia, Record 2009/16,
1476 16pp.

1477 Howard, HM, Smithies, RH and Pirajno F, 2006b, Geochemical and Nd isotopic signatures of mafic
1478 dykes in the western Musgrave Complex: Geological Survey of Western Australia Annual Review
1479 2005–06, p. 64–71.

1480 Howard, HM, Smithies, RH, Pirajno, F and Skwarnecki, MS 2006a, Bates, WA Sheet 4646:
1481 Geological Survey of Western Australia, 1:100 000 Geological Series.

1482 Howard, HM, Smithies, RH, Pirajno, F and Skwarnecki, MS 2007, Bell Rock, WA Sheet 4645:
1483 Geological Survey of Western Australia, 1:100 000 Geological Series.

1484 Howard, HM, Smithies, RH, Werner, M, Kirkland, CL and Wingate, MTD 2011a, Geochemical
1485 characteristics of the Alcurra Dolerite (Giles Event) and its extrusive equivalents in the Bentley
1486 Supergroup: Geological Survey of Western Australia, Record 2011/2, p. 27–30.

1487 Howard, HM, Werner, M, Smithies, RH, Kirkland, CL, Kelsey, DL, Hand, M, Collins, A, Pirajno, F,
1488 Wingate, MTD, Maier, WD and Raimondo, T 2011b, The geology of the west Musgrave Province
1489 and the Bentley Supergroup — a field guide: Geological Survey of Western Australia, Record
1490 2011/4, 119p.

1491 Howard HM, Smithies RH, Kirkland CL, Kelsey DE, Aitken A, Wingate MTD, Quentin de
1492 Gromard R, Spaggiari CV, Maier, WD 2015, The burning heart — The Proterozoic geology and
1493 geological evolution of the west Musgrave Region, central Australia, Gondwana Research, 27, 64-
1494 94

1495 Irvine, TN 1970, Crystallization sequences in magmas of the Muskox intrusion and some other
1496 layered intrusions: Geological Society of South Africa, Special Publication 1, p. 441–476.

1497 Irvine, TN, Andersen, JCO and Brooks, CK 1998, Included blocks (and blocks within blocks) in the
1498 Skaergaard Intrusion: Geological relations and the origins of rhythmic modally graded layers:
1499 Geological Society of America, Bulletin 110, p. 1398–1447.

1500 Kelsey, DE, Hand, M, Evins, P, Clark, C and Smithies, H 2009, High temperature, high geothermal
1501 gradient metamorphism in the Musgrave Province, central Australia: potential constraints on
1502 tectonic setting, in Biennial conference of the Specialist Group for Geochemistry, Mineralogy and
1503 Petrology, Kangaroo Island November 2009 edited by NE Timms, J Foden, K Evans and C Clark:
1504 Geological Society of Australia Abstracts No. 96, p. 28.

1505 Kelsey, DE, Hand, M, Smithies, H, Evins, P, Clark, C and Kirkland, CL 2010, What is the tectonic
1506 setting of long-lived Grenvillian-aged ultrahigh temperature, high geothermal gradient
1507 metamorphism in the Musgrave Province, central Australia?: Geological Society of America,
1508 Abstracts with Programs, 42(5), p. 516.

1509 King, RJ 2008, Using calculated pseudosections in the system NCKFMASHTO and SHRIMP II U–Pb
1510 zircon dating to constrain the metamorphic evolution of paragneisses in the Latitude Hills, West
1511 Musgrave Province, Western Australia: Geological Survey of Western Australia, Record 2009/15,
1512 67p.

1513 Kirkland, CL, Wingate, MTD and Bodorkos, S 2008a, 183496: orthogneiss, Mount West;
1514 Geochronology Record 747: Geological Survey of Western Australia, 5p.

1515 Kirkland, CL, Wingate, MTD and Bodorkos, S 2008b, 183459: charnockite, Latitude Hill,
1516 Geochronology Record 722: Geological Survey of Western Australia, 5p.

1517 Kirkland, CL, Wingate, MTD and Bodorkos, S 2008c, 183509: leucogranite dyke, Mount West;
1518 Geochronology Record 724: Geological Survey of Western Australia, 4p.

Kirkland, CL, Wingate, MTD and Bodorkos, S 2008d, 193850: leucogranite dyke, Mount Fanny; Geochronology Record 748: Geological Survey of Western Australia, 4p.

Kirkland, CL, Wingate, MTD and Bodorkos, S 2008e, 174761: porphyritic granite dyke, Bell Rock; Geochronology Record 721: Geological Survey of Western Australia, 4p.

Kirkland, CL, Wingate, MTD and Bodorkos, S 2008f, 185509: leucogranite, Mount Aloysius; Geochronology Record 725: Geological Survey of Western Australia, 4p.

Kirkland, CL, Wingate, MTD and Smithies, RH 2011, 194762: leucogabbro, Mount Finlayson; Geochronology Record 966: Geological Survey of Western Australia, 4p.

Kirkland, CL, Smithies, RH, Woodhouse, AJ, Howard, HM, Wingate, MTD, Belousova, EA, Cliff, JB, Murphy, RC and Spaggiari, CV 2013, Constraints and deception in the isotopic record; the crustal evolution of the west Musgrave Province, central Australia: Gondwana Research, v. 23, p. 759–781.

Latypov R, Hanski E, Lavrenchuk A, Huhma H, and Havela T 2011, A 'Three-Increase Model' for the Origin of the Marginal Reversal of the Koitelainen Layered Intrusion, Finland. Journal of Petrology, v. 52, p. 733-764.

Lesher, CM and Burnham, OM 2001, Multicomponent elemental and isotopic mixing in Ni–Cu–(PGE) ores at Kambalda, Western Australia: Canadian Mineralogist, v. 39, p. 421–446.

Li, ZX 2000, Palaeomagnetic evidence for unification of the North and West Australian craton by ca. 1.7 Ga: new results from the Kimberley Basin of northwestern Australia: Geophysical Journal International, v. 142, p. 173-180.

1539 Li, C and Ripley, EM 2010, The relative effects of composition and temperature on olivine-liquid
1540 partitioning: statistical deconvolution and implications for petrologic modelling: Chemical Geology,
1541 v. 275, p. 95–104.

1542 Li, C, Ripley, EM, Oberthür, T, Miller, JD Jr and Joslin, GD 2008, Textural, mineralogical and stable
1543 isotope studies of hydrothermal alteration in the main sulfide zone of the Great Dyke, Zimbabwe
1544 and the precious metals zone of the Sonju Lake Intrusion, Minnesota, USA: Mineralium Deposita,
1545 v. 43, p. 97–110.

1546 Liebenberg, L 1970, The sulfides in the layered sequence of the Bushveld igneous Complex:
1547 Geological Society of South Africa, Special Publication, v. 1, p. 108–208.

1548 Lightfoot, PC and Naldrett, AJ 1983, The geology of the Tabankulu section of the Insizwa Complex,
1549 Transkei, Southern Africa, with reference to the nickel sulphide potential: Transactions of the
1550 Geological Society of South Africa, v. 86, p. 169–187.

1551 Lipin, BR 1993, Pressure increases, the formation of chromite seams, and the development of the
1552 Ultramafic series in the Stillwater Complex, Montana: Journal of Petrology, v. 34, p. 955–976.

1553 Maier, WD 2005, Platinum-group element (PGE) deposits and occurrences: mineralization styles,
1554 genetic concepts and exploration criteria: Journal of African Earth Sciences, v. 41, p. 165–191.

1555 Maier, WD, Barnes, SJ, Gartz, V and Andrews, G 2003b, Pt–Pd reefs in magnetitites of the Stella
1556 layered intrusion, South Africa: a world of new exploration opportunities for platinum group
1557 elements: Geology, v. 31, p. 885–888.

1558 Maier, WD, Barnes, S-J and Groves, DI 2013b, The Bushveld Complex, South Africa: Formation of
1559 platinum–palladium, chrome and vanadium- rich layers via hydrodynamic sorting of a mobilized

cumulate slurry in a large, relatively slowly cooling, subsiding magma chamber: Mineralium Deposita, v. 48, p. 1–56.

Maier, WD and Eales, HV 1997, Correlation within the UG2 – Merensky Reef interval of the Western Bushveld Complex, based on geochemical, mineralogical and petrological data. Geological Survey of South Africa, Bulletin 120, 56p.

Maier, WD, Rasmussen, B, Li, C, Barnes, S-J and Huhma, H 2013a, The Kunene anorthosite complex, Namibia, and its satellite bodies: geochemistry, geochronology and economic potential: Economic Geology, v. 108, p. 953–986.

Metals X Ltd 2013, Globally significant nickel project, viewed 8 April 2014, <http://www.metalsx.com.au/system/assets/26/original/Nickel_Division.pdf>.

Morris, PA and Pirajno, F 2005, Geology, geochemistry, and mineralization potential of Mesoproterozoic sill complexes of the Bangemall Supergroup, Western Australia: Geological Survey of Western Australia of Western Australia, Report 99, 72p.

Morse, SA 1981, Kiglapait geochemistry IV: the major elements: Geochimica et Cosmochimica Acta, v. 45, p. 461–479.

Naldrett, AJ and Lehmann, J 1988, Spinel nonstoichiometry as the explanation for Ni-, Cu-, and PGE-enriched sulphides in chromitites, in Geo–Platinum 87 edited by HM Prichard et al.: Elsevier, Barking, p. 93–109.

Naslund, HR 1983, The effect of oxygen fugacity on liquid immiscibility in iron-bearing silicate melts: American Journal of Science, v. 283, p. 1034–1059.

1580 Nesbitt, RW, Goode, ADT, Moore, AC and Hopwood, TP 1970, The Giles Complex, central Australia:
1581 a stratified sequence of mafic and ultramafic intrusions: Special Publications of the Geological
1582 Society of South Africa, v. 1, p. 547–564.

1583 Nesbitt, RW and Talbot, JL 1966, The layered basic and ultrabasic intrusives of the Giles Complex,
1584 central Australia: Contributions to Mineralogy and Petrology, v. 13, p. 1–11.

1585 Norrish, K and Chappell, BW 1977, X-ray fluorescence spectrometry, in Physical Methods in
1586 Determinative Mineralogy, 2nd Edition edited by J Zussman: Academic Press, London, p. 201–272.

1587 Pascoe, A 2012, The geochemistry and petrogenesis of the mafic and ultramafic giles intrusions at
1588 Latitude Hill, west Musgrave Province, Western Australia: The University of Tasmania, Hobart, BSc
1589 Honours thesis (unpublished).

1590 Patino Douce, A.E. & Beard, J.S. (1995). Dehydration-melting of Biotite Gneiss and Quartz
1591 Amphibolite from 3 to 15 kbar. Journal of Petrology v. 36, 707-738.

1592 Philpotts, AR 1967, Origin of certain iron–titanium oxide and apatite rocks: Economic Geology, v.
1593 62, p. 303–315.

1594 Phosphate Australia Ltd 2014, Manchego Prospect: Musgrave Project, Western Australia, viewed 6
1595 May 2014, at <http://www.asx.com.au/asxpdf/20140103/pdf/42lz643zrngqwx.pdf>.

1596 Raedeke, LD 1982, Petrogenesis of the Stillwater Complex: The University of Washington, Seattle,
1597 PhD thesis (unpublished).

1598 Redstone Resources Ltd 2008a, Quarterly report for the period ending June 30th 2008, viewed 6
1599 May 2014, at
1600 <http://www.redstone.com.au/investor_centre_asx_announcements_files/2008_07_31_01.pdf>.

1601 Redstone Resources Ltd 2008b, Report of the Annual General Meeting, viewed 8 April 2014, at
1602 <http://www.asx.com.au/asxpdf/20081127/pdf/31dvzvjbkp7f5b.pdf>.

1603 Reynolds, IM 1985, The nature and origin of titaniferous magnetite-rich layers in the Upper Zone
1604 of the Bushveld Complex: a review and synthesis: Economic Geology, v. 80, p. 1089–1108.

1605 Rollinson HR (2013) Using geochemical data: evaluation, presentation, interpretation, Routledge,
1606 Oxon, UK.

1607 Scrimgeour, IR and Close, DF 1999, Regional high pressure metamorphism during intracratonic
1608 deformation: the Petermann orogeny, central Australia: Journal of Metamorphic Geology, v. 17, p.
1609 557–572.

1610 Seat, Z 2008, Geology, petrology, mineral and whole-rock chemistry, stable and radiogenic isotope
1611 systematics and Ni–Cu–PGE mineralisation of the Nebo–Babel intrusion, west Musgrave, Western
1612 Australia: The University of Western Australia, Perth, PhD thesis (unpublished).

1613 Seat, Z, Beresford, SW, Grguric, BA, Gee, MA and Grassineau, NV 2009, Reevaluation of the role of
1614 external sulfur addition in the genesis of Ni–Cu–PGE deposits: evidence from the Nebo–Babel Ni–
1615 Cu–PGE deposit: West Musgrave, Western Australia: Economic Geology, v. 104, p. 521–538.

1616 Seat, Z, Beresford, SW, Grguric, BA, Waugh, RS, Hronsky, JMA, Gee, MMA, Groves, DI and
1617 Mathison, CI 2007, Architecture and emplacement of the Nebo–Babel gabbro-norite-hosted
1618 magmatic Ni–Cu–PGE sulfide deposit, West Musgrave, Western Australia: Mineralium Deposita, v.
1619 42, p. 551–582.

1620 Sharpe, MR 1981, The chronology of magma influxes to the eastern compartment of the Bushveld
1621 Complex, as exemplified by its marginal border group: Journal of the Geological Society of London,
1622 v. 138, p. 307–326.

1623 Sheraton, JW and Sun, S-s 1995, Geochemistry and origin of felsic igneous rocks of the western
1624 Musgrave Block: AGSO Journal, v. 16, p. 107–125.

1625 Silver, PG, Behn, MD, Kelley, K, Schmitz, M and Savage, B 2006, Understanding cratonic flood
1626 basalts: Earth and Planetary Science Letters, v. 245, p. 190–201.

1627 Smithies, RH, Howard, HM, Evins, PM, Kirkland, CL, Bodorkos, S and Wingate, MTD 2009, The west
1628 Musgrave Complex — some new geological insights from recent mapping, geochronology, and
1629 geochemical studies: Geological Survey of Western Australia, Record 2008/19, 20p.

1630 Smithies, RH, Howard, HM, Evins, PM, Kirkland, CL, Kelsey, DE, Hand, M, Wingate, MTD, Collins,
1631 AS, Belousova, E and Allchurch, S 2010, Geochemistry, geochronology and petrogenesis of
1632 Mesoproterozoic felsic rocks in the western Musgrave Province of central Australia, and
1633 implication for the Mesoproterozoic tectonic evolution of the region: Geological Survey of
1634 Western Australia, Report 106, 73p.

1635 Smithies, RH, Howard, HM, Evins, PM, Kirkland, CL, Kelsey, DE, Hand, M, Wingate, MTD, Collins, AS
1636 and Belousova, E 2011, Mesoproterozoic high temperature granite magmatism, crust–mantle
1637 interaction and the intracontinental evolution of the Musgrave Province: Journal of Petrology,
1638 doi:10.1093/petrology/egr010.

1639 Smithies, RH, Howard, HM, Kirkland, CL, Werner, M, Medlin, CC, Wingate, MTD and Cliff, JB 2013,
1640 Geochemical evolution of rhyolites of the Talbot Sub-basin and associated felsic units of the
1641 Warakurna Supersuite: Geological Survey of Western Australia, Report 118, 74p.

1642 Smithies, RH, Kirkland, CL, Korhonen, FJ, Aitken, ARA, Howard, HM, Maier, WD, Wingate, MTD,
1643 Quentin de Gromard, R and Gessner, K 2015, The Mesoproterozoic thermal evolution of the

1644 Musgrave Province in central Australia – Plume vs. the geological record: Gondwana Research, v.
1645 27, p. 64-94

1646 Smithies, RH, Howard, HM, Kirkland, CL, Korhonen, FJ, Medlin, CC, Maier, WD, Quentin de
1647 Gromard, R, and Wingate, MTD, in press. Piggyback Supervolcanoes - Long-Lived, Voluminous,
1648 Juvenile Rhyolite Volcanism in Mesoproterozoic Central Australia: Journal of Petrology, in press.

1649 Sobolev, SV, Sobolev, AV, Kuzmin, DV, Krivolutskaya, NA, Petrunin, AG, Arndt, NT, Radko, VA and
1650 Vasiliev, YR 2011, Linking mantle plumes, large igneous provinces and environmental
1651 catastrophes: Nature, v. 477, p. 312–316.

1652 Sprigg, RC and Wilson, RB 1959, The Musgrave mountain belt in South Australia: Geologische
1653 Rundschau, v.c47, p. 531–542.

1654 Staubmann, M 2010, The petrogenesis and economic potential of the Southern Cavenagh Range
1655 Intrusion (West Musgraves), Western Australia: The University of Tasmania, Hobart, BSc Honours
1656 thesis (unpublished).

1657 Stewart, AJ 1995, Resolution of conflicting structures and deformation history of the Mount
1658 Aloysius granulite massif, western Musgrave Block, central Australia: AGSO Journal of Australian
1659 Geology and Geophysics, v. 16, p. 91–105.

1660 Sun, S.-s, and McDonough, WF 1989, Chemical and isotopic systematics of oceanic basalts:
1661 implications for mantle composition and processes, in Magmatism in the Ocean Basins edited by
1662 AD Saunders andMJ Norry: Geological Society Special Publication, 42, p. 313–345.

1663 Sun, S-S, Sheraton, JW, Glikson, AY and Stewart, AJ 1996, A major magmatic event during 1050–
1664 1080 Ma in central Australia, and an emplacement age for the Giles Complex: AGSO Journal of
1665 Australian Geology and Geophysics, 24, p. 13–15.

1666 Tegner, C, Wilson, JR and Brooks, CK 1993, Intraplutonic quench zones in the Kap Edvard Holm
1667 layered gabbro complex, east Greenland: Journal of Petrology, v. 34, p. 681–710.

1668 Teigler, B and Eales, HV 1996, The Lower and Critical Zones of the western limb of the Bushveld
1669 Complex, as indicated by the Nooitgedacht boreholes: Geological Survey of South Africa, Bulletin
1670 111, 126p.

1671 Tollari, N, Baker, D and Barnes, S-J 2008, Experimental effects of pressure and fluorine on apatite
1672 saturation in mafic magmas, with reference to layered intrusions and massif anorthosites:
1673 Contributions to Mineralogy and Petrology, v. 156, p. 161–175.

1674 Tollari, N, Toplis, MJ and Barnes, S-J 2006, Predicting phosphate saturation in silicate magmas: an
1675 experimental study of the effects of melt composition and temperature: Geochimica et
1676 Cosmochimica Acta, v. 70, p. 1518–1536.

1677 Toplis, MJ and Carroll, MR 1995, An experimental-study of the influence of oxygen fugacity on Fe–
1678 Ti oxide stability, phase-relations, and mineral–melt equilibria in ferro-basaltic systems: Journal of
1679 Petrology, v. 36, p. 1137–1170.

1680 Toplis, MJ and Carroll, MR 1996, Differentiation of ferro-basaltic magmas under conditions open
1681 and closed to oxygen: implications for the Skaergaard intrusion and other natural systems: Journal
1682 of Petrology, v. 37, p. 837–858.

1683 Traka Resources Ltd 2011, Quarterly Activities Report for the three months ended 30 June 2011.

1684 Traka Resources Ltd 2013, Musgrave Project, viewed 29 August 2013, at
1685 <http://www.trakaresources.com.au>.

1686 Ulmer, GC 1969, Experimental investigation of chromite spinels: Economic Geology, Monograph 4,
1687 p 114–131.

1688 Wade, BP 2006, Unravelling the tectonic framework of the Musgrave Province, central Australia:
1689 The University of Adelaide, Adelaide, PhD thesis (unpubished).

1690 Waight, TE, Maas, R and Nicholls, IA 2000, Fingerprinting feldspar phenocrysts using crystal
1691 isotopic composition stratigraphy: implications for crystal transfer and magma mingling in S-type
1692 granites: Contributions to Mineralogy and Petrology, v. 139, p. 227–239.

1693 White, RW, Clarke, GL and Nelson, DR 1999, SHRIMP U–Pb zircon dating of Grenville-age events in
1694 the western part of the Musgrave Block, central Australia: Journal of Metamorphic Geology, v. 17,
1695 p. 465–481.

1696 Wilson, AH, Naldrett, AJ and Tredoux, M 1989, Distribution and controls of platinum group
1697 element and base metal mineralization in the Darwendale subchamber of the Great Dyke,
1698 Zimbabwe: Geology, v. 17, p. 649–652.

1699 Wingate, MTD and Evans, DAD 2003, Palaeomagnetic constraints on the Proterozoic tectonic
1700 evolution of Australia: Yoshida, M, Windley, BF and Dasgupta, S (eds), Proterozoic East Gondwana:
1701 Supercontinent Assembly and Breakup. Geological Society, London, Special Publications, v. 206, p.
1702 77-91.

1703 Wingate, MTD, Pirajno, F and Morris, PA 2004, Warakurna large igneous province: a new
1704 Mesoproterozoic large igneous province in west-central Australia: Geology, v. 32, p. 105–108.

1705 Yang, S, Maier, WD, Hanski, E, Lappalainen, M, Santaguida, F and Määttä, S 2013a, Origin of ultra-
1706 nickeliferous olivine in the Kevitsa Ni–Cu–PGE mineralized intrusion, Lapland, Finland:
1707 Contributions to Mineralogy and Petrology, v. 166, p. 81–95.

1708 Yang S, Maier WD, Lahaye Y, O'Brien, H 2013b, Strontium isotope disequilibrium of plagioclase in
1709 the Upper Critical Zone of the Bushveld Complex: evidence for mixing of crystal slurries, Cont Min
1710 Petrol DOI 10.1007/s00410-013-0903-4

1711 Zhao, J-X, McCulloch, MT and Korsch, RJ 1994, Characterisation of a plume-related ~800 Ma
1712 magmatic event and its implications for basin formation in central-southern Australia: Earth and
1713 Planetary Science Letters, v. 121, p. 349–367.

1714

1715 **Figure captions**

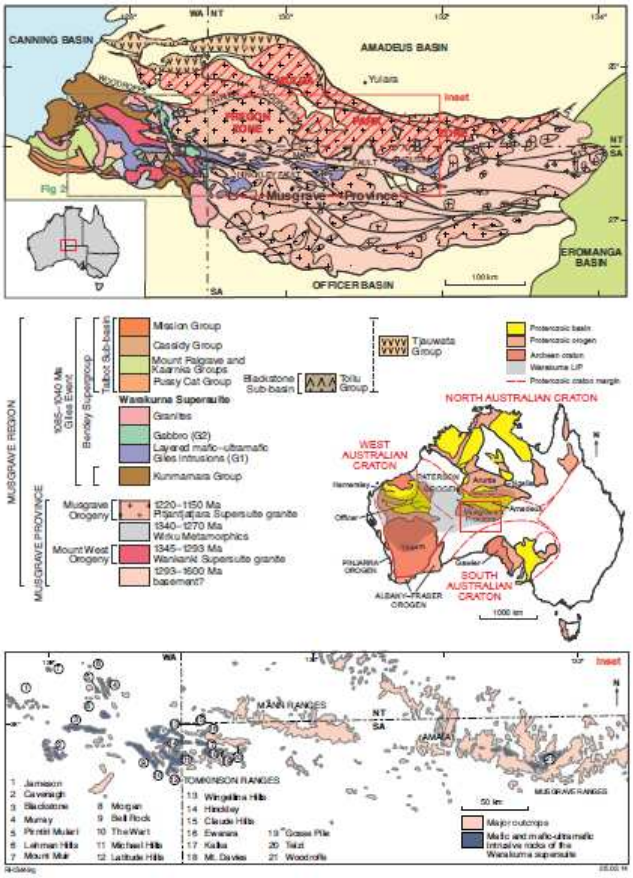

1716

1717 Figure 1. Simplified geological map of the Musgrave Province, with mafic-ultramafic intrusions
1718 highlighted in bottom panel. From Maier et al. (2014).

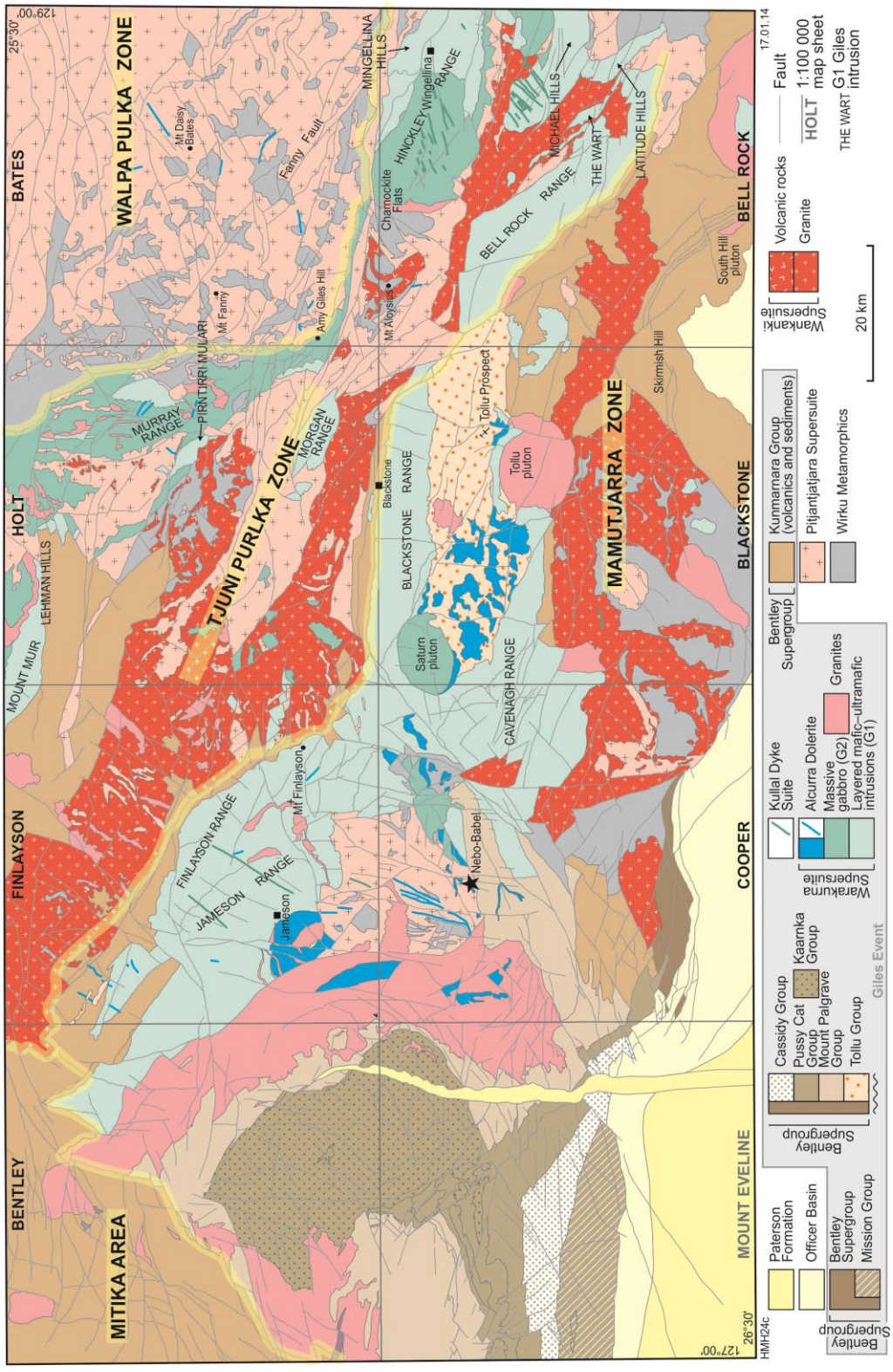

1719

1720 Figure 2. Interpreted bedrock geology map of the west Musgrave Province. Location of Nebo-

1721 Babel deposits is indicated by black star. From Maier et al. (2014).

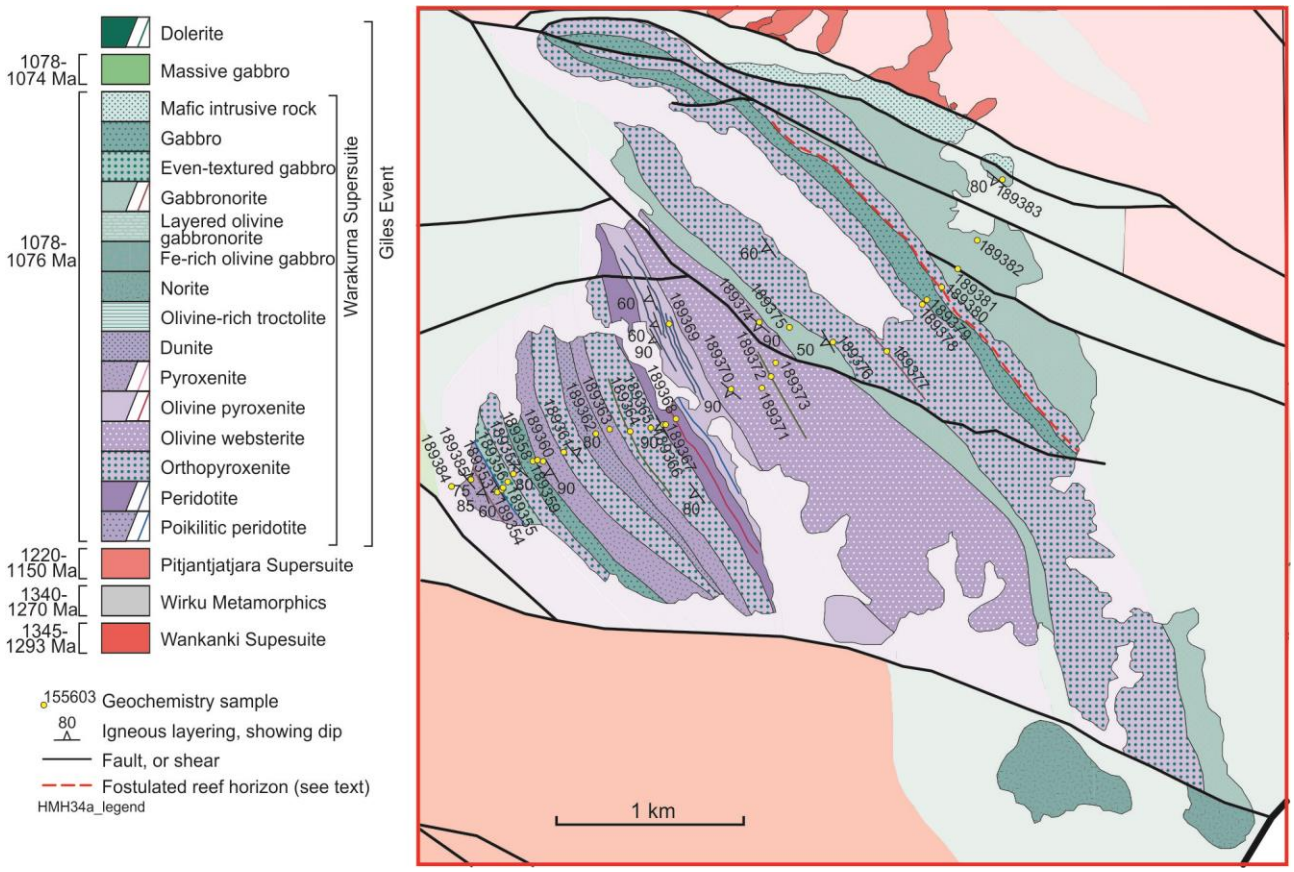

1722

1723 Figure 3. Interpreted bedrock geological map of the Pirntirri Mulari intrusion, showing sample

1724 localities (yellow circles). Stippled line indicates position of postulated reef horizon. Light shaded

1725 areas indicate regions of regolith cover. Modified from Maier et al. (2014).

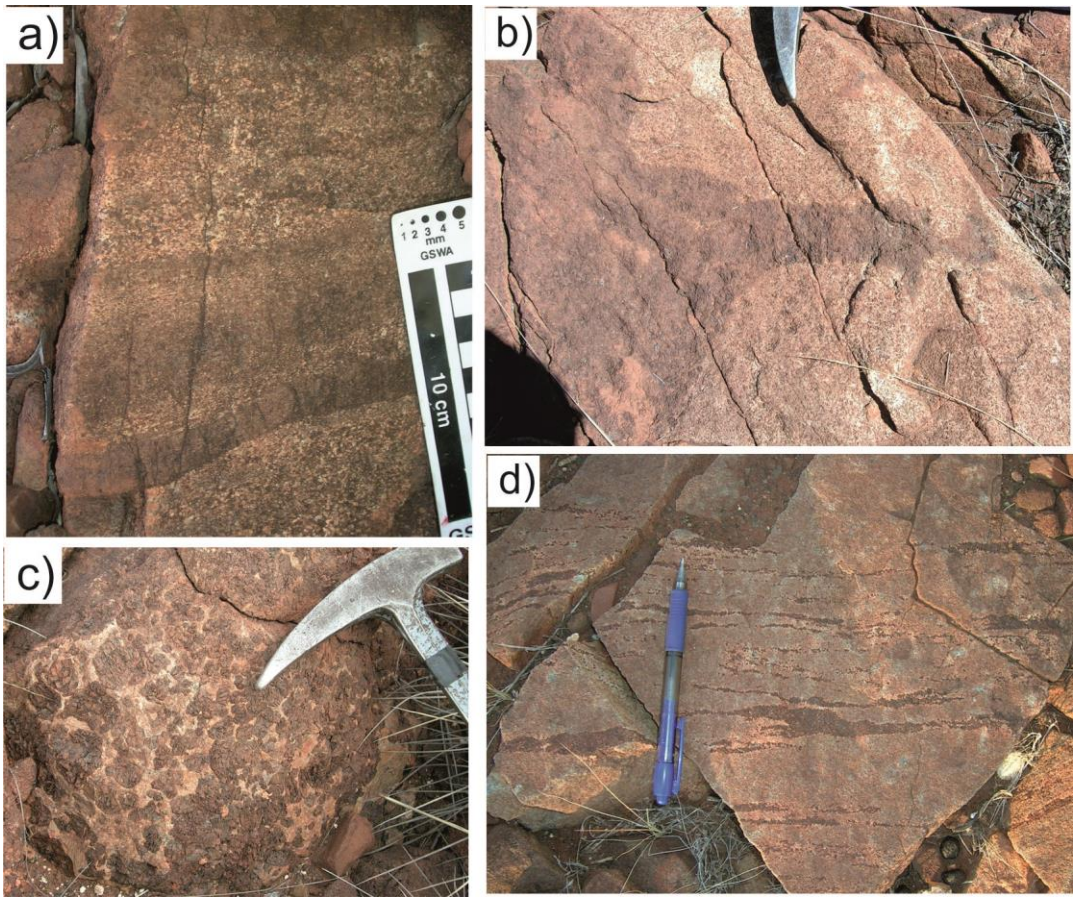

Figure 4. Textures of rocks in the Pirntirri Mulari intrusion. a) Centimetre-scale interlayering of pyroxenite and gabbronorite showing sharp bottom contact and upward grading; note small lenses and schlieren of pyroxenite within gabbronorite (near GSWA 189359); b) pegmatoidal layer within medium-grained pyroxenite (GSWA 189360); c) contact between pyroxenite and overlying gabbronorite; finger-like structure of pyroxenite is interpreted as injection of pyroxenite mush into gabbronorite (near GSWA 189374); d) schlieren of pyroxenite within leucogabbronorite (near GSWA 189358). Adapted from Maier et al. (2014).

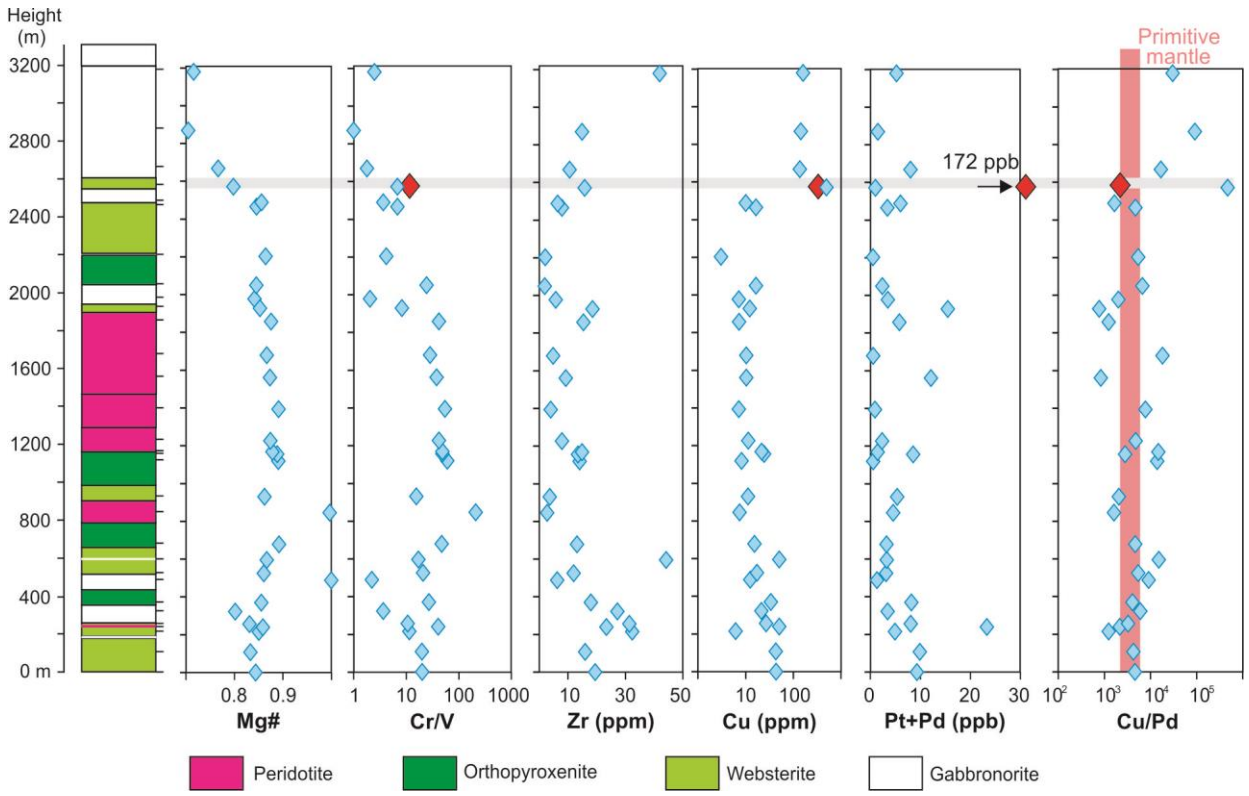

1734

1735 Figure 5. Compositional variation with stratigraphic height in the Pirntirri Mulari intrusion. Red
1736 diamonds indicate the platinum group element – rich sample analysed by Redstone Resources Ltd,
1737 and horizontal shaded bar indicates postulated position of platinum group element reef. Range of
1738 primitive mantle composition (for Cu/Pd) is based on Barnes and Maier (1999) and Becker et al.
1739 (2006). Figure from Maier et al. (2014).

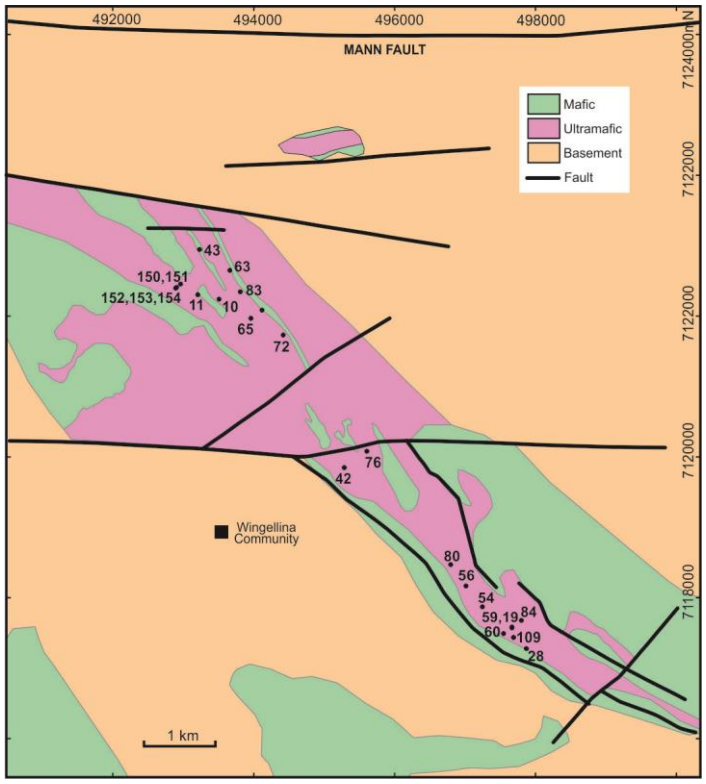

1740

1741 Figure 6. Simplified geological map of Wingellina Hills intrusion, showing location of boreholes

1742 where platinum group element mineralization has been intersected. Figure provided by Metals X

1743 Ltd, with permission. Figure from Maier et al. (2014).

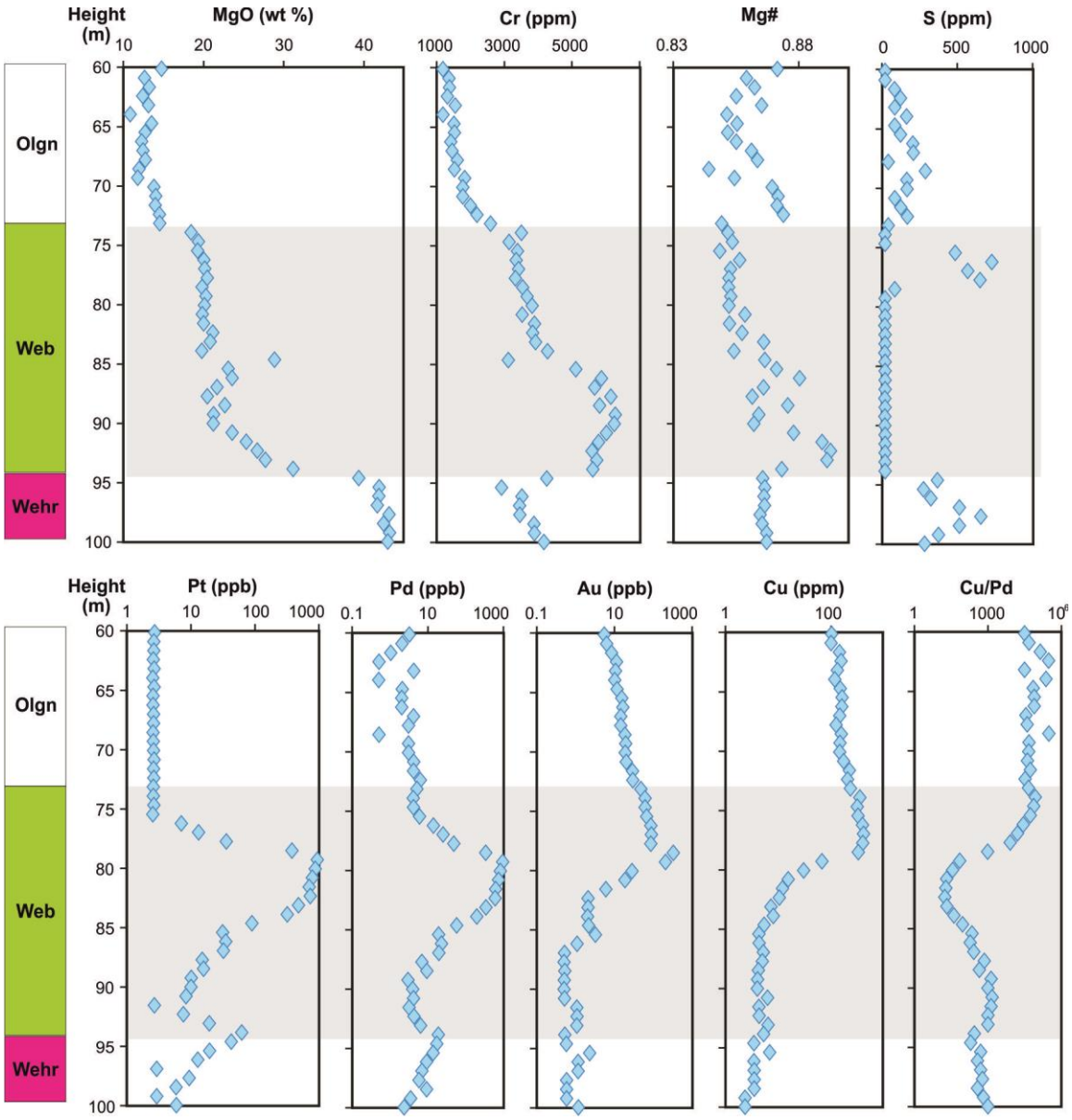

1744

1745 Figure 7. Log of percussion drillhole WPRC0–064, Wingellina Hills intrusion (Web = websterite,

1746 Wehr = wehrlite). From Maier et al. (2014).

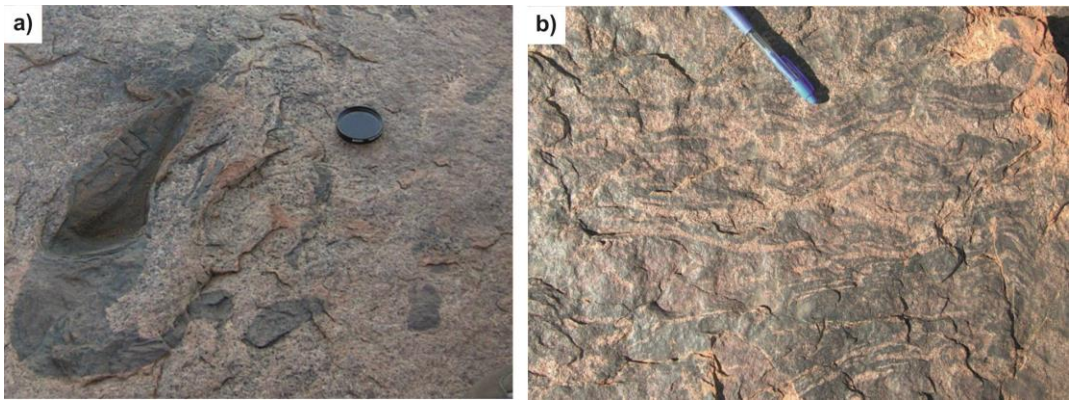

1747

1748 Figure 8. a,b) Examples of mingling textures between G2 gabbro and granite in the West Hinckley

1749 Range. Figure from Maier et al. (2014).

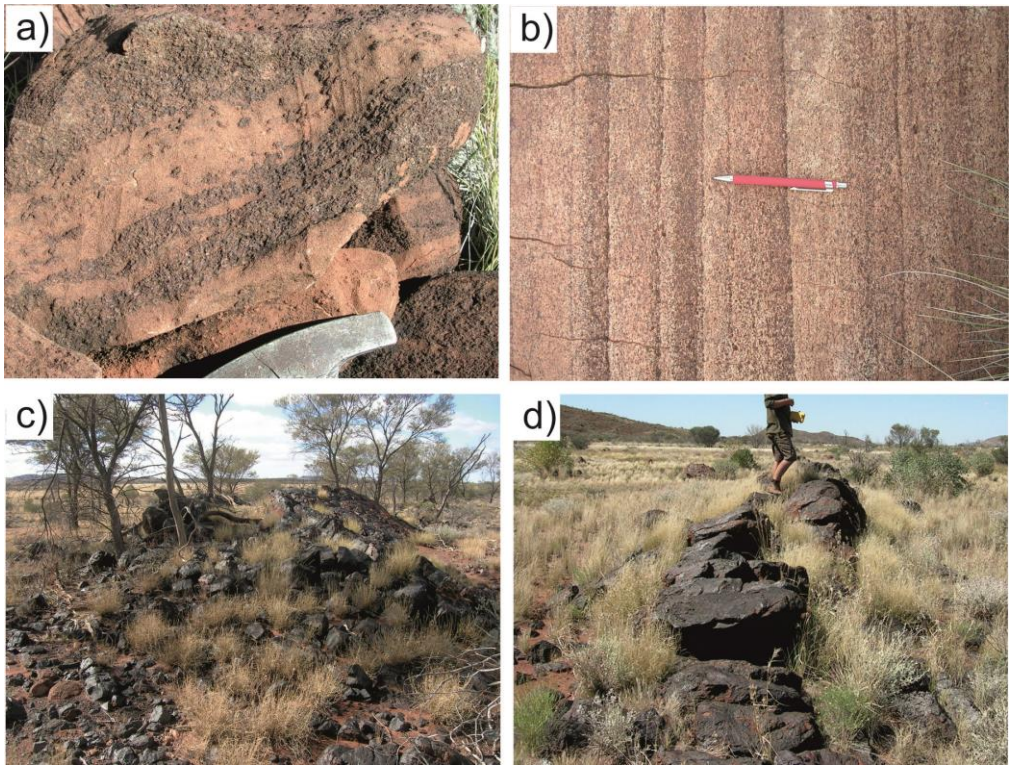

1750

1751 Figure 9. Field photographs of samples from the Lehman Hills, Jameson and Blackstone intrusions:

1752 a) banded horizon containing schlieren, lenses and fragments of fine-grained gabbronorite, and

1753 medium- to coarse-grained pyroxenite (Lehman Hills, near GSWA 189310); c) basal magnetite

1754 layer, Jameson Range; note shallow dip of layer to the right (locality GSWA 194642); e) modally

1755 graded layering in olivine gabbronorite at Jameson Range (MGA 363526E 7149428N). f) steeply

1756 south-dipping magnetite layer, southern edge of Blackstone Range (GSWA 194679). Adapted from

1757 Maier et al. (2014).

1758

1759

1760

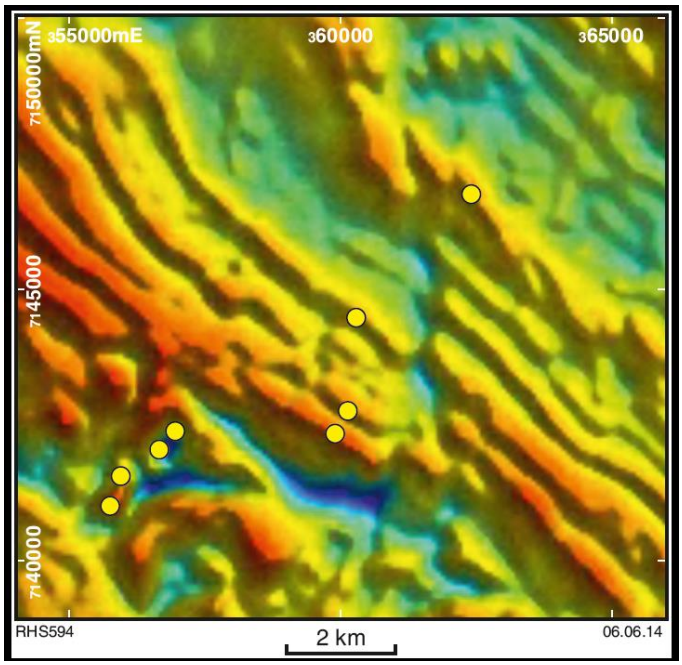

1761

1762 Figure 10. Aeromagnetic total magnetic intensity (TMI) image of the area to the northwest of

1763 Jameson, showing interpreted trend of magnetite layers (aeromagnetic highs) within the Jameson

1764 intrusion. Yellow circles are GSWA sample sites. Figure from Maier et al. (2014).

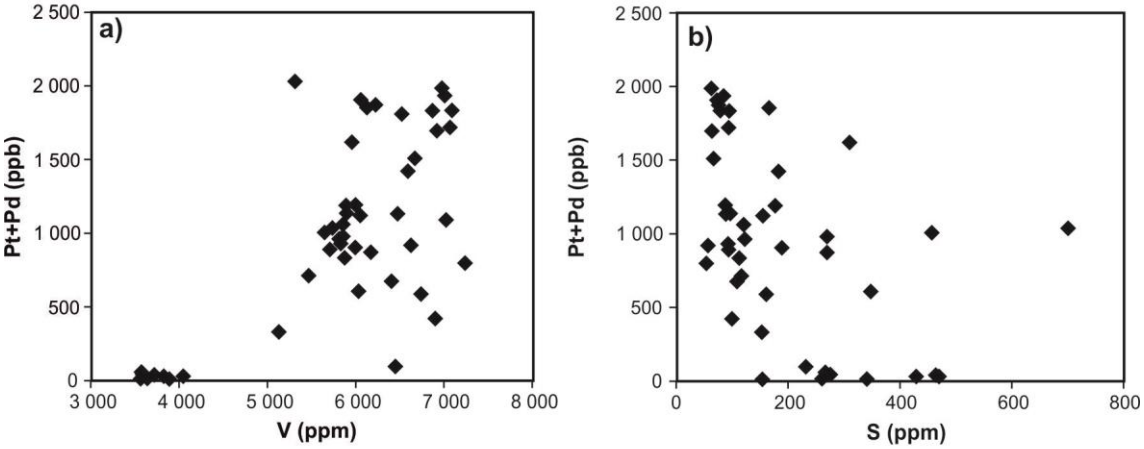

1765

1766 Figure 11. Composition of basal magnetite layer within the Jameson intrusion, based on 32

1767 samples collected along strike by Traka Resources (Traka Resources Ltd, 2011, written comm., 21

1768 October): a) Pt+Pd vs V; b) Pt+Pd vs S. Adapted from Maier et al. (2014).

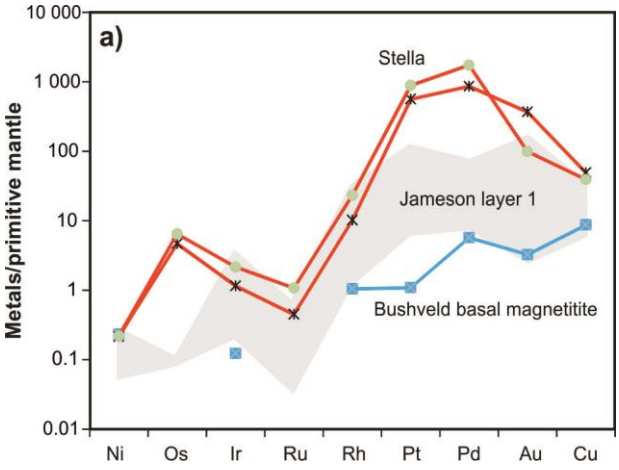

Figure 12. Metal patterns of the basal magnetite layer of the Jameson intrusion (shaded field), compared to basal magnetite layer in Upper Zone of Bushveld Complex (blue line) and PGE-rich magnetite layers of Stella intrusion, South Africa (red lines). Adapted from Maier et al. (2014).

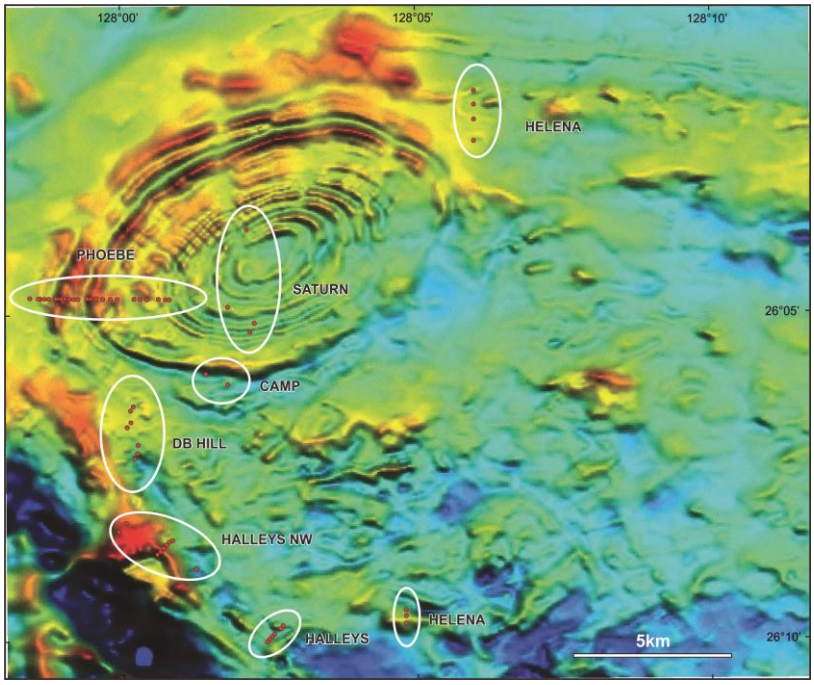

Figure 13. Aeromagnetic image of the Saturn intrusion, between the Cavenagh intrusion (lower left) and the Blackstone intrusion (to the north of the image). Red circles are sampling points for various transverses (named and enclosed in ellipses). Note the concentric pattern defining the Saturn intrusion. Figure from Maier et al. (2014).

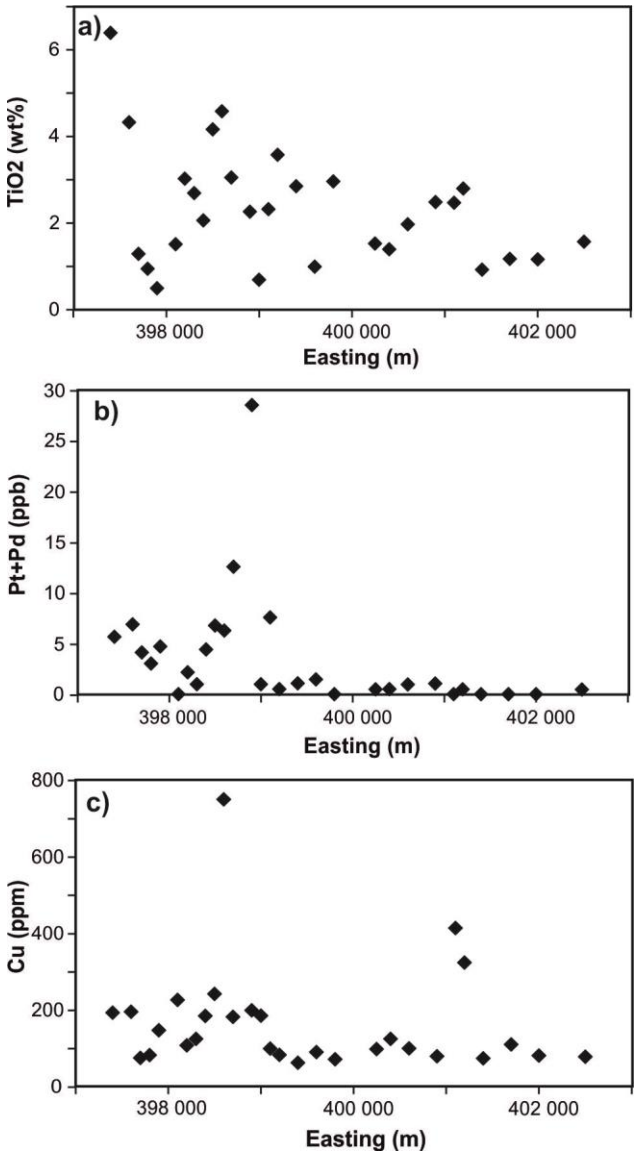

1778

1779 Figure 14. Compositional traverse (west to east) across the Saturn intrusion at Phoebe (see Fig. 27
1780 for sample localities). Note increase in PGE and Cu concentrations approximately halfway along
1781 the traverse. Plots of: a) TiO2; b) Pt+Pd; c) Cu vs Eastings. Adapted from Maier et al. (2014).

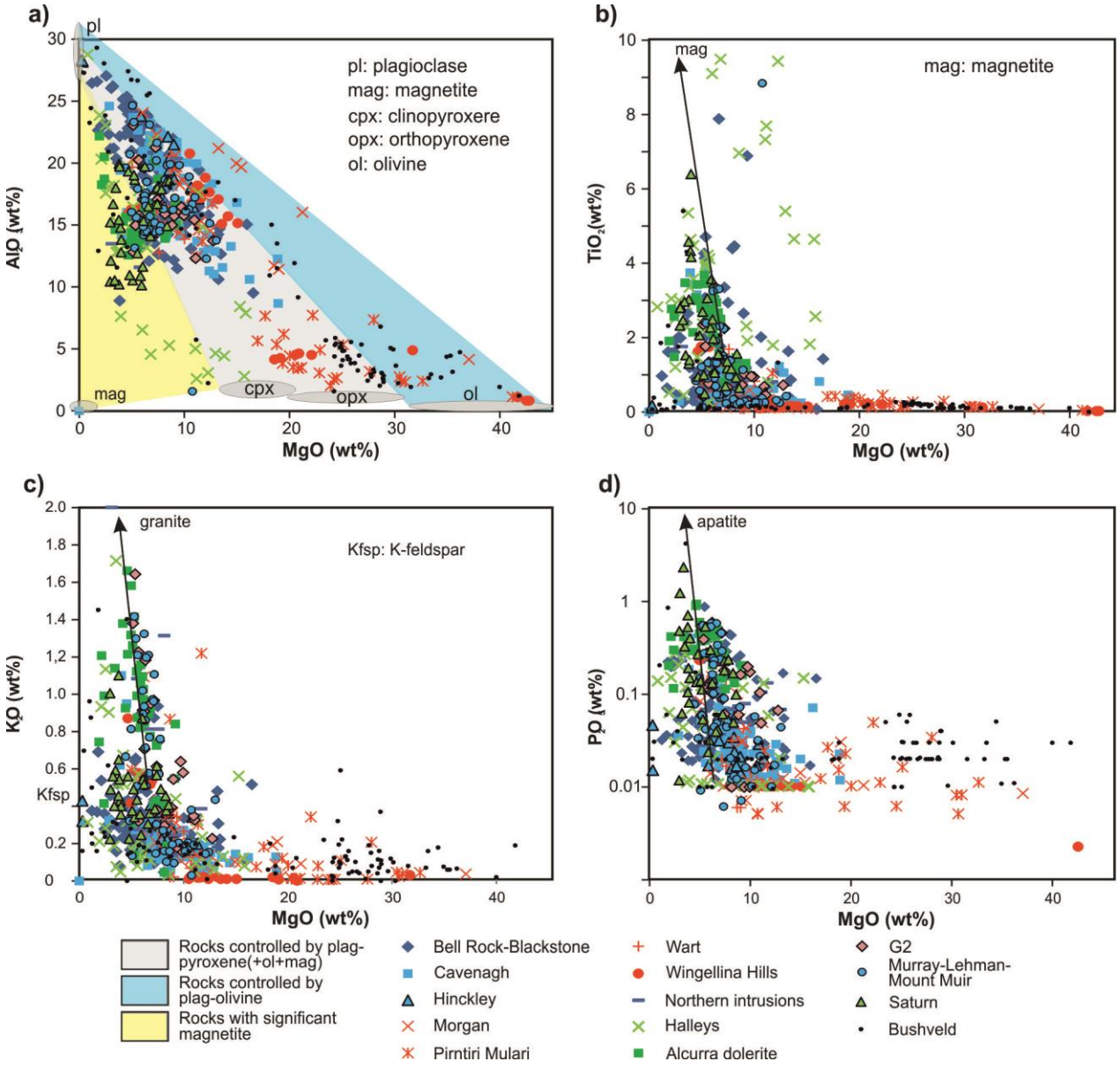

1782

1783 Figure 15. Binary variation diagrams vs MgO of selected major elements in the Giles intrusions: a)
1784 Al_2O_3; b) TiO_2; c) K_2O; d) P_2O_5. Coloured fields in (a) denote cumulates whose compositions are
1785 principally controlled by variation in modal proportions of plagioclase and olivine (blue) and
1786 plagioclase+pyroxene (grey). Yellow field indicates rocks that contain significant magnetite.
1787 Vectors in b)–d) indicate that some cumulates contain substantial magnetite, apatite, and granite
1788 components. 'Northern' intrusions include intrusive fragments to the north of Mt Muir and
1789 Hinckley Range. Figure from Maier et al. (2014).

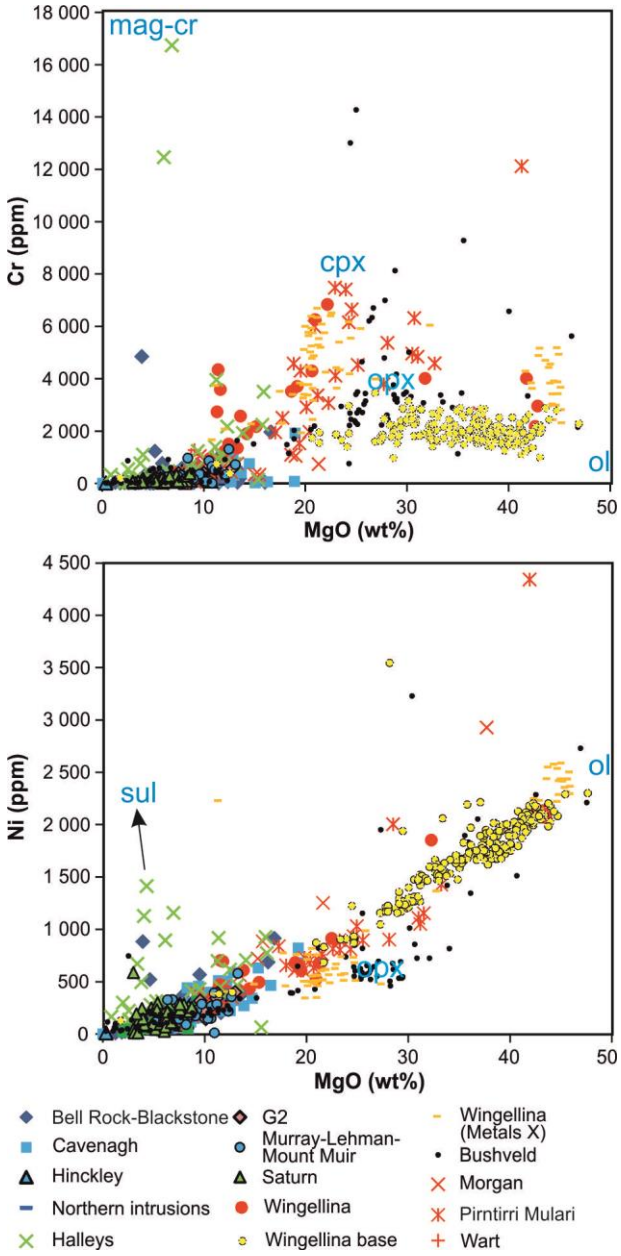

1790

1791 Figure 16. Rocks of the Giles intrusions plotted into binary variation diagrams vs MgO of: a) Cr; and

1792 b) Ni. Approximate compositions of selected silicate and oxide minerals are shown in blue

1793 lettering. Mineral abbreviations as for Figure 19. Figure from Maier et al. (2014).

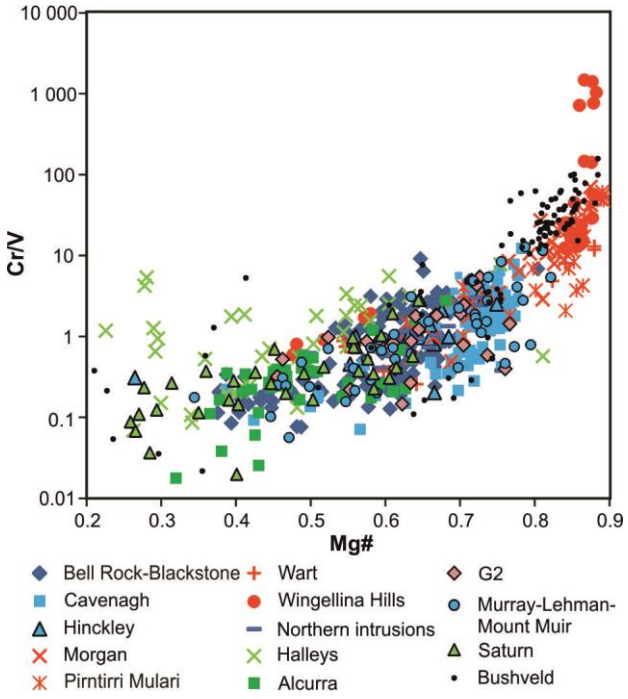

1794

1795 Figure 17. Binary variation diagram of Cr/V vs Mg# for the Giles intrusions. Bushveld data are from

1796 Maier et al. (2013b). 'Northern' intrusions include intrusive fragments North of Mt Muir and the

1797 Hinckley Range. Cavenagh data include samples from Staubmann (2010). Figure from Maier et al.

1798 (2014).

1799

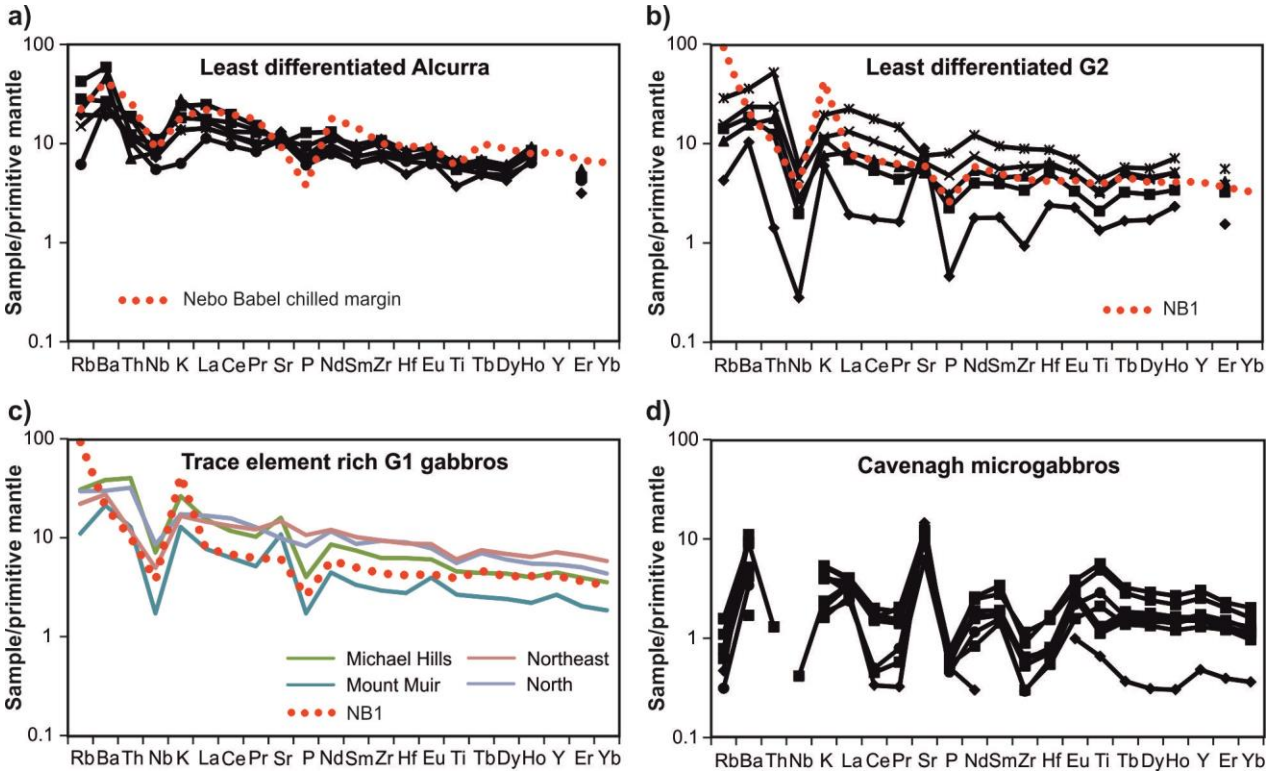

1800

1801 Figure 18. Primitive mantle-normalized multi-element variation diagrams for rocks of the Giles

1802 Event that may be liquids, including: a) unevolved samples of the Alcurra dolerite suite; b)

1803 unevolved samples of the G2 gabbros; c) G1 gabbros enriched in incompatible trace elements; and

1804 d) Cavenagh microgabbros. Normalization factors are from Sun and McDonough (1989). Adapted

1805 from Maier et al. (2014).

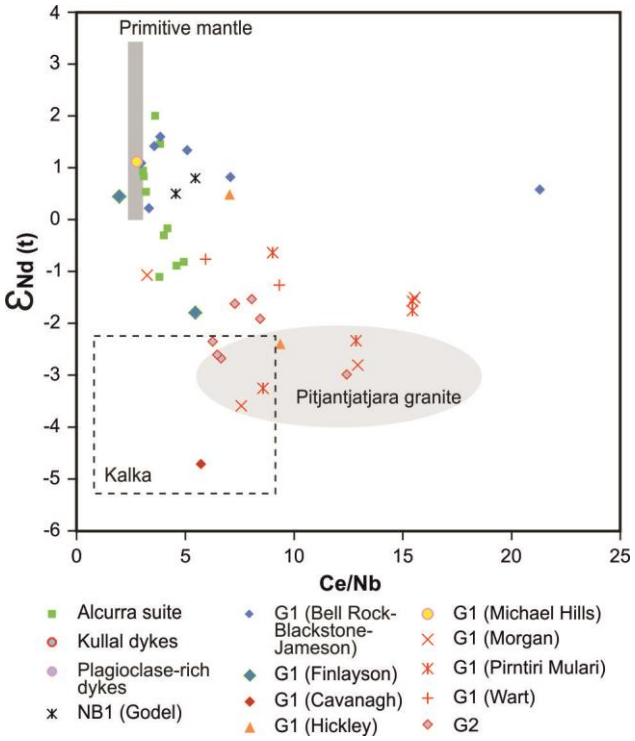

1806

1807 Figure 19. Plot of εNd vs Ce/Nb for the Giles intrusions. Note that troctolitic G1 intrusions and the
1808 Alcurra Dolerite suite plot near the mantle range, whereas the other intrusions contain an
1809 enriched component. The compositional field of Pitjantjatjara granite contains the 10th–90th
1810 percentile of Ce/Nb data. Data for Kalka intrusion are from Wade (2006). Figure from Maier et al.
1811 (2014).

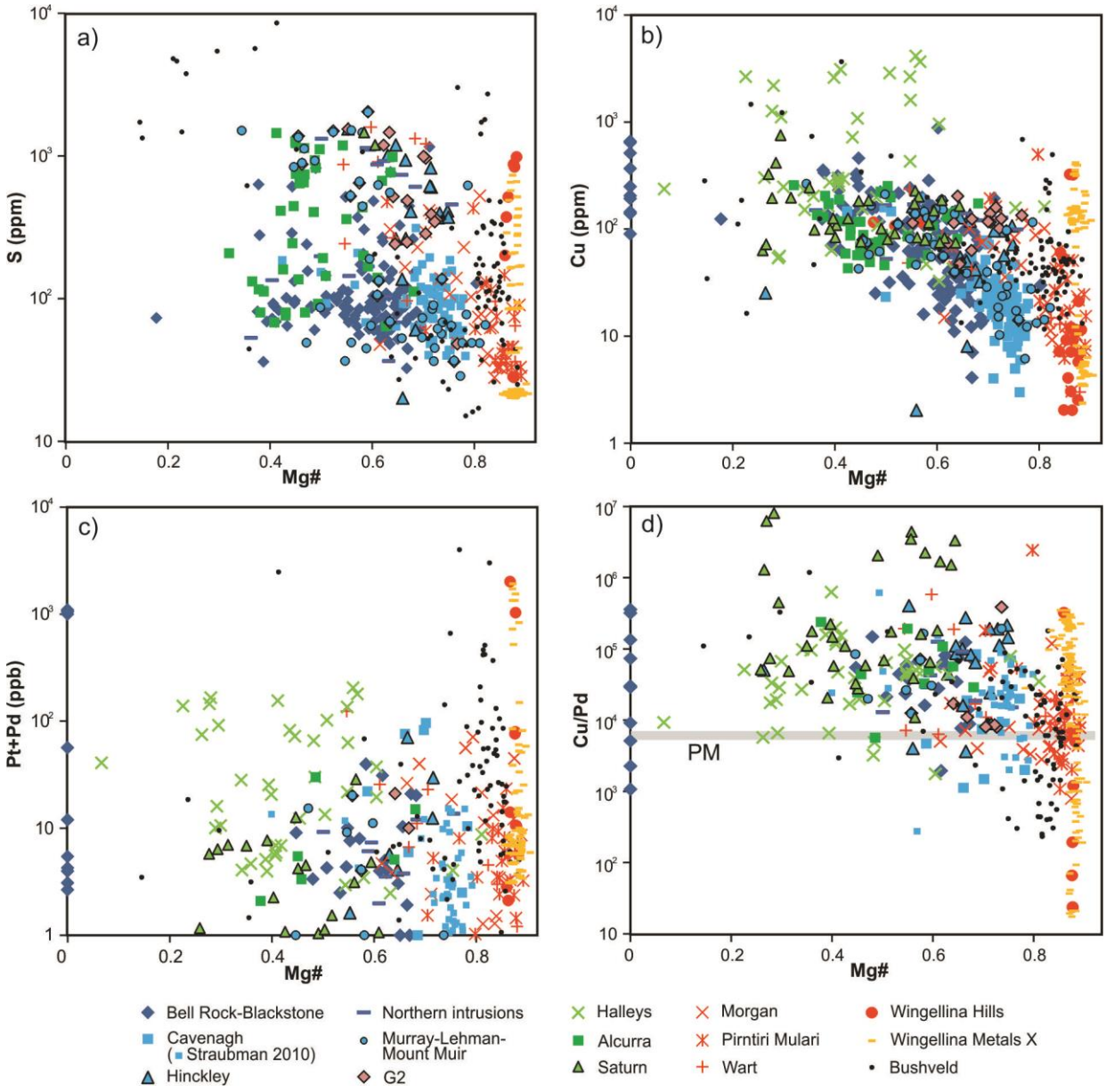

1812

1813 Figure 20. Binary variation diagrams vs Mg# of: a) S; b) Cu; c) Pt+Pd; d) Cu/Pd. Primitive mantle

1814 value in d) is from Barnes and Maier (1999). Adapted from Maier et al. (2014).

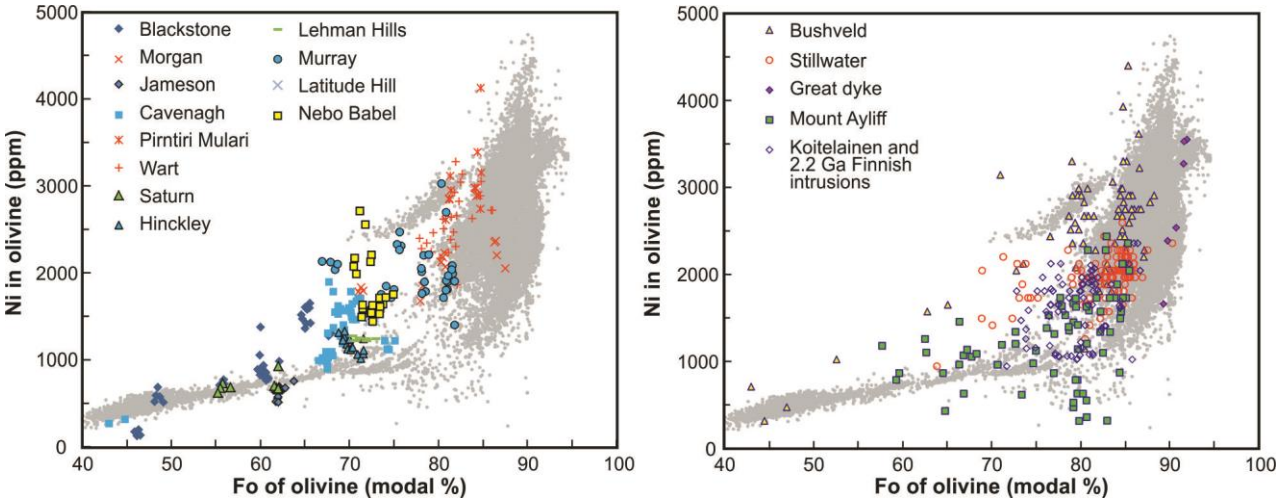

1815

1816 Figure 21. Plot of Ni vs Fo in olivine: a) data from the west Musgrave Province; b) global data of

1817 layered intrusions (data compiled from Teigler and Eales, 1996; Maier and Eales, 1997; Lightfoot et

1818 al., 1984; Raedeke, 1982; E Hanski, unpublished data). Grey shading is background data, from

1819 Sobolev et al. (2011). Figure from Maier et al. (2014).

1820

1821

1822

1823

1824

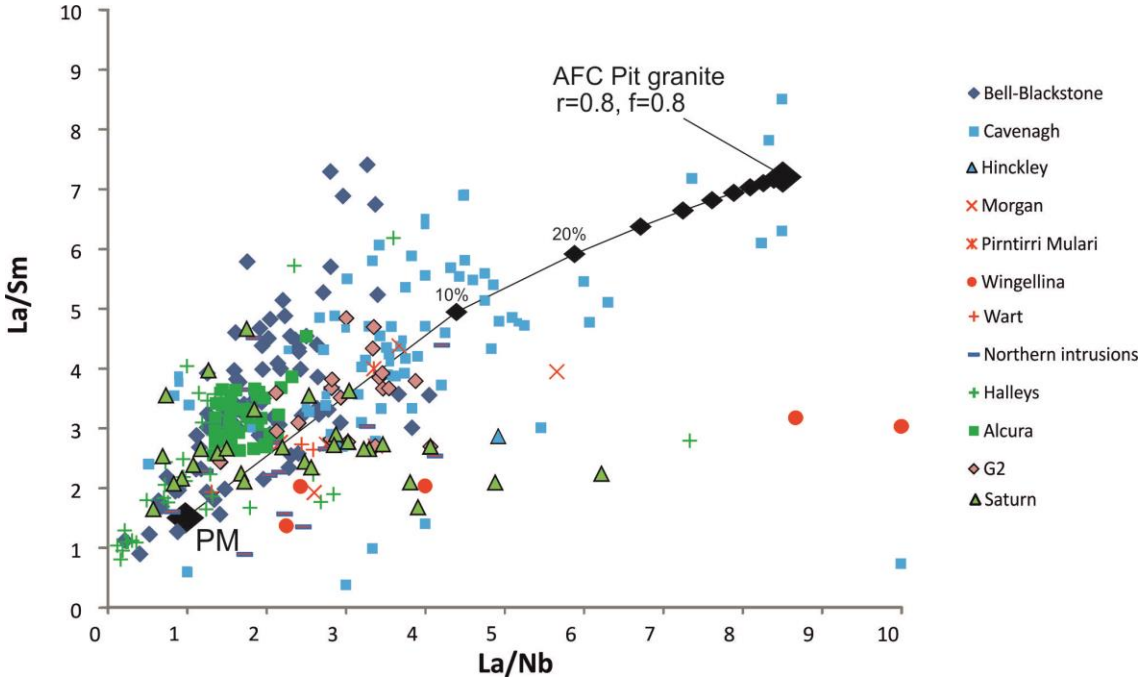

1825

1826 Figure 22. Binary variation diagrams of La/Sm vs La/Nb: Most of the troctolitic intrusions
1827 (Mantamaru), the Alcurra Dolerite suite, and the Halleys and Saturn intrusions have primitive
1828 mantle-like trace element ratios, whereas many of the other intrusions (notably Cavenagh,
1829 Hinckley Range, Murray Range, and the ultramafic intrusions) contain a crustal component,
1830 possibly of Pitjantatjara granite (Pit granite). Solid line represents mixing line between picrite (with
1831 trace element contents assumed to be 4x primitive mantle, i.e. equivalent to ~25% partial mantle
1832 melting) and a contaminated magma produced by AFC (r=0.8, f=0.8) of picrite with a 17% partial
1833 melt of Pitjantjarra granite (calculated by assuming modal proportions determined during
1834 experimental melting of biotite gneiss at 875°, 3kbar, Patino Douce and Beard, 1995, and D values
1835 summarized in Rollinson, 2013).

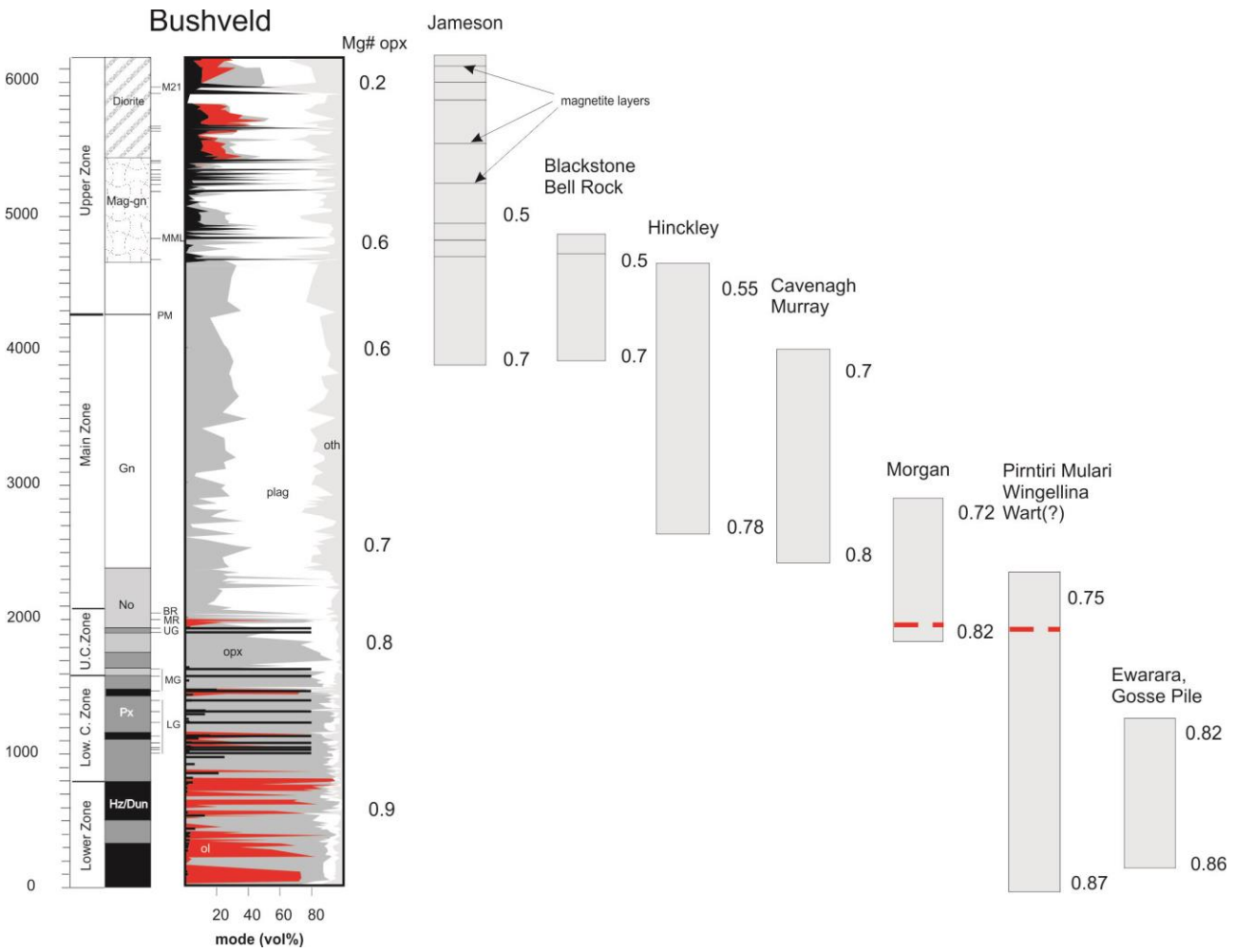

1836

1837 Figure 23. Stratigraphic comparison of Giles intrusions with Bushveld Complex. (Bushveld log and

1838 data from Maier et al., 2013b). Low. C. Zone = Lower Critical Zone. U.C. Zone = Upper Critical Zone.

1839 Figure from Maier et al. (2014).

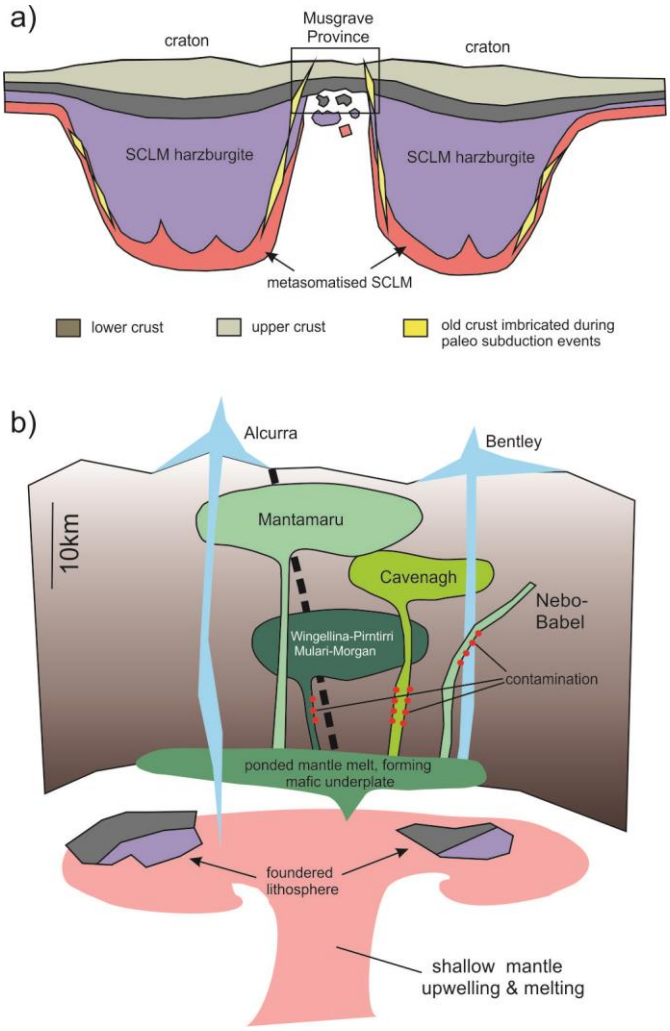

1840

1841 Figure 24. Schematic model of emplacement of the Giles intrusions: a) foundering of crust and

1842 new SCLM; b) ponding and ascent of mantle melts. Note that the horizontal dimension is greatly

1843 compressed for added clarity. See text for discussion. SCLM = subcontinental lithospheric mantle.

1844 Figure from Maier et al. (2014).

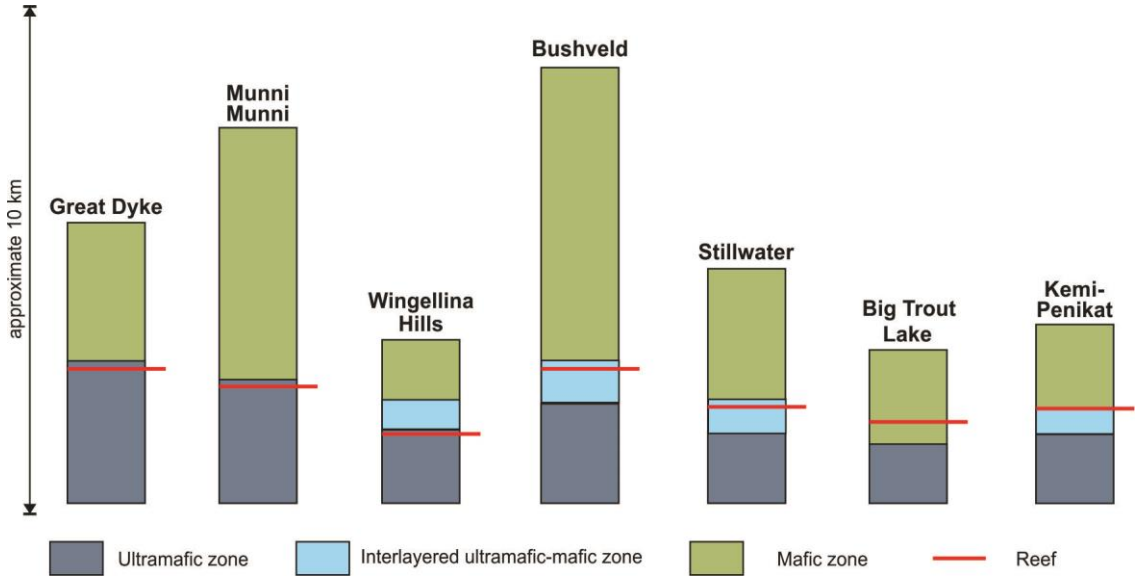

1845

1846 Figure 25. Comparison of the positions of the PGE reef in a number of well-characterized layered

1847 intrusions. Figure from Maier et al. (201is 4).